



Review

Tetrathiafulvalene-based group XV ligands: Synthesis, coordination chemistry and radical cation salts

Dominique Lorcy^{a,*}, Nathalie Bellec^a, Marc Fourmigué^{a,*}, Narcis Avarvari^{b,*}^a Sciences Chimiques de Rennes, UMR 6226 CNRS-Université de Rennes 1, Matière Condensée et Systèmes Electroactifs (MaCSE), Campus de Beaulieu, 35042 Rennes, France^b Laboratoire Chimie et Ingénierie Moléculaire d'Angers (CIMA), UMR 6200 CNRS-Université d'Angers, UFR Sciences, Bât. K, 2 Bd. Lavoisier, 49045 Angers Cedex, France

Contents

1. Introduction	1399
2. Syntheses of tetrathiafulvalenyl ligands	1399
2.1. Tetrathiafulvalenes with N-ligands	1399
2.1.1. Pyridine directly linked to the TTF core	1400
2.1.2. Ethylenic and acetylenic spacer groups	1400
2.1.3. Spacer groups involving ethylenedithio junctions	1402
2.1.4. Spacer groups incorporating amide and ester functionalities	1402
2.1.5. Thiopicoline derivatives: S,N ligands	1403
2.1.6. N,N chelating ligand: bipyridine	1404
2.1.7. Other N,N chelating ligands	1406
2.1.8. Pyrazines	1407
2.1.9. Oxazolines and imidazoles	1408
2.1.10. Miscellaneous	1409
2.2. Tetrathiafulvalenyl phosphines	1409
2.2.1. Phosphine directly linked to the donor core	1409
2.2.2. Phosphine linked through a non-conjugated spacer group	1409
2.2.3. Redox properties	1410
2.3. Tetrathiafulvalenyl stibines	1411
3. Complexes: synthesis and structure	1411
3.1. The Cr, Mo, W triad (group 6)	1411
3.2. The Mn, Tc, Re triad (group 7)	1414
3.3. The Fe, Ru, Os triad (group 8)	1417
3.3.1. The Fe, Ru, Os triad with N-ligands	1417
3.3.2. The Fe, Ru, Os triad with P-ligands	1419
3.4. The Co, Rh, Ir triad (group 9)	1420
3.4.1. The Co, Rh, Ir triad with N-ligands	1420
3.4.2. The Co, Rh, Ir triad with P-ligands	1422
3.4.3. The Co, Rh, Ir triad with N,S or P,N-ligands	1423
3.5. The Ni, Pd, Pt triad (group 10)	1423
3.5.1. The Ni, Pd, Pt triad with N-ligands	1423
3.5.2. The Ni, Pd, Pt triad with P-ligands	1424
3.5.3. The Ni, Pd, Pt triad with P,N-ligands	1426
3.6. The Cu, Ag, Au triad (group 11)	1426
3.6.1. The Cu, Ag, Au triad with N-ligands	1426
3.6.2. The Cu, Ag, Au triad with P-ligands	1430
3.7. The Zn, Cd, Hg triad (group 12)	1431
4. Cation radical salts of TTF metal complexes	1432
4.1. Cation radical salts of the copper complex Cu1	1432
4.2. Cation radical salts of the molybdenum complex Mo1	1433
4.3. Cation radical salts of the nickel complex Ni2	1434

* Corresponding author. Tel.: +33 2 23 23 62 73; fax: +33 2 23 23 67 38.

E-mail addresses: dominique.lorcy@univ-rennes1.fr (D. Lorcy), marc.fourmigue@univ-rennes1.fr (M. Fourmigué), narcis.avarvari@univ-angers.fr (N. Avarvari).

5. Catalytic applications of complexes based on TTF ligands	1434
6. Conclusions and perspectives	1436
Acknowledgement	1436
References	1436

ARTICLE INFO

Article history:

Received 24 July 2008

Accepted 15 September 2008

Available online 25 September 2008

Keywords:

Tetrathiafulvalene

N-ligand

P-ligand

Coordination

Redox active ligands

Radical cation salts

Catalysis

Conducting materials

Molecular magnetism

ABSTRACT

This review deals with the synthesis, properties and applications of metal complexes of tetrathiafulvalene-based group XV (N, P, As, Sb) ligands. The different synthetic methods for the preparations of tetrathiafulvalenes (TTFs) incorporating coordination functions such as N atoms (essentially sp^2 N atoms in pyridines, pyrazines, bipyridines, imines, etc.) and P atoms (essentially in tertiary phosphines) are reviewed, together with the redox properties of these free ligands, showing in most cases that the electron donating ability of the TTF core is only scarcely affected upon association with the coordinating group. Metal complexes of such ligands have been reported with a large variety of metal centers, from group 6 (Cr, Mo, W) to group 12 (Zn, Cd, Hg). Their structural and electronic and magnetic properties are described, with an emphasis on the evolution of the properties of the ligand (redox potentials, ^{31}P NMR chemical shifts) upon coordination. Two applications of these complexes are further discussed, elaboration of multi-functional conducting materials upon TTF oxidation, redox modulation of the reactivity of the metal complex used as catalyst.

© 2008 Elsevier B.V. All rights reserved.

1. Introduction

The synthesis and coordination chemistry of electro-active molecules functionalized by various mono or polydentate ligands have developed steadily during the past two decades. A prominent redox-active class of compounds is represented by tetrathiafulvalene (TTF) derivatives, which have been extensively studied in the search for molecular conductors and superconductors [1,2]. In this respect, the association of the redox active TTF unit with coordinating heteroatom-based groups is particularly promising in the perspective of preparing electroactive transition metal complexes with original structural and electronic properties. First, the metal may serve as a template in order to assemble two or more TTF units, by means of metal-ligand interactions, in a rigid predefined manner ruled by the stereochemical preferences of the metal ion and the number of free coordination sites. Interplay between the electron donating properties of the electroactive ligand and the electron density on the metallic center could possibly occur, especially when the ligand is directly bound to TTF. In addition, the functional redox ligands may be further activated and assembled into electroactive supramolecular edifices by chemical or electrochemical oxidation. Such radical cation salts would provide unique models to probe the structural and electronic consequences of mixing the metal d and ligand π electrons and spins. In addition, when the coordinated metal is paramagnetic, the coexistence of magnetic and conducting properties hold much promise for the development of bifunctional molecular materials, a field of much current activity [3–6]. Electroactive complexes could provide new interesting applications in the field of luminescent compounds and also in that of homogenous catalysis.

Among the numerous TTF ligand systems investigated in these last 20 years, those containing pyridine or bipyridine ligands in the one hand, those containing phosphines in the other hand are the most extensively studied so far, particularly for the elaboration of metal complexes. In this review article, we therefore concentrate on group XV ligands containing N, P or Sb atoms, readily available for further metal coordination. We will first describe in Section 2 the different synthetic methods developed for the syntheses of these original electroactive ligands together with a strong emphasis on the evolution of their electrochemical properties depending on the nature and location of the coordinating group. Section 3 is

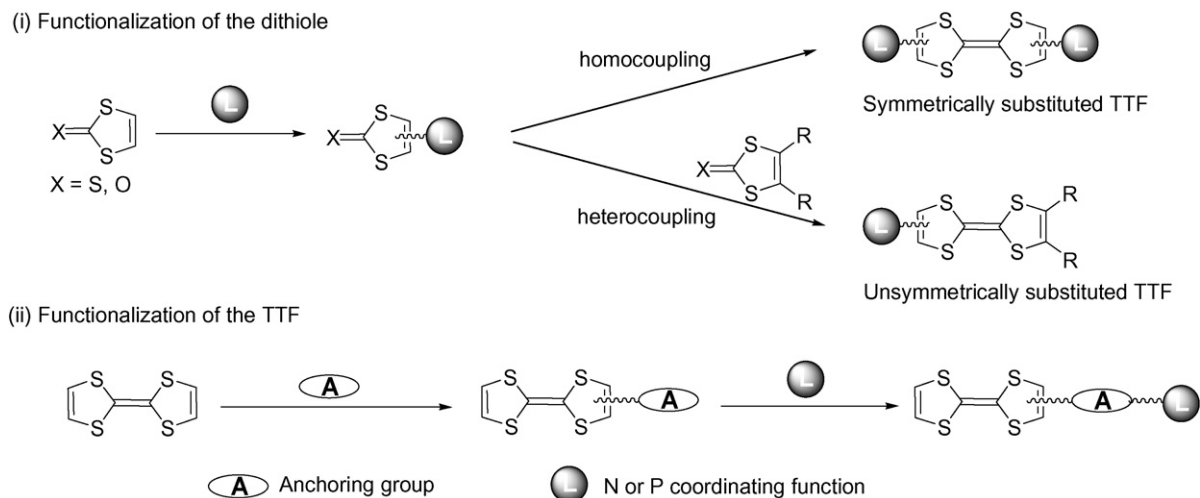
devoted to a thorough description of the different metal complexes reported so far with these ligands, from group 6 (Cr, Mo, W) to group 12 (Zn, Cd, Hg) metal triad, as no N or P complexes have been described so far, neither with the early transition metals, nor with lanthanide or actinides. In Section 4, we describe in detail the few reported examples of cation radical salts derived from these TTF-containing complexes, while in Section 5, we report on the catalytic applications of several Pd and Ir complexes.

2. Syntheses of tetrathiafulvalenyl ligands

For almost four decades, the imagination of the chemists involved in the field of molecular materials based on TTF gave rise to numerous TTF derivatives which have been thoroughly reviewed along the years by Schukat and Fanghänel [7]. The various strategies used to prepare these numerous functionalized TTF derivatives have also been recently reviewed [8]. However, until now, no compendium of TTFs as electroactive ligands has been reported, this is the object of the present part of this section. The synthetic approaches used towards these electroactive ligands are essentially based on two strategies (Scheme 1): (i) functionalization of the dithiole core by the coordination function, followed by its homo- or heterocoupling to the symmetrically or unsymmetrically substituted TTFs and (ii) functionalization of the preformed donor core with a reactive group which will then serve as an anchorage for introducing the coordinating part on the TTFs. In this section, we will first focus on the synthesis of N electroactive ligands, followed by the P-ligands and Sb-ligands as no TTF functionalized with arsenic-containing moieties has been described so far.

2.1. Tetrathiafulvalenes with N-ligands

The use of TTF organic donors containing a sp^2 nitrogen atom as potential coordinating site has been intensively developed within the last decade. Among the various heterocycles grafted on the TTF core, we will focus on the pyridine, bipyridine, pyrazine, thiopicoline, etc. Since the synthesis of the first TTF-pyridine in 1984 by Okamoto et al., a large variety of N sp^2 TTF ligands has been synthesized. It was however only at the beginning of the 21st century that transition metal complexes have been reported, and since then, the development of this field became clearly oriented towards



Scheme 1. Two main synthetic approaches for the synthesis of N and P TTF ligands.

the coordination chemistry of these electroactive ligands. As a consequence, many potentially interesting TTF-N ligands described before 2000 have never been engaged in metal complexes.

2.1.1. Pyridine directly linked to the TTF core

The first pyridine-substituted TTF **1** has been prepared by Okamoto et al. in 1984 through the reaction of bis-(2-pyridyl)acetylene with CS_2 at 100°C under high pressure for 12 h (Scheme 2). The goal of this work was to couple the electron-rich TTF π -system with a metal complex into a single conjugated and repeating framework [9]. This visionary and pioneering work was followed by the synthesis of the mono-substituted TTF **2** by Iyoda et al. in 1992 through the palladium-catalyzed coupling of trialkylstannyl-TTF with 2-bromopyridine (Scheme 3) [10].

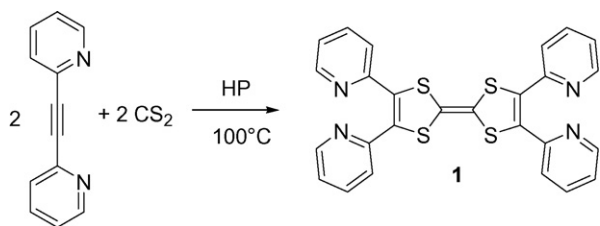
The same synthetic procedure involving TTF- SnR_3 has been used with 2,6-dibromopyridine [11] or 4-bromopyridine as reactants [12]. N-methylation afforded for example the corresponding N-methyl-4-pyridinium-TTF, a TTF-A diad molecule (A = electron acceptor moiety) exhibiting intramolecular charge transfer (ICT). This Stille coupling reaction is particularly attractive as the stannylated TTF derivatives are readily available in very good yields from lithiation of the preformed TTF core and reaction with trialkylstannylchloride. Reactivity of the different halogenated pyridines in this Stille palladium-catalyzed condensation is, as expected, in the

order $\text{Py-I} > \text{Py-Br} \gg \text{Py-Cl}$. This chemical approach has been successfully developed for the synthesis of mono and bis-pyridyl-TTFs (Scheme 4) [13–15] and was also extended to the synthesis of 3-quinolyl and 3,5-pyrimidyl [13] derivatives **10** and **11**. The mono and bis-pyridyl-TTFs can also be prepared from the unsymmetrical or symmetrical coupling using the 4-pyridyl-1,3-dithiole-2-one in the presence of neat triethylphosphite but in rather low yields [16–18]. The pyridine substituent directly linked to the donor core has no significant electron withdrawing effect on the redox properties of the donor core as the oxidation potentials remain very close to those of the non-substituted TTFs [10–17] (Table 1).

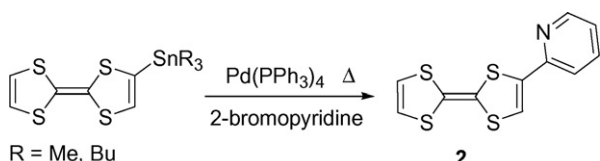
2.1.2. Ethylenic and acetylenic spacer groups

The pyridine unit has also been grafted on the TTF core through various conjugated linkers. For instance, the first example in this series, TTF- $\text{CH}=\text{CH}$ -4-pyridine **14a**, was described by Casoux et al. [19] in 1999. It was obtained by a Wittig reaction between formyl-TTF and the ylide generated in basic medium from the 4-picolyltriphenylphosphonium chloride, hydrochloride (Scheme 5).

According to the same Wittig approach, the mono and the bis-pyridylethenyl-TTF derivatives **14b**, **15** and **16** were prepared (Scheme 5) [20–22]. These pyridyl-TTF derivatives were first investigated as precursors of donor-acceptor diads, in TTF-(π -



Scheme 2. Synthesis of tetrakis(2-pyridyl)TTF.



Scheme 3. Synthesis of 2-pyridyl-TTF by Stille coupling.

Table 1

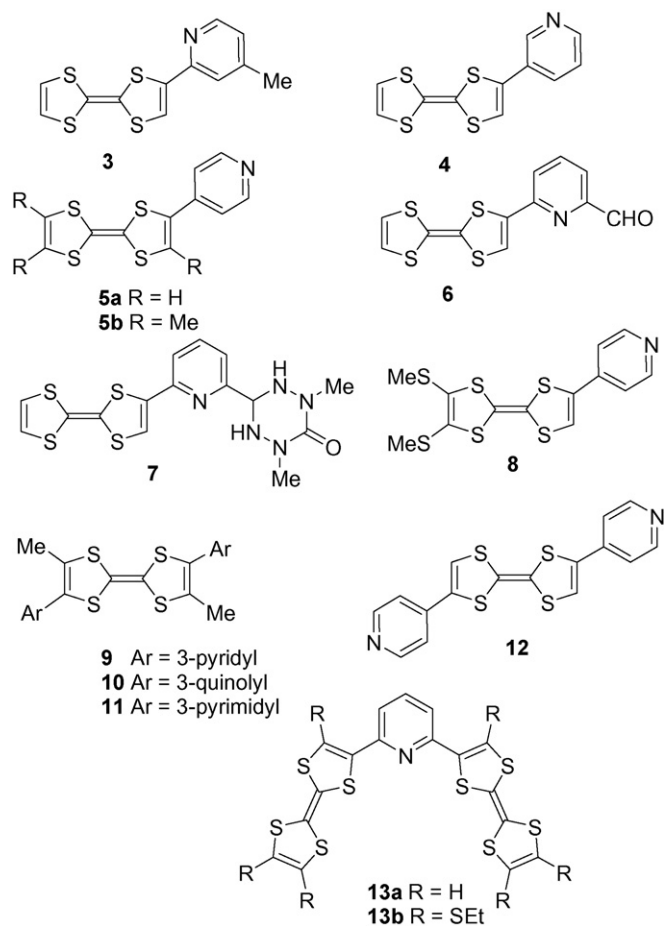
Oxidation potential of TTF-pyridines **2–13** (in V, scanning rate 100 mV/s, using TBAPF₆ as supporting electrolyte and Pt working electrode).

Compound	E^1	E^2	Solvent, ref. electrode	Reference
2	0.39	0.85	PhCN vs. Ag/AgCl ^a	[10]
2	0.54	1.09	CH_2Cl_2 vs. SCE	[13]
3	0.51	1.07	CH_2Cl_2 vs. SCE	[13]
4	0.58	1.08	CH_2Cl_2 vs. SCE	[13]
5a	0.47	0.70	DMF vs. Ag/AgCl ^a	[14]
5b	0.31	0.70	CH_3CN vs. Ag/AgCl	[12]
6	0.43	0.82	CH_3CN vs. Ag/AgCl ^b	[15]
7	0.43 ^c	0.82	CH_3CN vs. Ag/AgCl ^b	[15]
8	0.49	0.76	CH_3CN vs. Ag/AgCl	[17]
9	0.55	1.02	CH_2Cl_2 vs. SCE	[13]
10	0.65	1.08	CH_2Cl_2 vs. SCE	[13]
11	0.55	1.02	CH_2Cl_2 vs. SCE	[13]
13a	0.29	0.87	PhCN vs. SCE ^a	[11]
13b	0.54	0.82	PhCN vs. SCE ^a	[11]

^a TBAClO₄ as supporting electrolyte.

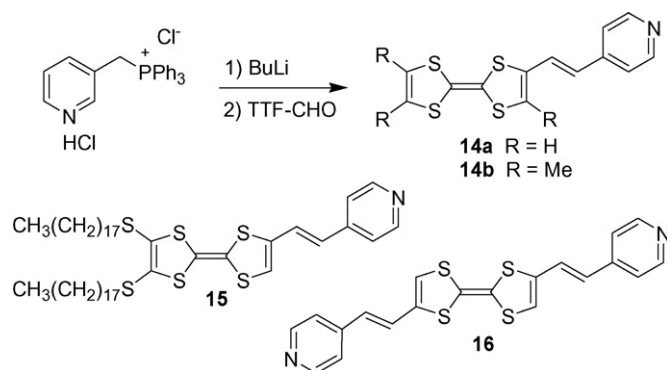
^b Glassy carbon as the working electrode.

^c $E_{\text{p/ox}} = 0.76$ V corresponding to the formation of verdazyl radical.

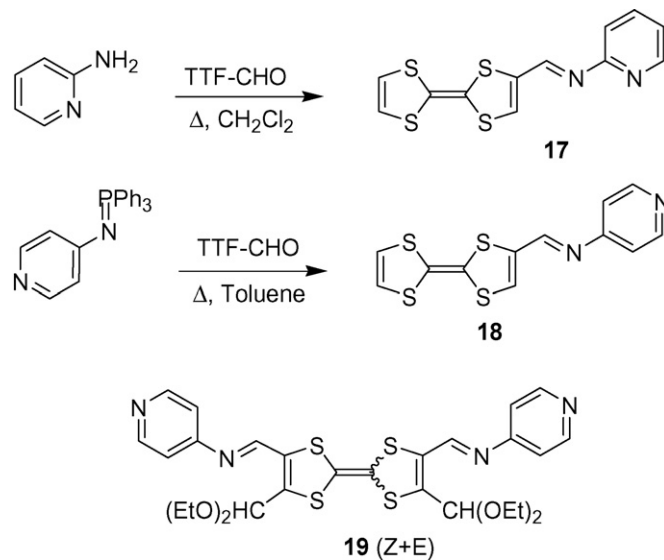


Scheme 4. Structure of TTF-pyridine ligands.

spacer)-acceptor systems where the *N*-methylpyridinium moiety is the acceptor group. These salts were simply obtained by reacting TTF-CH=CH-pyridine molecules with a large excess of methyl iodide [19]. Langmuir-Blodgett monolayers of the amphiphilic TTF derivative **15** show second-order non-linear optical properties [20]. Mono- and bis(pyridylethenyl) TTF derivatives **14a** and **16** also exhibit remarkable sensing and coordinating properties of the Pb²⁺ cation. Upon coordination, the electron accepting ability of the pyridyl group is enhanced, which in turn causes a decrease in electron density in the TTF core, with a modification of the UV-vis absorption bands and the NMR proton resonances [21].



Scheme 5. Synthesis of the pyridylethenyl-TTF.



Scheme 6. Synthesis of the pyridylimino-TTF.

An imine bridge, rather than the ethylenic one, has also been used as a conjugated linker between TTF and pyridine. One further advantage of this imine bridge is the possibility for its nitrogen atom to also participate to metal coordination, affording for example in **17** (Scheme 6) a bidentate chelating ligand with the pyridyl group [23]. Two synthetic approaches have been described towards these electroactive ligands, either a Schiff base condensation of formyl-TTF with 2-aminopyridine [23], or an aza-Wittig reaction between formyl-TTF and an iminophosphorane [24]. The latter reaction was also carried out on 4,4'-diformyl-TTF, producing the disubstituted imine-pyridine derivative **19** as a mixture of two isomers (*Z* and *E*).

A comparison of the imino or ethenyl junctions, based on B3LYP/6-31G calculations performed on **14a** (R=H) and **18**, showed that they both exhibit the same efficiency in the conjugation of the delocalized system and that the electron accepting ability of the imine nitrogen atom lowers only slightly the HOMO and LUMO energies of **18** [24]. This was confirmed by the analysis of the redox potentials as the E_{ox} of the imino derivatives are slightly higher than those of their ethenyl analogues (Table 2) [23,24]. These imino pyridyl TTFs exhibit the same binding affinity and selectivity for Pb²⁺ as those observed for their analogues bearing an ethylenic or acetylenic (*vide infra*) spacer.

Indeed, a series of acetylenic TTF derivatives have been recently designed and synthesized by Wu et al. in order to investigate the electronic communication between the TTF and the pyridine

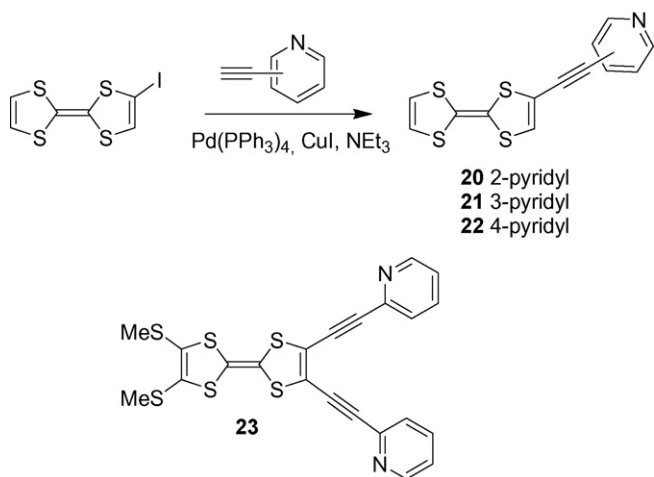
Table 2

Oxidation potential of TTF- π -spacer-pyridines **14–23** (in V, scanning rate 100 mV/s, using TBAPF₆ as supporting electrolyte and Pt working electrode).

Compound	E^1	E^2	Solvent	Reference
14a	0.44	0.80	CH ₃ CN vs. SCE	[19]
14b	0.40	–	PhCl vs. SCE	[22]
16	0.58	0.94	CH ₃ CN vs. SCE	[21]
17	0.49	0.88	CH ₃ CN vs. Ag/AgCl ^a	[23]
18	0.47	0.86	DCM/ACN vs. Ag/AgCl ^b	[24]
19	0.58	0.98	DCM/ACN vs. Ag/AgCl ^b	[24]
20	0.48	0.83	CH ₃ CN vs. SCE	[25]
21	0.46	0.82	CH ₃ CN vs. SCE	[25]
22	0.48	0.84	CH ₃ CN vs. SCE	[25]
23	0.15	0.43	CH ₂ Cl ₂ vs. Fc/Fc ⁺	[26]

^a Glassy carbon as the working electrode.

^b TBABF₄ as supporting electrolyte.



Scheme 7. Synthesis of pyridylethynyl-TTFs.

moiety upon Pb^{2+} coordination [25]. These pyridyl-C≡C-TTFs were synthesized according to a Sonogoshira coupling reaction between iodo-TTFs with ethynylpyridines to afford the 2-, 3- and 4-pyridylethynyl-TTF derivatives **20–22** (Scheme 7). Varying the spacer unit between the TTF and pyridine unit from a double bond to a triple bond leads to positive shifts for the first and second oxidation potentials of the TTF moieties. Also, the extent of intramolecular charge-transfer interactions through the triple bond is smaller than through the double bond [25].

Bis(2-pyridylethynyl)TTF **23** was prepared from the bis-iodo TTF following the same strategy, Sonogoshira coupling reaction of the dihalogenated TTF with an excess of ethynylpyridine in the presence of CuI , $\text{Pd}(\text{PPh}_3)_4$ and triethylamine (Scheme 7) [26]. Interestingly, the X-ray structure of **23** shows that the two pyridylethynyl units are almost coplanar with the C=C double bond of the TTF core (Fig. 1) while the two nitrogen atoms do not point toward each other, at variance with the structures observed in its copper salts (see Section 3.6.1).

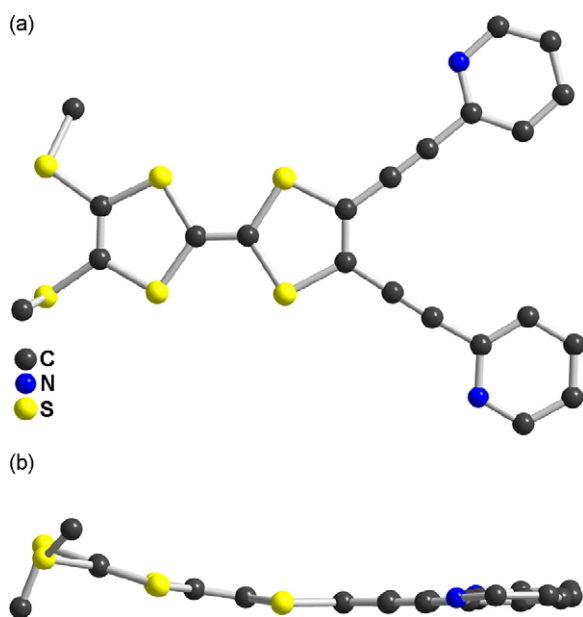
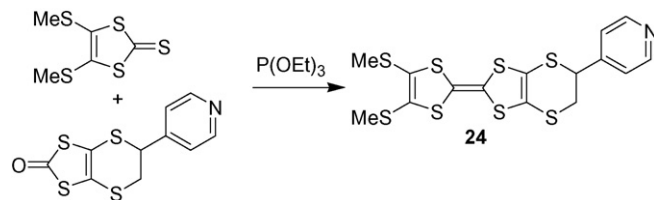


Fig. 1. Molecular structure of TTF **23** (a) showing the disposition of the pyridine substituents and (b) side view of the TTF [26].



Scheme 8. Cross-coupling reaction of dithioles affording pyridyl-EDT-TTF.

2.1.3. Spacer groups involving ethylenedithio junctions

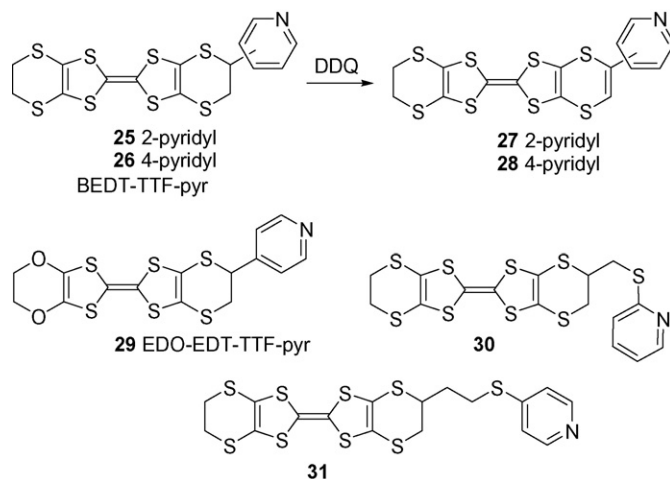
The pyridine substituent has also been covalently linked to the TTF core via non-conjugated spacer groups, as for example on the ethylenic bridge of EDT-TTF derivatives such as **24**. The chemical route used for these TTF derivatives is based on the cross coupling of 4,5-di(thioalkyl)-1,3-dithiole-2-thione and 4,5-(4-pyridyl)ethylenedithio-1,3-dithiole-2-one in the presence of trimethylphosphite (Scheme 8) [27].

An interesting aspect of this non-amphiphilic derivative **24**, besides its potential ligand behavior, lies in its ability to form stable Langmuir-Blodgett films with only 25% molar ratio of fatty acid. These films become semiconducting after iodine doping [28]. According to the same cross coupling reaction, either BEDT-TTF or EDO-EDT-TTF derivatives substituted by a pyridine have been prepared [29–31]. All these donor molecules **25–31** (Scheme 9), apart from achiral **27** and **28**, are obtained as racemic mixtures which were not separated. As expected, the TTF and the pyridine moieties in **29** are not coplanar, but exhibit a dihedral angle of $80.1(1)^\circ$ [31].

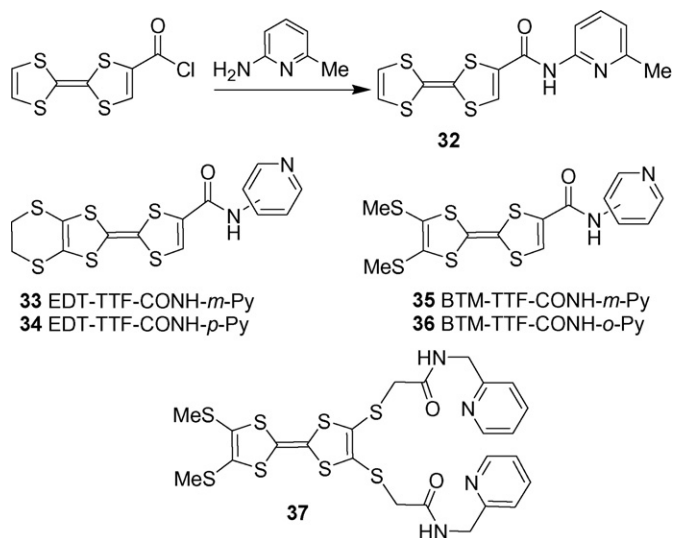
2.1.4. Spacer groups incorporating amide and ester functionalities

A series of amido pyridines have been prepared by reacting various TTF-acyl chlorides with *ortho*- [32], *meta*- and *para*-aminopyridine [33], in order to introduce an additional hydrogen bonding functionality on the molecule (Scheme 10).

For example, the setting of hydrogen bonds between **32** and complementary guests such as butanoic acid has been evidenced as well as the possibility of modulating the host-guest hydrogen bonding interactions in solution, in function of the redox state of the TTF [32]. Due to the hydrogen-bond donor/acceptor character of the amide and pyridine groups, specific hydrogen-bonded motifs are observed in the solid state, such as ribbons for the *meta* isomer EDT-TTF-CONH-*m*-py **33**, or infinite chains for the *para* isomer **34** (Fig. 2) [33]. The *ortho* derivative **36** exhibits a high selectivity for H_2PO_4^- over a wide range of anions [34] through



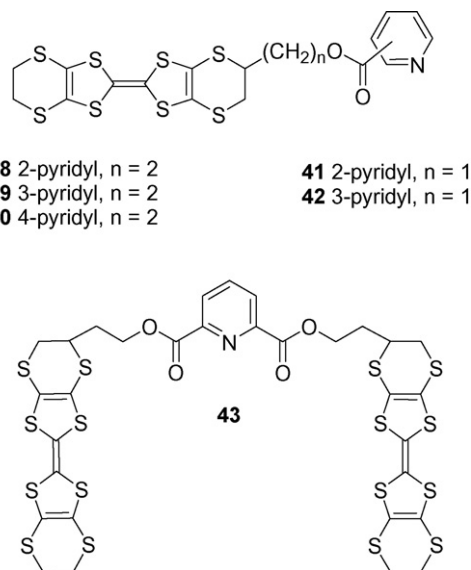
Scheme 9. Pyridyl-EDT-TTF.



Scheme 10. Amide as anchoring group between TTF and pyridine.

hydrogen bonding interactions. A bis(amidomethylpyridyl)-TTF (**37**) incorporating also the amide and pyridyl coordinating units, but non-conjugated together, has recently been reported as a highly effective redox responsive receptor towards M^{2+} transition metal cations (Cd^{2+} , Ni^{2+} and Co^{2+}) (Scheme 10) [35].

Flexible links based on the ester functionality were also introduced in TTF pyridine derivatives upon reaction of various pyridine acyl chlorides with TTFs functionalized with an alcohol group, affording **38–43** in good yields (Scheme 11) [30,36]. The redox properties of these pyridine ligands incorporating amide or ester functionalities within the spacer group are summarized Table 3.



Scheme 11. Ester as anchoring group between TTF and pyridine.

2.1.5. Thiopicoline derivatives: *S,N* ligands

Alkylation of a thiolate or a dithiolate with a halomethylpyridine derivative is a very convenient and easy route for functionalizing the dithiole or the TTF core. This route was first used by Kilburn et al. in 1989 for the synthesis of a macrocycle containing one TTF and two pyridine units [37]. Addition of 2,6-bis(bromomethyl)pyridine to the disodium salt of the 1,3-dithiole-2-thione-4,5-dithiolate leads to the corresponding macrocycle in excellent yield which by intramolecular coupling in the presence of triethylphosphite afforded the macrocycle **44** (Scheme 12). As expected for this type of constrained macrocycle, the TTF core in **44** is highly distorted.

Alkylation of the thiolate group of preformed TTF cores in the presence of bis-electrophilic reagents allowed the formation of donors incorporating two TTF units. For instance, Zhu and coworkers, reacting EDT-TTF-thiolate with 2,6-bis(chloromethyl)pyridine isolated the dimeric TTF **45** (Scheme 13) [38]. Under the same

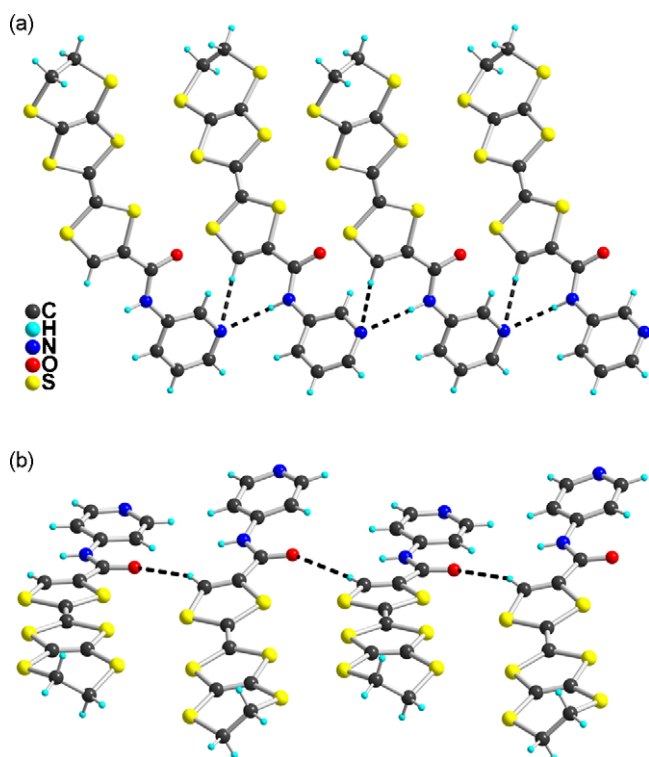


Fig. 2. View of the hydrogen-bonded motifs formed by (a) the *meta* isomer EDT-TTF-CONH-*m*-py **33** and (b) the *para* isomer **34** [33].

Table 3

Oxidation potential of TTF ligands **24–43** (in V, scanning rate 100 mV/s, using 0.1 M TBAPF₆ as supporting electrolyte and Pt as working electrode).

Compound	E^1	E^2	Solvent	Reference
24	0.45	0.80	CH ₂ Cl ₂ vs. Ag/AgCl ^a	[28]
25	0.45	0.87	CH ₂ Cl ₂ vs. SCE ^b	[29]
26	0.45	0.82	CH ₂ Cl ₂ vs. SCE ^b	[29]
27	0.48	0.89	CH ₂ Cl ₂ vs. SCE ^b	[29]
28	0.50	0.89	CH ₂ Cl ₂ vs. SCE ^b	[29]
29	0.52	0.83	PhCN vs. SCE ^{c,d}	[31]
30	0.48	0.89	CH ₂ Cl ₂ vs. Ag/AgCl	[30]
31	0.50	0.89	CH ₂ Cl ₂ vs. Ag/AgCl	[30]
32	0.57	irr.	CH ₂ Cl ₂ vs. Me ₅ Fc/Me ₅ Fc ⁺	[32]
33	0.66	0.90	THF vs. SCE ^e	[33]
34	0.67	0.92	THF vs. SCE ^e	[33]
35	0.74	0.94	THF vs. SCE ^e	[33]
37	0.59	0.87	DCM/ACN vs. Ag/AgCl	[35]
38	0.49	0.90	CH ₂ Cl ₂ vs. Ag/AgCl	[30]
39	0.50	0.90	CH ₂ Cl ₂ vs. Ag/AgCl	[30]
40	0.50	0.90	CH ₂ Cl ₂ vs. Ag/AgCl	[30]
43	0.43	0.50 ^f	CH ₂ Cl ₂ vs. Ag/AgCl	[30]

^a 0.2 M TBAPF₆ as supporting electrolyte.

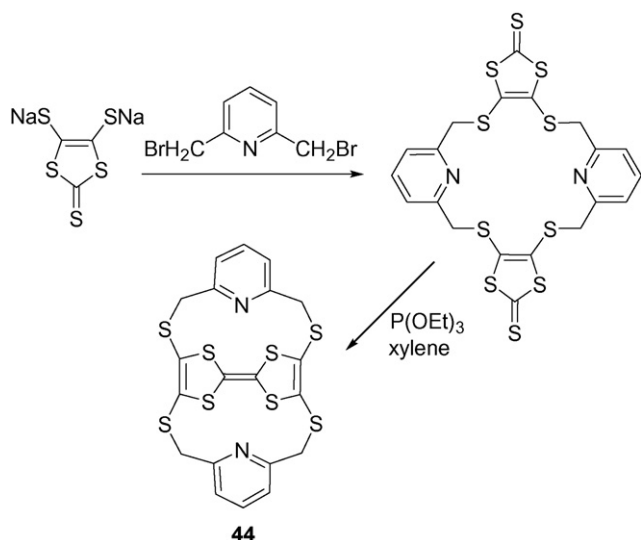
^b Scanning rate 50 mV/s.

^c TBABF₄ as supporting electrolyte.

^d Scanning rate 10 mV/s.

^e 0.05 M TBAPF₆ as supporting electrolyte.

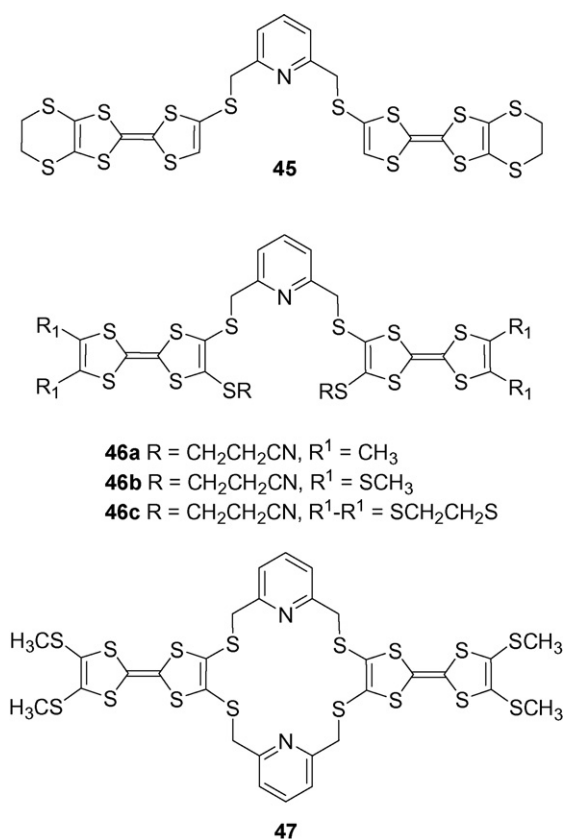
^f $E_{ox}^3 = 0.82$ V, irreversible process.



Scheme 12. Macrocycle containing one TTF unit and two pyridines.

conditions, Fabre et al. prepared a series of dimeric TTFs where the TTFs are either connected through one single spacer group **46a–c**, or with two pyridine units as spacer groups as in **47** (Scheme 13) [39].

All these dimeric TTFs (**45–47**) exhibit similar redox behavior upon cyclic voltammetry investigations (Table 4). Three distinct reversible oxidation waves were observed and the relative intensity of each wave suggests two successive one-electron redox processes followed by a two-electron reversible oxidation step [38,39]. The



Scheme 13. Dimeric TTF linked by a pyridine.

Table 4

Oxidation potentials of thiopicoline derivatives **44–47** (in V, using 0.1 M TBAPF₆ as supporting electrolyte, platinum electrode, scan rate 100 mV/s).

Compound	E ¹	E ²	E ³	Solvent	Reference
44	0.27	0.57		1,1,2-TCE vs. Ag/AgCl ^a	[37]
45	0.40	0.54	0.86	CH ₂ Cl ₂ vs. SCE	[38]
46a	0.504	0.580	0.952	CH ₂ Cl ₂ vs. SCE	[39]
46b	0.616	0.668	0.962	CH ₂ Cl ₂ vs. SCE	[39]
46c	0.604	0.696	0.995	CH ₂ Cl ₂ vs. SCE	[39]
47	0.506	0.672	0.934	CH ₂ Cl ₂ vs. SCE	[39]

^a 0.1 M TBAClO₄ as supporting electrolyte and scan rate 200 mV/s.

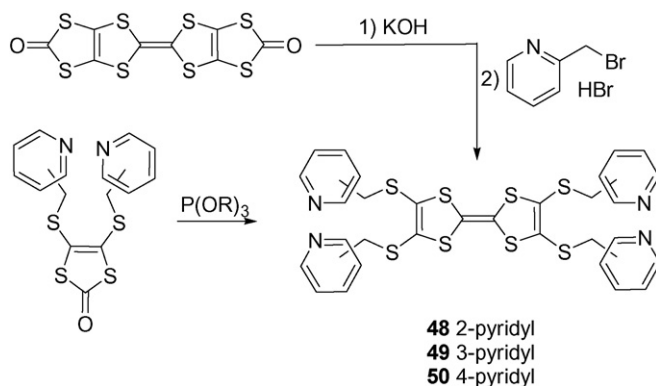
splitting of the first system into two monoelectronic waves was attributed, thanks to the flexibility of the space group, to the formation of a π -dimer stabilizing the formation of the radical cation species. Removal of the second electron to the bis-radical cation induces the opening out of the sandwich structure. Then, the two non-interacting cation radical species oxidize concomitantly into the bis dication [40].

Several mono-, bis- and tetrakis(pyridylmethylthio)-TTF have been described recently. Decurtins et al. reported a straightforward synthesis of tetrakis(2-pyridylmethylthio)TTF **48** based on the reactivity of the tetrathiole TTF, generated from the 2,2'-bis(1,3,4,6-tetrathiapentalen-5-one) with KOH, in the presence of 2-bromomethylpyridine hydrobromide (Scheme 14) [41]. The analogous tetrakis(3-pyridylmethylthio) and tetrakis(4-pyridylmethylthio)-TTF **49** and **50** have also been synthesized using a different approach which is based on the coupling of the already functionalized 1,3-dithiole-2-one, the corresponding 4,5-bis(pyridylmethylthio)-1,3-dithiole-2-one, in the presence of tri-isopropylphosphite (Scheme 14) [42].

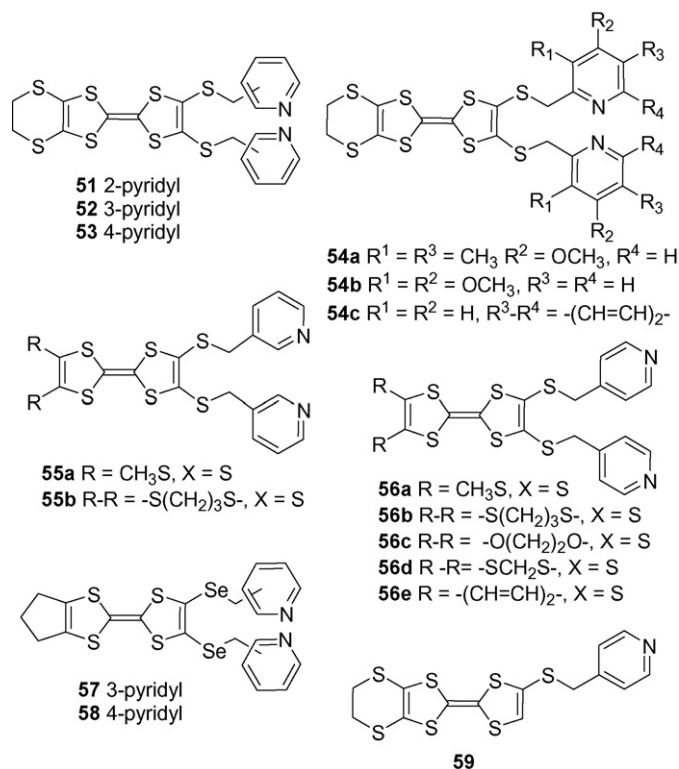
An extensive series of bis(pyridylmethylthio)-TTF derivatives **51–59** was prepared by two different routes (Scheme 15): (i) unsymmetrical phosphite coupling involving a pyridyl-functionalized 1,3-dithiole-2-one molecule or (ii) alkylation of a TTF dithiolate with the appropriate halomethylpyridine derivative [42–46]. It is worth noting that according to the second strategy and starting from bis(cyanoethylseleno)TTF derivatives, the corresponding TTFs **57** and **58** bearing two 3- or 4-pyridyl groups linked to the selenium atom have been synthesized [43]. It can be observed that, for all these derivatives, the substitution of the pyridine ring in either the *ortho*, *meta* or *para* position has no effect on the redox potential values (Table 5).

2.1.6. *N,N* chelating ligand: bipyridine

Compared to pyridine, bipyridine TTF derivatives have been scarcely studied although 2,2'-bipyridine is an interesting bidentate ligand widely used for chelating various metals. Bipyridine-TTF



Scheme 14. Syntheses of tetrakis(pyridylmethylthio)-TTF.



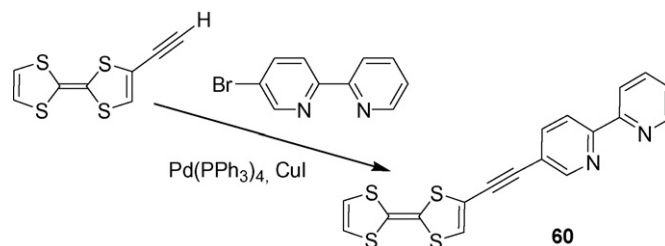
Scheme 15. Pyridylmethylthio-TTFs.

derivatives have been synthesized using the same synthetic approaches as the ones used for the pyridine-TTF derivatives. Depending on the type of reaction used, bipyridine can be linked, either directly to the donor core or through a conjugated or non-conjugated spacer group. For instance, Decurtins et al. chose the Sonogashira coupling reaction for connecting the bipyridine through an ethynyl spacer: the reaction of 2-ethynyl-TTF with 5-bromo-2,2'-bipyridine catalyzed by CuI and $\text{Pd}(\text{PPh}_3)_4$ afforded the ethynylbipyridine-linked mono (**60**) (Scheme 16) and bis-TTF (**61**) (Scheme 17) [47].

Pilkington et al. prepared, thanks to a Stille coupling reaction, the derivative **62** where the bipyridine is directly linked to the TTF unit (Scheme 17) [15]. The reaction of different TTF acyl chlorides with

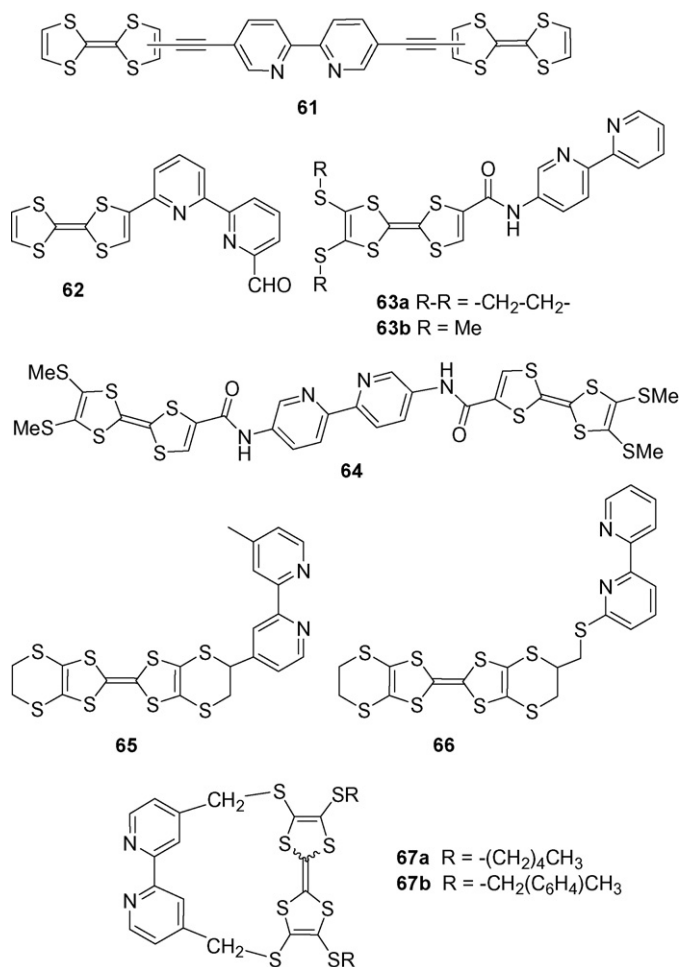
Table 5
Oxidation potentials of thiopicoline derivatives **49–58** (in V, using 0.1 M TBAPF₆ as supporting electrolyte, platinum as working electrode, scan rate 100 mV/s).

Compound	E^1	E^2	Solvent	Reference
49	0.49	0.86	CH_2Cl_2 vs. SCE	[42]
50	0.50	0.88	CH_2Cl_2 vs. SCE	[42]
51	0.58	0.97	CH_2Cl_2 vs. Ag/AgCl	[44]
52	0.54	0.90	CH_2Cl_2 vs. SCE	[42]
53	0.53	0.87	CH_2Cl_2 vs. SCE	[42]
54a	0.68	1.07	CH_2Cl_2 vs. Ag/AgCl	[45]
54b	0.60	0.91	CH_2Cl_2 vs. Ag/AgCl	[45]
54c	0.58	0.97	CH_2Cl_2 vs. Ag/AgCl	[45]
55a	0.54	0.89	CH_2Cl_2 vs. SCE	[42]
55b	0.61	0.98	CH_2Cl_2 vs. SCE	[43]
56a	0.52	0.88	CH_2Cl_2 vs. SCE	[42]
56b	0.61	0.98	CH_2Cl_2 vs. SCE	[43]
56c	0.80	1.05	CH_2Cl_2 vs. SCE	[43]
56d	0.80	1.05	CH_2Cl_2 vs. SCE	[43]
56e	0.64	1.00	CH_2Cl_2 vs. SCE	[43]
57	0.44	0.87	CH_2Cl_2 vs. SCE	[43]
58	0.44	0.87	CH_2Cl_2 vs. SCE	[43]



Scheme 16. Sonogashira coupling reaction of ethynyl-TTF.

5-amino-2,2'-bipyridine and 5,5'-diamino-2,2'-bipyridine allowed Avarvari and Batail to prepare the 5-amido-2,2'-bipyridine TTF derivatives **63a** and **63b** and the 5,5'-diamido-2,2'-bipyridine bis-TTF **64** [33]. 6-Vinyl-2,2'-bipyridine has also been used as precursor [48] of the ethylenedithio derivatized molecule **65**. Tetrathiafulvalene cyclophanes **67a** and **67b** incorporating bipyridine have been synthesized following the efficient deprotection/alkylation of TTF-bis(thiolate), starting from bis(cyanoethylthio)TTF derivatives and using 4,4'-bis(bromomethyl)-2,2'-bipyridine as alkylating agent [49]. The cyclophanes were obtained as a mixture of two *cis*- and *trans*-isomers of the TTF moiety. The electrochemical data of TTF ligands **60–67** are collected in Table 6, except for compound **61** due to its poor solubility. All of them show two reversible oxidation waves, even in the case of the bis-TTF **64**.



Scheme 17. TTF-bipyridine ligands.

Table 6

Oxidation potentials of TTF-bipyridine compounds **60–69** (in V, using 0.1 M TBAPF₆ as supporting electrolyte, platinum as working electrode, scan rate 100 mV/s).

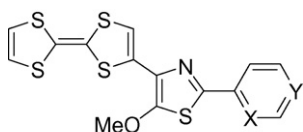
Compound	E^1	E^2	Solvent	Reference
60	0.32	0.67	DCM/ACN vs. SCE ^{a,b}	[47]
62	0.43	0.82	CH ₃ CN vs. Ag/AgCl ^c	[15]
63a	0.66	0.89	THF vs. SCE ^d	[33]
63b	0.73	0.93	THF vs. SCE ^d	[33]
64	0.75	0.95	DMF vs. SCE	[33]
65	0.55	0.95	CH ₂ Cl ₂ vs. SCE	[48]
66	0.49	0.90	CH ₂ Cl ₂ vs. Ag/AgCl	[30]
67a	0.64	1.03	CH ₃ CN vs. SCE	[49]
67b	0.63	1.01	CH ₃ CN vs. SCE	[49]

^a $E_{\text{red}} = -1.15$ V.

^b Scanning rate 1 mV/s.

^c Glassy carbon as working electrode.

^d 0.05 M TBAPF₆ as supporting electrolyte.



68 X = N, Y = CH
69 X = CH, Y = N

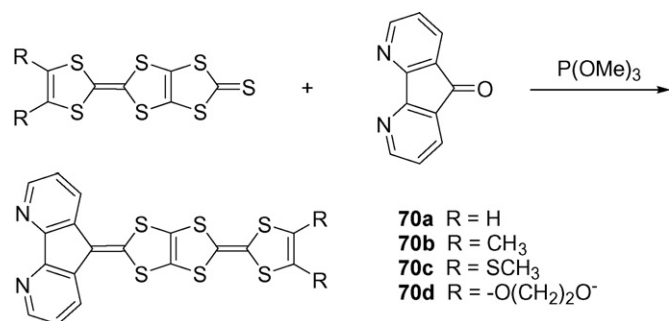
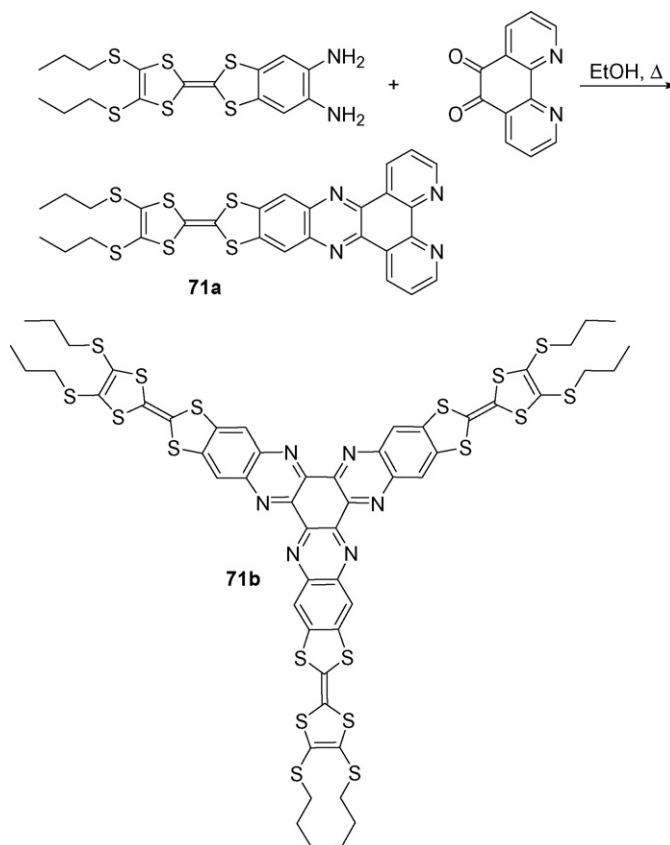
Scheme 18.

2.1.7. Other *N,N* chelating ligands

TTFs **68** and **69** (Scheme 18) linked to a 1,3-thiazol-2-yl-pyridine and prepared *via* the Stille coupling reaction, could be considered as potential ligands, even if they were essentially investigated for their fluorescent properties [50].

The diazafluorene moiety has shown a powerful chelating ability with various transition metals and has been also incorporated on a TTF backbone. Indeed, the synthesis of TTFs **70a–d** was carried out using a trimethylphosphite cross-coupling reaction of 4,5-diazafluoren-9-one with a 1,3-dithiole-2-thione fused to a TTF core (Scheme 19) [51].

Another synthetic approach was used to prepare the TTF-fused dipyrindophenazine **71a** (Scheme 20), obtained through the direct condensation of 1,10-phenanthroline-5,6-dione with a TTF diamine precursor in 65% yield. One can notice the electron withdrawing effect of the dipyrindophenazine moiety as the oxidation potentials of **71a** amount to $E_{1/2}^1 = 0.73$ V and $E_{1/2}^2 = 1.08$ V (vs. Ag/AgCl) [52a]. It should be mentioned also the formation of a redox active tri-star molecule **71b** as a potential ligand merging TTF and hexa-azatriphenylene (HAT) chemistry by simply using the same TTF diamine precursor in the presence of hexaketocyclohexane octahydrate [52b].

**Scheme 19.** Synthesis of diazafluorene-functionalized TTFs.**Scheme 20.** Synthesis of TTF-fused dipyrindophenazine **71a** and the tri-star molecule **71b**.

Tetrathiafulvalene-phenanthroline macrocycles (Scheme 21) have been reported as precursors of catenates. These macrocycles were prepared from the reaction of a bis(tosylated)TTF with 2,9-diphenol-1,10-phenanthroline (dpp) in high dilution conditions using Cs₂CO₃ as a base, affording **72** in 13% yield [53]. In a similar fashion, TTF-phenanthroline macrocycles **73a** and **73b** were prepared starting from the appropriate functionalized TTF and used as sensor unit [54]. Oxidation potentials of these donor molecules are reported in Table 7.

Finally, the only terpyridine TTF derivative **74** described so far, is prepared as outlined below (Scheme 22) [36].

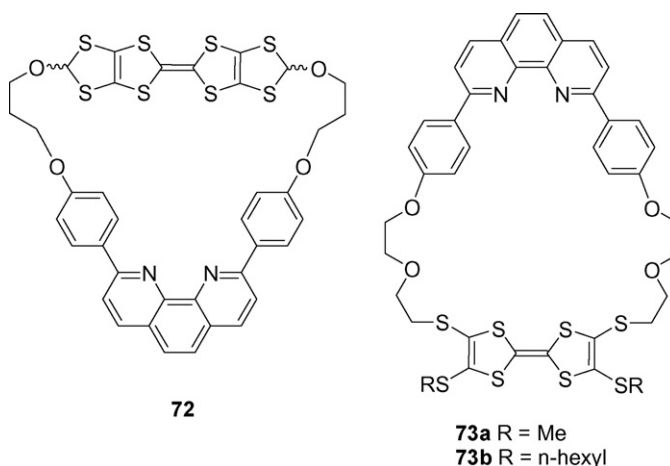
**Scheme 21.** Electroactive macrocycles containing a TTF core and a dpp unit.

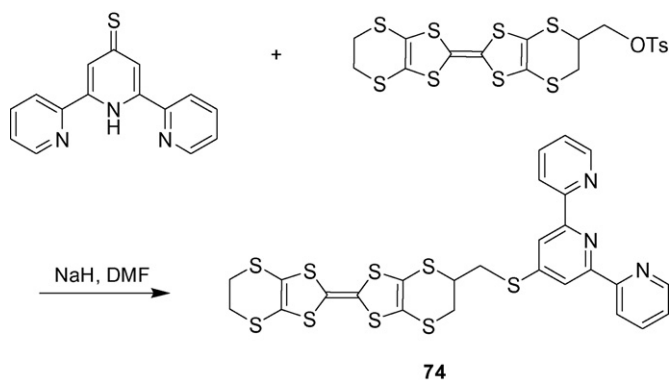
Table 7

Oxidation potentials of the *N,N*-chelating TTF ligands **68–73** (in V, using 0.1 M TBAPF₆ and platinum electrode, scan rate 100 mV/s).

Compound	E^1	E^2	E^3	Solvent	Reference
68	0.31	0.89		CH ₂ Cl ₂ vs. Ag/AgCl	[50]
69	0.39	0.89		CH ₂ Cl ₂ vs. Ag/AgCl	[50]
70a	0.07	0.42	1.32 irr.	PhCN vs. Fc/Fc ⁺ a	[51]
70b	0.05	0.37	1.27 irr.	PhCN vs. Fc/Fc ⁺ a	[51]
70c	0.17	0.38	1.32 irr.	PhCN vs. Fc/Fc ⁺ a	[51]
70d	0.08	0.36	1.31 irr.	PhCN vs. Fc/Fc ⁺ a	[51]
71a	0.73	1.08 irr. ^b		CH ₂ Cl ₂ vs. Ag/AgCl	[52]
73a	0.49	0.75		CH ₂ Cl ₂ vs. Ag/AgCl	[54]
73b	0.53	0.78		CH ₂ Cl ₂ vs. Ag/AgCl	[54]

^a 0.1 M TBAClO₄ as supporting electrolyte.

^b $E_{red}^{1/2} = -1.17$ V.

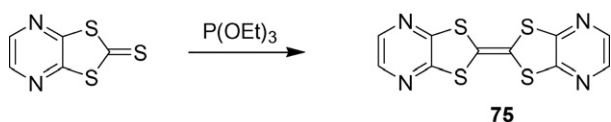
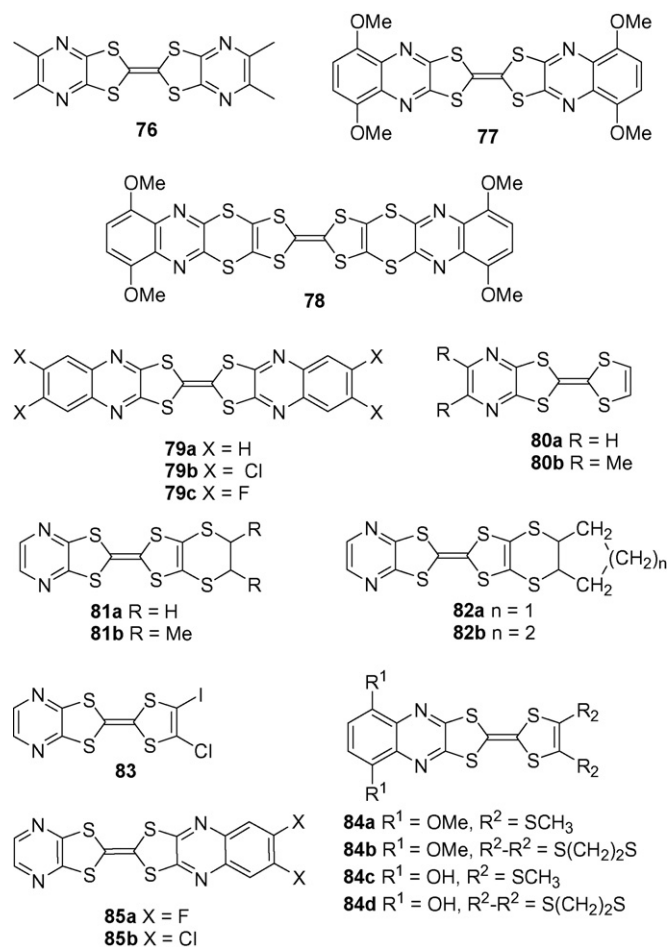
**Scheme 22.**

2.1.8. Pyrazines

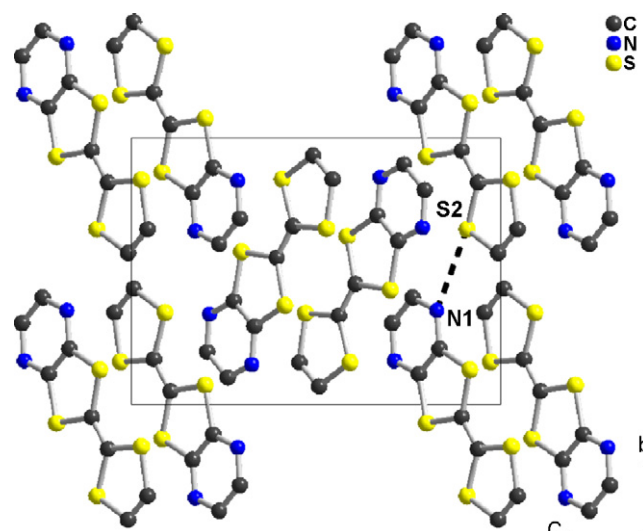
The first pyrazino-fused TTF **75** was prepared by Papavassiliou et al. in 1985, thanks to the triethylphosphite self-coupling reaction of a pyrazinotrithiocarbonate, itself prepared from dichloropyrazine (Scheme 23) [55]. At that time, the goal of this work was to increase dimensionality within charge transfer salts, thanks to the presence of the lone pair on the nitrogen atoms, by analogy with those of the outer sulfur atoms in BEDT-TTF [1a].

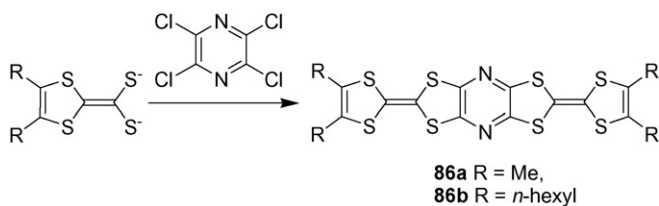
Following this work, several symmetrical (**76–79**), or unsymmetrical (**80–85**) TTFs bearing one or two fused pyrazine rings have been prepared by trialkyl phosphite cross-coupling reactions of the appropriate pyrazino-1,3-dithiole-2-one or 2-thione (Scheme 24) [56–61]. Selenium analogues have also been prepared according to this strategy [62].

In the solid state (Fig. 3), the simplest derivative **80a** was shown to crystallize into inversion-centered head-to-tail dyads with short inter-heteroatom contacts (N1...S2: 3.10(1) Å) [63], illustrating the original ideas developed by Papavassiliou et al. [55], albeit the dipyrazino-TTF derivative **75** does not exhibit such short intermolecular distances [64]. It is worth mentioning here an extensive series of such TTFs incorporating halogenated quinoxaline rings, which were investigated as semiconductors in field effect transistor (FET) devices, since these derivatives show excellent n- or p-type performances with high carrier mobility due to the presence of the halogen groups [65].

**Scheme 23.** Bis-pyrazino-fused TTF.**Scheme 24.** Pyrazino-fused TTFs.

Pyrazino-fused TTF dimers **86a** and **86b** have been prepared through the nucleophilic substitution of tetrachloropyrazine by the dilithium salts of (4,5-dialkyl-1,3-dithiole-2-ylidene)methane dithiolate (Scheme 25) [66]. Interestingly, these fused pyrazino bis-TTF derivatives, when soluble, exhibit four reversible sequential

**Fig. 3.** Projection view of the unit cell of **80a** showing the short S...N inter-heteroatom contact (dotted line) [63].



Scheme 25.

Table 8

Oxidation potentials of TTF-pyrazine ligands **75–88** (in V, using 0.1 M TBAPF₆ and platinum electrode, scan rate 100 mV/s).

Compound	E^1	E^2	Solvent	Reference
75	0.89	1.17	CH ₃ CN vs. SCE ^a	[62a]
76	0.99	1.28	CH ₃ CN vs. SCE ^a	[62a]
77	1.30 irr.	–	PhCN vs. SCE	[61]
78	1.09 irr.	–	CH ₂ Cl ₂ vs. SCE	[61]
79a	1.15	–	PhCN vs. SCE	[64]
80a	0.68	–	–	[71]
82a	0.74	1.05	PhCN vs. SCE	[62b]
82b	0.72	1.03	PhCN vs. SCE	[62b]
83	0.45	0.73 irr.	PhCN vs. Fc/Fc ⁺ ^b	[60]
84a	0.75	1.13	CH ₂ Cl ₂ vs. SCE	[61]
84b	0.72	1.17 irr.	CH ₂ Cl ₂ vs. SCE	[61]
84c	0.79	1.14 ^c	CH ₂ Cl ₂ vs. SCE	[61]
84d	0.79	1.08 ^d	CH ₂ Cl ₂ vs. SCE	[61]
86b	0.49	0.71 ^e	CH ₂ Cl ₂ vs. SCE	[69]
88a	0.56	0.90	CH ₂ Cl ₂ vs. Ag/AgCl	[44]
88b	0.69	0.97	CH ₂ Cl ₂ vs. Ag/AgCl	[70]

^a 0.1 M TEAClO₄, 50 mV/s.

^b Glassy carbon working electrode, 0.1 M TBABF₄.

^c $E_{ox}^3 = 1.23$ V.

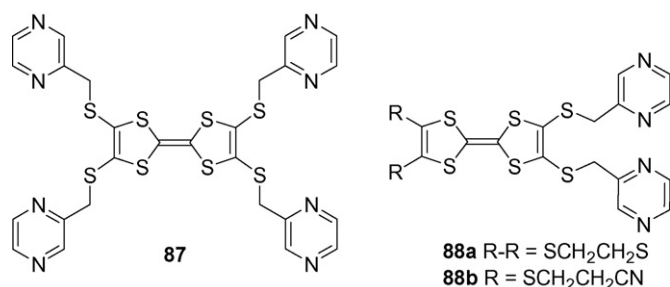
^d $E_{ox}^3 = 1.28$ V.

^e $E_{1/2}^3 = 1.24$ V and $E_{1/2}^4 = 1.50$ V.

oxidation steps (Table 8), as also observed in analogous benzo- [67] and diphosphino-fused [68] TTF dimers, indicating a strong interaction between the two redox centers through the planar, conjugated link. The cation radical species generated electrochemically exhibits an intense and broad band in the near-IR region which was assigned, thanks to theoretical calculations, to an intervalence transition [69].

More flexible structures involving one or several pyrazine groups as additional functionalities in **87** and **88** have been also grafted on the TTF core. For instance, Decurtins et al. prepared the tetrakis(pyrazylmethylthio)TTF **87** by alkylating TTF tetrathiolate with 2-chloropyrazine (Scheme 26) [41].

The corresponding unsymmetrical TTFs **88a** and **88b** have been also prepared by analogy with the corresponding pyridine derivatives (see Section 2.1.5) either by the coupling of the appropriate 1,3-dithiole-2-thiones and 1,3-dithiole-2-ones in the presence of



Scheme 26. Tetrakis and bis(pyrazylmethylthio)TTF.

Table 9

Oxidation potentials of TTF oxazolines and imidazoles (in V, using 0.1 M TBAPF₆ and platinum electrode, scan rate 100 mV/s).

Compound	E^1	E^2	Solvent	Reference
89a	0.52	0.91	CH ₃ CN vs. Fc/Fc ⁺ ^a	[73]
90a	0.65	1.13	CH ₂ Cl ₂ vs. Ag/AgCl	[74]
91a	0.63	1.09	CH ₂ Cl ₂ vs. Ag/AgCl	[74]
94	–0.06	0.20	DMF vs. Fc/Fc ⁺	[79]
95	–0.11	0.15	DMF vs. Fc/Fc ⁺	[79]

^a 0.2 M TBAPF₆ as supporting electrolyte.

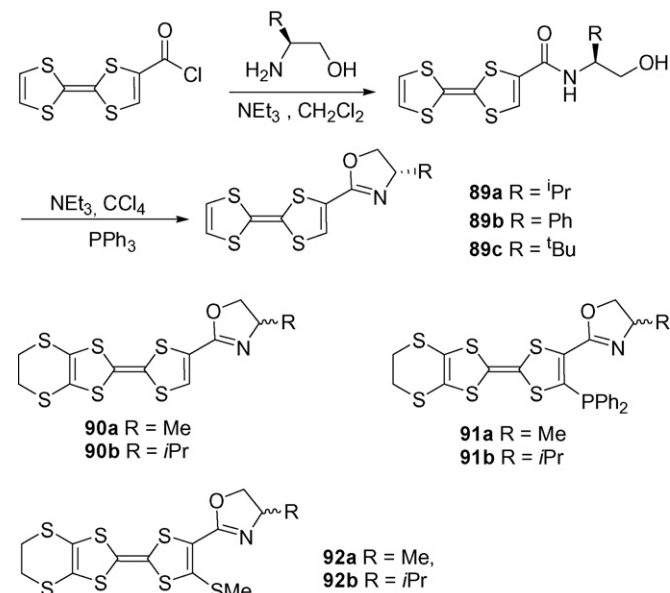
triethylphosphite [44] or through the functionalization of the pre-formed dithiolate TTF core [70].

The influence of the pyrazine group on the electron-donating ability of the TTF core has been analyzed electrochemically. Introduction of the fused pyrazine rings increases significantly the oxidation potentials. For instance, a potential difference of 670 mV is observed between the first oxidation potential of TTF ($E^1 = 0.35$ V vs. SCE in C₆H₅CN) with the one of bis-pyrazino-fused TTF **75** ($E^1 = 1.02$ V vs. SCE in C₆H₅CN) [64]. This strong anodic shift of the oxidation potential of the bis(pyrazino) and the pyrazino-fused TTFs allowed for the coordination of these derivatives with Cu²⁺ ions, as charge transfer could not occur [72]. On the other hand, pyrazine groups linked to the TTF core through a non-conjugated spacer group such as thiomethyl one, only weakly modify the electron donating ability of the donor core (Table 8).

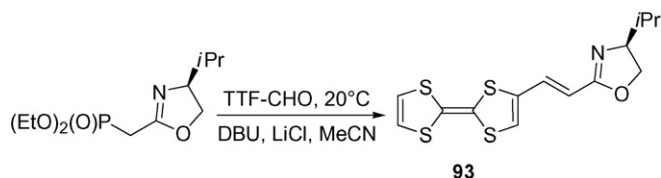
2.1.9. Oxazolines and imidazoles

Tetrathiafulvalene-substituted oxazolines **89a–c** were first reported by Chesney and Bryce [73]. These chiral ligands were easily obtained in their enantiopure forms from the commercially available homochiral amino-alcohols upon reaction with tetrathiafulvalene carbonyl chloride (Scheme 27). The resulting β -hydroxy amide was cyclized and dehydrated under Appel conditions (PPh₃, CCl₄ and NEt₃). These ligands were investigated as catalysts for asymmetric palladium-catalyzed allylic substitution reactions (see Section 5).

According to a similar synthetic pathway, Fourmigué and Avarvari have described the preparation of racemic and enantiopure EDT-TTF derivatives **90a** and **90b** (Scheme 27) [74,75]. Cyclization of



Scheme 27. TTF oxazoline derivatives.



Scheme 28.

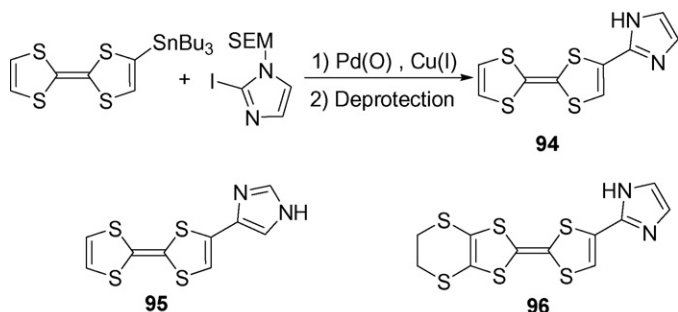
the intermediate β -hydroxy amide was performed in the presence of methanesulfonyl chloride. EDT-TTF phosphino-oxazoline **91a** and **91b** have been synthesized by lithiation of EDT-TTF oxazoline **90a** and **90b**, followed by reaction with chlorodiphenylphosphine [74,75]. While the methyl-oxazoline TTF derivatives **90a** were investigated as chiral conducting cation radical salts [76], the diphenylphosphino isopropylloxazoline TTFs **91b** was used as catalyst precursor in asymmetric allylic substitution and asymmetric imine hydrogenation reactions (see Section 5). For the EDT-TTF oxazoline **92** bearing a thiomethyl rather than a $-PPh_2$ substituent α to the oxazoline ring, single crystal X-ray diffraction analyses revealed the setting of intramolecular $O \cdots S$ non-bonded interactions characterized by short $S \cdots O$ distances and linear $O \cdots SMe$ motifs [77].

A π -extended tetrathiafulvenyl oxazoline **93** with a rigid conjugated spacer unit between the TTF and the chiral oxazoline was also described by Bryce in his first paper, from the reaction of formyl-TTF with an *in-situ* generated Wittig–Horner reagent (Scheme 28) [73]. This compound showed no ability to catalyze the allylic substitution reaction.

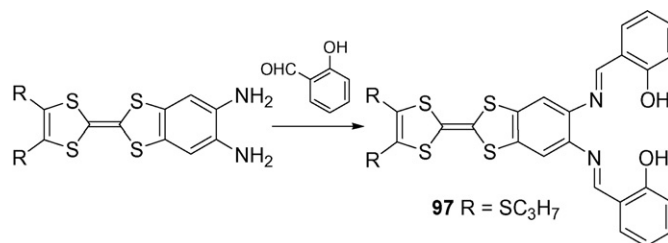
TTF derivatives having imidazole moieties have been investigated by Saito and Morita as interesting building blocks for H-bonded charge transfer complexes and assembled metal complexes [78]. TTFs **94** and **95** were prepared according to the Stille coupling reaction of TTF– $SnBu_3$ with N-protected 2- and 4-iodoimidazole using Pd(0) and Cu(I) catalysts followed by deprotection reaction of the imidazole core (Scheme 29, Table 9) [79]. EDT-TTF **96** was prepared according to a similar strategy [80].

2.1.10. Miscellaneous

Tetradentate tetrathiafulvalene-fused salphen complexes might generate simple models for biologically metalloproteins and metalloenzymes. Accordingly, a TTF-salphen ligand **97** was synthesized via the condensation reaction of salicylaldehyde with a TTF diamine precursor (Scheme 30). Deprotonation of the phenol functions of TTF **97** provides a tetradentate N_2O_2 coordination sphere for metal ions [81]. TTF-salphen ligand **97** undergoes two well-separated quasi reversible one-electron oxidation processes at $E_{1/2}^1 = 0.60$ V and in CH_2Cl_2 vs. Ag/AgCl.



Scheme 29. TTF imidazole derivatives.



Scheme 30. Synthesis of TTF-fused Schiff-base ligand.

2.2. Tetrathiafulvalenyl phosphines

The synthetic strategy toward TTF derivatives bearing a phosphino substituent is exclusively based on the functionalization of preformed TTF derivatives, given the high reactivity of the phosphorus group in the presence of oxidizing or electrophilic reagents. Two main approaches have been used: either the lithiation of the TTF core followed by reaction with phosphorus halides, or the deprotection of (cyanoethylthio)TTF derivatives, followed by alkylation of the generated thiolate groups with haloalkyl chains bearing a phosphino substituent. Depending on the synthetic approach used, the phosphine group can be either directly linked to the donor core or linked through a non-conjugated flexible chain.

2.2.1. Phosphine directly linked to the donor core

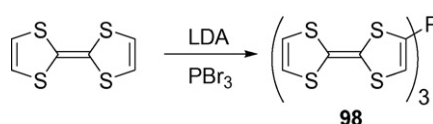
The first example of a tetrathiafulvalenyl phosphine was reported in 1991 by Fourmigué via the monolithiation of the unsubstituted TTF core followed by the reaction with PBr_3 (Scheme 31) [82], affording the tris(tetrathiafulvalenyl)phosphine **98a**.

Following this first report, a series of TTFs containing aryl- and alkylphosphines were prepared according to this chemical pathway, by varying the nature of the phosphorus halide, PPh_2Cl [83], PEt_2Cl [84], $PPhCl_2$ [85,86], $PEtCl_2$ [84] or PBr_3 [86] (Scheme 32), affording a variety of TTF-phosphines, bis(TTF)phosphines and tris(TTF)phosphines. Depending on the amount of base used in the lithiation step, it is possible to form the mono-, the bis-(4,4') and the tetrakis lithiated species [87]. Upon reaction with $ClPPh_2$, only the monosubstituted **100a**, and the tetrakisphosphino-TTF **103** were formed [88,89].

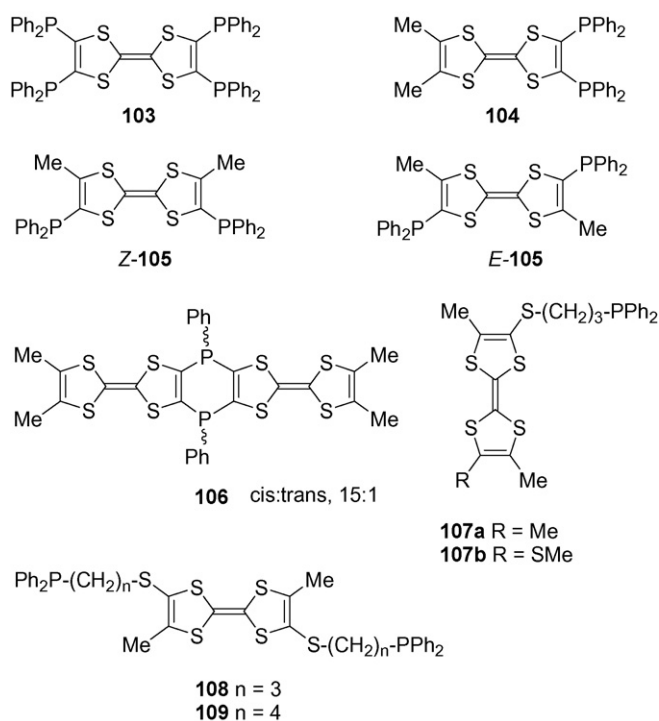
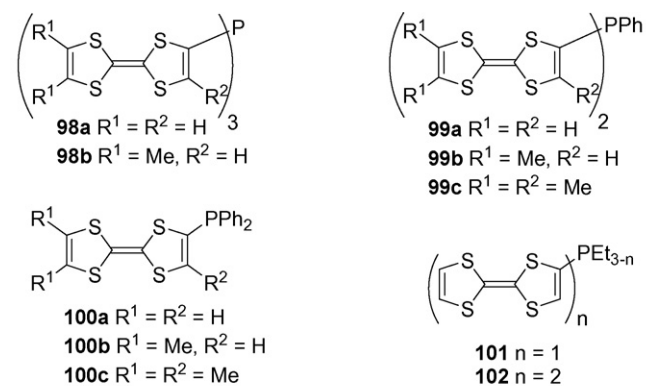
In that respect, the *ortho* chelating diphosphine **104** would be particularly appealing but cannot be prepared from TTF itself as the dilithiation affects the two dithiole rings. In order to prepare selectively an *ortho*-dilithiated TTF species through bimetalation, the unsymmetrically substituted 4,5-dimethyl-TTF has been used as starting material [83] to afford the chelating derivative **104** (Scheme 33). The dilithiated *o*-dimethyltetrathiafulvalene can also lead to **106**, a 1,4-dihydro-1,4-diphosphinine fused with two TTF cores, by using one equivalent of phenyl dichlorophosphine ($PhPCl_2$) as electrophile [68]. This TTF dimer is obtained as a *cis-trans* mixture in which the *cis* isomer is largely predominant.

2.2.2. Phosphine linked through a non-conjugated spacer group

The second approach towards phosphino-TTFs developed by Lorcy et al. is based on the deprotection of cyanoethylthio-TTF followed by the alkylation of the thiolate group with a (haloalkyl)(diphenyl)phosphine-borane reagent (Scheme 34).

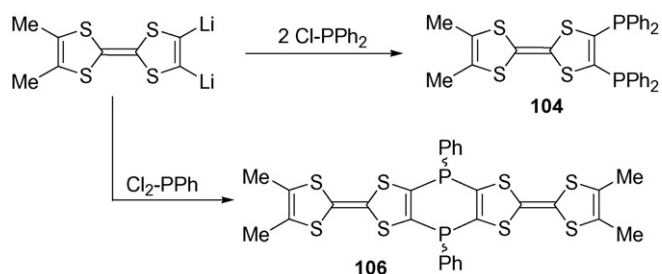
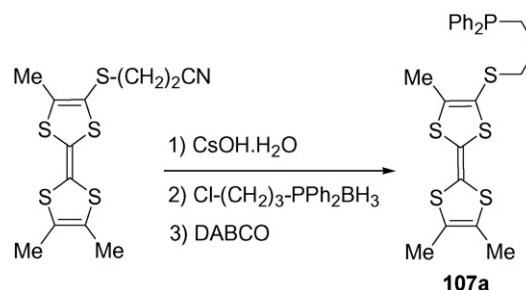


Scheme 31.



Scheme 32. TTF phosphines.

Phosphine borane complexes can be considered as excellent protecting groups of phosphines as these complexes are very stable in the presence of electrophiles or oxidizing agents. Moreover, the removal of the borane can be easily performed using soft conditions compatible with the TTF core. Mono- and bis-functionalized phosphino TTFs have been synthesized according to this strategy (Scheme 34) [90,91]. It consists first in the preparation of the haloalkyl(diphenyl)phosphine-borane reagent starting from a α -w-

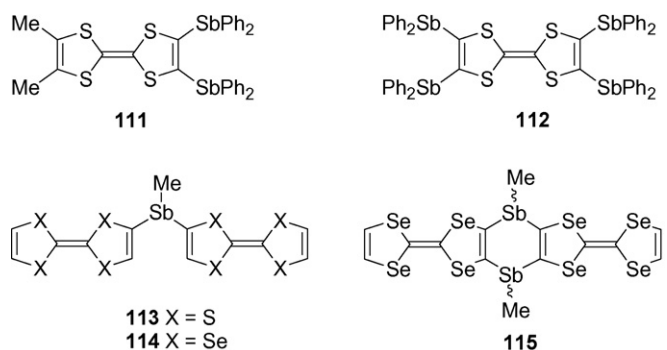
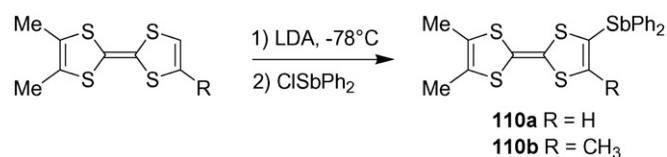
Scheme 33. *ortho*-Chelating diphosphino TTF.

Scheme 34.

dihalopropane or butane chain with one equivalent of the lithium salt of diphenylphosphine-borane $Ph_2P(Li)BH_3$. According to this approach, it is possible to insert between the coordinating function and the TTF core an aliphatic bridging chain of variable length [92]. Moreover, the presence in the same chain of sulfur and phosphorus atoms transforms these P-ligands **107–109** into potential (P,S) ligands.

2.2.3. Redox properties

All these phosphino-TTFs are electroactive ligands and exhibit, when analyzed by cyclic voltammetry, two reversible oxidation waves typical for TTF derivatives (Table 10). The presence of the phosphorus atom directly linked to the donor core induces an anodic shift of both redox processes, a shift more or less pronounced depending on the number of diphenylphosphino groups present on the TTF moiety (Table 10). Among all these TTFs, only one is reported to exhibit an irreversible reduction, presumably attributed to the reduction of the oxidized ethylphosphine substituent. Concerning the phosphines containing at least two TTF cores, sequential oxidation to the mono-, di-, tri-, and tetracations can be observed due to interactions between the redox moieties. Similarly, the *cis*-1,4-dihydro-1,4-diphosphinine-fused TTF **106** oxidizes in a four-electron process such as TTF dimers with fully conjugated bridges such as benzo- [67] or pyrazine rings [66]. This dimer, upon electrocrystallization experiment in the presence of Linquist anion $Mo_6O_{19}^{2-}$ leads to a salt where one TTF core is oxidized into cation radical but also the phosphine into the phosphine oxide [68].



Scheme 35.

Table 10Oxidation potentials of TTF-phosphines **98–109** (in V, scan rate 100 mV/s, using TBAPF₆) and ³¹P NMR chemical shifts.

Compound	E ¹	E ²	Solvent	δ (ppm)	Reference
98a	0.28	0.52	DMF vs. SCE	−33.6	[82]
98a	0.47	0.86	CH ₂ Cl ₂ vs. SCE	−33.6	[83]
98a	0.35/0.47/0.54	0.86	CH ₂ Cl ₂ vs. SCE	−33.6	[86]
98b	0.27/0.38/0.47	0.78	CH ₂ Cl ₂ vs. SCE	−33.06	[86]
99a	0.37/0.47	0.84	CH ₂ Cl ₂ vs. SCE	−22.9	[83]
99b	0.28/0.38	0.88	CH ₂ Cl ₂ vs. SCE	−23.2	[85]
99c	0.23/0.36	0.76/0.87	CH ₂ Cl ₂ vs. SCE	−40.2	[85]
100a	0.38	0.74	CH ₃ CN vs. SCE	−13.1	[83]
100b	0.32	0.70	CH ₂ Cl ₂ vs. SCE	−13.4	[86]
100c	0.23	0.74	CH ₂ Cl ₂ vs. SCE	−22.1	[88]
101^a	0.50	0.93	C ₆ H ₅ CN vs. Ag/AgCl	−	[84]
103	0.33	0.73	CH ₂ Cl ₂ vs. SCE	−18.2	[89]
104	0.34	0.71	CH ₃ CN vs. SCE	−18.8	[83]
104	0.27	0.81	CH ₂ Cl ₂ vs. SCE	−18.8	[89]
105Z	0.31	0.76	CH ₂ Cl ₂ vs. SCE	−18.3	[89]
105E	0.31	0.76	CH ₂ Cl ₂ vs. SCE	−18.3	[89]
<i>cis</i> - 106	0.43/0.55	0.93/1.05	CH ₂ Cl ₂ vs. Ag/AgCl	−21.5 ^b	[68]
107a	0.32	0.76	CH ₂ Cl ₂ vs. SCE	−16.4	[91]
107b	0.44	0.84 ^c	CH ₂ Cl ₂ vs. SCE	−16.4	[90]
108	0.46	0.83	CH ₂ Cl ₂ vs. SCE	−16.4	[92]
109	0.39	0.82 ^c	CH ₂ Cl ₂ vs. SCE	−16.7	[92]

^a E_{red} = −0.3 V.^b *trans*-**106** δ (ppm) = −25.6.^c Quasi irreversible process.

2.3. Tetrathiafulvalenyl stibines

Tetrathiafulvalenyl stibines (Scheme 35) have been first investigated by Fourmigué et al. [93] in order to generate stable cation radical salts. Indeed, it is known that Sb(III) derivatives are harder to oxidize to the Sb(V) stibine oxides than the corresponding phosphines derivatives. Mono **110a** and **110b**, bis-**111** and tetrastibine-TTF **112** were prepared by lithiation of the corresponding TTF core followed by the addition of the appropriate amount of ClSbPh₂. Due to the electron rich character of the diphenylstibino substituent, these derivatives are excellent candidates for electrocrystallization experiments as the first redox potential of the tetrastibine TTF **112** is 0.28 V (Table 11).

Dimeric TTF and tetraselenafulvalenes (TSFs) linked by a single or a double methylantimony bridge have been described recently by Ashikawa et al. [94]. Compound **113** was obtained from the reaction of the lithium derivative of TTF with 0.5 equivalent of MeSbI₂. Similarly, the treatment of bis(lithiated) TSF with one equivalent of MeSbI₂ afforded compound **115** as a *cis-trans* mixture together with compound **114**. Singly bridged **113** and **114** show three reversible oxidation waves (Table 11).

3. Complexes: synthesis and structure

3.1. The Cr, Mo, W triad (group 6)

While no chromium complexes containing TTF-pyridine or TTF-phosphine ligands have been reported so far, all the

Table 11Oxidation potentials of tetrathiafulvalenyl stibines **110–115** in V, using 0.1 M TBAPF₆ and platinum electrode, scan rate 100 mV/s).

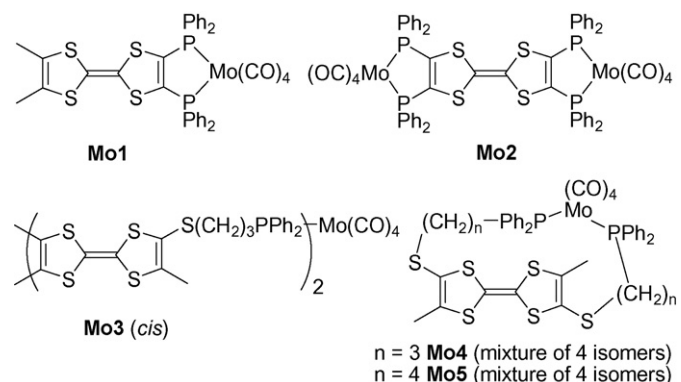
Compound	E ¹	E ²	E ³	Solvent	Reference
110a	0.35	0.90		CH ₂ Cl ₂ vs. Ag/AgCl	[93]
110b	0.34	0.87		CH ₂ Cl ₂ vs. Ag/AgCl	[93]
111	0.30	0.83		CH ₂ Cl ₂ vs. Ag/AgCl	[93]
112	0.28	0.76		CH ₂ Cl ₂ vs. Ag/AgCl	[93]
113	−0.11	0.01	0.40	PhCN vs. Ag/AgNO ₃ ^a	[94]
114	0.05	0.17	0.49	PhCN vs. Ag/AgNO ₃ ^a	[94]

^a Glassy carbon as working electrode.

molybdenum-based complexes known to date contain TTF-phosphines and the fragment Mo(CO)₄, with the metallic center in the 0 oxidation state. The common synthetic procedure involves the thermal displacement of both piperidine ligands from the precursor *cis*-Mo(CO)₄(piperidine)₂ upon moderate heating (50 or 80 °C) in toluene in the presence of the TTF-phosphine. The first complexes were described with the chelating bis(phosphine) *o*-DMTTF-(PPh₂)₂ (**104**) and the bis-chelating tetraphosphine TTF-(PPh₂)₄ (**103**), which provided the monometallic (**104**)[Mo(CO)₄] (**Mo1**) and bimetallic (**103**)[Mo(CO)₄]₂ (**Mo2**) derivatives (Scheme 36) [95].

The formation of the chelated complexes has been unambiguously proved by the massive downfield shift of Δδ = +71 ppm observed in ³¹P NMR with respect to the free ligands, a likely signature of the five member metallacycle. Later on [96], a single crystal X-ray analysis allowed the determination of the solid state structure of the complex **Mo1**, as well as that of the corresponding radical cation salt (see Section 4.2). As expected, the coordination environment around the metallic center is octahedral, with the two phosphorus atoms disposed in a *cis* conformation within the metallacycle, which is folded along the P...P axis by about 25° (Fig. 4).

As a general feature, in the TTF-phosphines metal-carbonyl complexes, the M–C bonds *trans* to the P-ligands are shorter by about 0.03–0.04 Å than the two remaining ones, as a consequence of the

**Scheme 36.** TTF-phosphines molybdenum complexes.

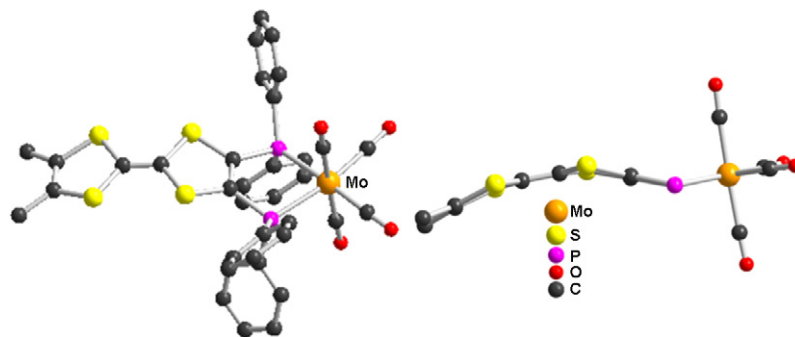


Fig. 4. X-ray structure of **Mo1** (left) with a side view (right, Ph groups omitted) of the molecule. H atoms have been omitted [96].

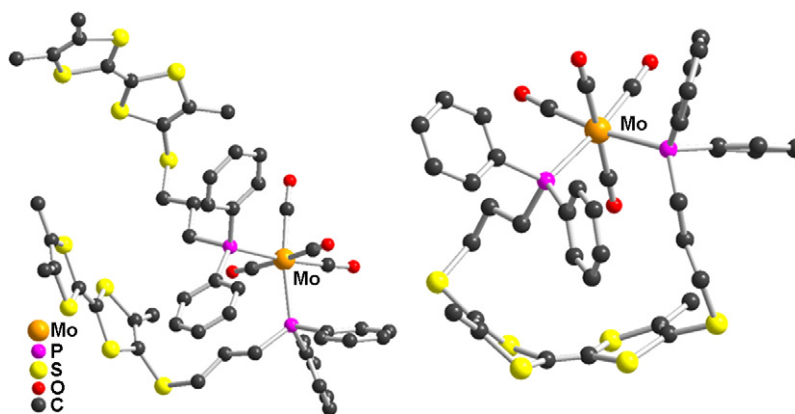


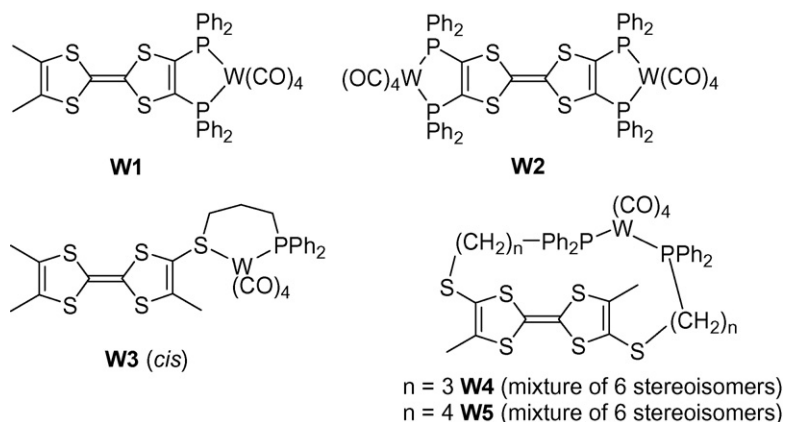
Fig. 5. X-ray structures of **Mo3** (left) [91] and of *trans* TTF/*cis* P-M-P **Mo4** (right) [92]. H atoms have been omitted.

stronger M to CO π -back retrodonation. Very likely, because of the steric hindrance provided by the $\text{Mo}(\text{CO})_4$ fragment and the phenyl rings, preventing the stacking of the TTF units, only formation of discrete centrosymmetric dyads, with the shortest intermolecular S...S distance of 3.62 Å, is observed. Cyclic voltammetry measurements show rather large anodic shifts for the first oxidation waves when compared to the free ligands, amounting to 200 mV for **Mo1** and 380 mV for **Mo2**.

The complex **Mo3** (Scheme 36) containing the long chain bridged TTF monophosphine $\text{Me}_3\text{TTF-S}(\text{CH}_2)_3\text{PPh}_2$ (**107a**) was synthesized through a similar synthetic procedure [91]. As in the previous cases, the formation of the expected complex was monitored by ^{31}P NMR spectroscopy, yet the downfield shift with respect to the ligand is now much weaker ($\Delta\delta = +43$ ppm). Its single crystal

X-ray structure proved the *cis* coordination of two phosphines on a $\text{Mo}(\text{CO})_4$ fragment (Fig. 5). Intermolecular S...S contacts slightly above 3.6 Å are observed between neighboring molecules forming centrosymmetric dimers, in which the TTF units are disposed perpendicularly each other.

Finally, the use of *cis/trans* mixtures of the bis(phosphines) **108** and **109** in reaction with the *cis*- $\text{Mo}(\text{CO})_4(\text{piperidine})_2$ precursor at higher temperature (80 °C) than precedently afforded the *ansa* type complexes **Mo4** and **Mo5** as mixtures of six stereoisomers, namely *cis* TTF/*trans* P-M-P, *cis* TTF/*cis* P-M-P, *trans* (R)TTF/*cis* P-M-P, *trans* (S)TTF/*cis* P-M-P, *trans* (R)TTF/*trans* P-M-P and *trans* (S)TTF/*trans* P-M-P, with an estimated ratio *trans* P-M-P/*cis* P-M-P of 5:2 from ^{31}P NMR spectra [92]. The rationale for the formation of *trans* P-M-P complexes, unlike the previous example, relies on



Scheme 37. TTF-phosphines $\text{W}(\text{CO})_4$ complexes.

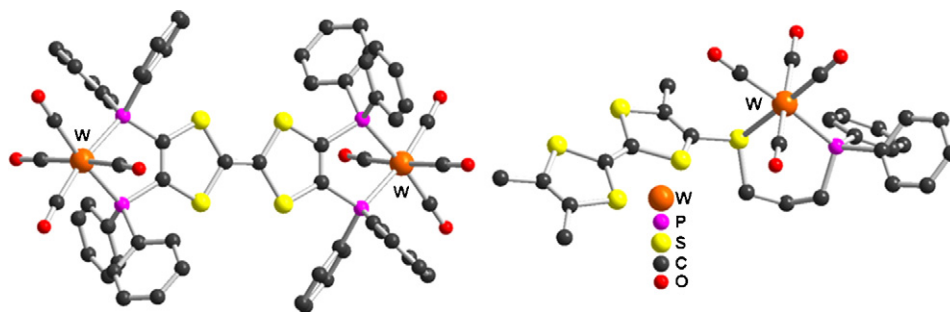


Fig. 6. X-ray structures of **W2** (left) [95] and of **W3** (right) [91]. H atoms have been omitted.

an isomerisation process favored by the higher temperature of the reaction. The structure of the racemic mixture *trans* (*R/S*)TTF/*cis* P-M-P **Mo4** could be determined by single crystal X-ray analysis (Fig. 5). Obviously, the formation of the 17-membered metallacycle is accompanied by a pronounced folding of both dithiole rings with angles about the S...S hinges of 19° and 36°. Within the series of complexes **Mo3–Mo5** the coordination of the electroactive phosphine(s) to the metallic fragment has no sizeable effect on the electrodonating properties of the TTF core, as ascertained by the same potential values for the ligands and the corresponding complexes, very likely because of the large separation between the TTF unit and the coordinating groups, unlike the case of **Mo1** and **Mo2**.

As in the case of molybdenum, all the TTF-containing tungsten complexes are based on TTF-phosphines. However, even though most of them involve coordination on a W(CO)₄ fragment, a couple of examples are known with the W₆S₈ cluster [84]. The complexes containing the W(CO)₄ unit (Scheme 37) have been synthesized by paralleling the preparation of the molybdenum analogues, upon thermal displacement of the piperidine ligands from the precursor *cis*-W(CO)₄(piperidine)₂.

Note however that the complex **W3** involved first the substitution of only one piperidine ligand, and then, upon chromatographic work up, the second piperidine was displaced by the sulfur atom of the bridge, thus providing a *cis* chelated (P,S) six-member metallacycle [91]. In the reaction conditions, formation of a bis(phosphino) complex, analogue of **Mo3**, was not observed. Once again, the monitoring of the complexation reactions by ³¹P NMR spectroscopy was very useful, with the mention that the downfield shifts are less important ($\Delta\delta = +54$ ppm for **W1** and **W2**) than in the case of molybdenum. The structure of the bimetallic complex **W2**, determined by X-ray analysis on single crystals, shows the expected octahedral coordination of the two W(CO)₄ fragments, with the metallic cen-

ters involved in the formation of five member metallacycles which are folded by about 17° along the P...P vectors (Fig. 6, left) [95]. Obviously, because of the huge steric hindrance around the TTF unit, no short S...S intermolecular interaction is observed.

Once again, as discussed in the case of their Mo counterparts, quite large anodic shifts of +220 mV are measured for the first oxidation processes to generate the radical cation species of **W1** and **W2**. This shift is only of +40 mV in the complex **W3**, despite the close vicinity between the organometallic fragment and the TTF unit. X-ray investigations on this complex revealed the *cis* chelating conformation of the (P,S) bridge (Fig. 6, right) [91]. Moreover, since the steric hindrance is much less pronounced than in **W2**, intermolecular S...S contacts as short as 3.75–3.88 Å are observed within TTF stacks.

The *ansa* type complexes **W4** and **W5** have been isolated as mixtures of the six possible stereoisomers (*trans* P-M-P/*cis* P-M-P 5:2, *vide supra*), yet, only the *cis* TTF/*trans* P-W-P one crystallized in both cases (Fig. 7) [92].

It is worth noting that the folding of the dithiole rings along the S...S hinges is larger in the *a priori* more strained 17-member metallacycle **W4** (17° and 28°) than in the 19-member metallacycle **W5** (9° and 11°). Cyclic voltammetry measurements indicate that the cyclization, upon formation of the metallacycles, does not induce any change in the electrodonating properties of the TTF core. Interestingly, both isomers afforded 2:1 neutral donor/acceptor crystalline complexes with the acceptor molecule tetracyanoquinodimethane (TCNQ), as deduced from structural parameters analyses, as well as from the absence of any EPR signal. This behavior is very likely due to the large difference between the oxidation potential of the complexes (0.41–0.45 V) and the reduction potential of TCNQ (0.18 V).

As mentioned earlier, the neutral electroactive cluster W₆S₈ has been also used to assemble 6 or 12 TTF units around it,

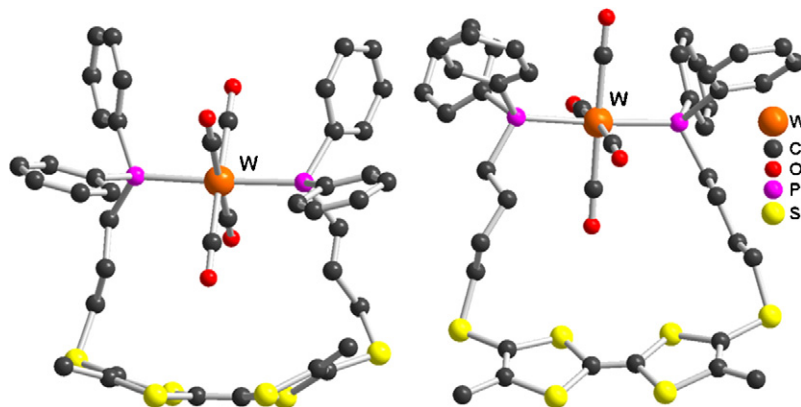
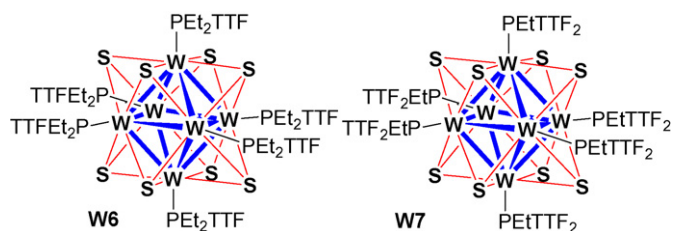
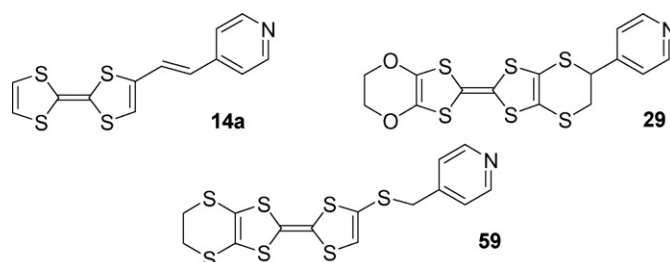


Fig. 7. X-ray structures of *cis* TTF/*trans* P-W-P **W4** (left) and of *cis* TTF/*trans* P-W-P **W5** (right) [92].



Scheme 38. W_6S_8 clusters with TTF-phosphines.



Scheme 39. TTF-pyridines involved in Mn complexes.

in a nearly isotropic fashion, with the aim to deliver electron active three-dimensional systems. The synthesis of $W_6S_8(\mathbf{101})_6$ (**W6**) and $W_6S_8(\mathbf{102})_6$ (**W7**) clusters has been performed by the thermal displacement of the 4-*t*-butylpyridine (4-*tbp*) ligands from the precursor $W_6S_8(4\text{-}tbp)_6$ by the TTF phosphines PEt_2TTF (**101**) and $PEtTTF_2$ (**102**), respectively (Scheme 38) [84].

The structures of both clusters have been proved by single crystal X-ray analyses. Three polymorphs could be crystallized for the cluster **W6**, one of them belonging to the hexagonal system (Fig. 8). In this one, the cluster is located on 3-fold inversion axes, leading to equivalent environments for each of the six TTFs.

However, the shortest intermolecular TTF...TTF contacts of 3.37 Å have been noticed in the case of another polymorph of **W6**, crystallized in the triclinic system. Cyclic voltammetry measurements demonstrate undoubtedly the concomitant reversible oxidation of the TTF units in radical cations, and then dications, at practically the same potential as in the free ligand. The oxidation of the cluster core seems to occur together with that of the TTFs in the corresponding radical cations, while the one electron reduction process, typical for this type of cluster, could be evidenced. Unfortunately, only polycrystalline powders were obtained upon chemical oxidation of **W6**, for which conductivity measurements show semiconducting behavior. The number of TTF units around the W_6S_8 cluster core is 12 in the compound **W7**, as it was demonstrated by a structural analysis (Fig. 8, right). They form an almost isotropic electroactive building block. Moreover, short TTF...TTF separations of 3.50 Å are observed in two perpendicular planes. It appears though that the lack of solubility of **W7** hampered so far its engagement into oxidized conducting materials. However, it is clear that the use of molecular forms of metallic clusters as templates for the assembling of several TTF units holds much promise for the straightforward access towards multidimensional precursors (see also the rhenium section).

3.2. The Mn, Tc, Re triad (group 7)

The very few manganese complexes described to date are based on TTF-pyridines and they were obviously synthesized within the general frame of the multifunctional materials in order to associate in the same material, localized d electrons on the Mn(II) centers (spin $S = 5/2$) with delocalized π electrons in the radical cation salts. The first couple of examples, described by Ouahab et al., involved the bis-coordination of the $Mn(hfac)_2$ fragment with the ligands *trans*-1,2-TTF-(4'-Py)-ethene (**14a**) and EDO-EDT-TTF-(4'-Py) (**29**) (Scheme 39) in *cis* and *trans*, respectively.

The complexes *cis*- $Mn(hfac)_2(\mathbf{14a})_2$ (**Mn1**) and *trans*- $Mn(hfac)_2(\mathbf{29})_2$ (**Mn2**) have been conventionally synthesized upon reaction of the precursor $Mn(hfac)_2 \cdot 3H_2O$ with roughly stoichiometric amounts of the ligands. In the case of **Mn1** the quality of the crystals was sufficient to determine solely the *cis* arrangement of the TTF ligands by X-ray analysis. The magnetic susceptibility of the complex as a function of temperature follows a Curie law, in agreement with the existence of isolated paramagnetic centers of spin $S = 5/2$ [97]. In the complex **Mn2**, for which the solid state structure was determined accurately, the two ligands **29**, disposed in *trans* around the $Mn(hfac)_2$ fragment, are crystallographically equivalent as they correspond each other through the inversion center located on the metal (Fig. 9).

A set of short intermolecular S...S contacts, within TTF layers possessing a β -type packing, has been identified, yet, the comparison of the bond lengths of the free and coordinated ligands proves that TTFs are at neutral state. Although this type of arrangement is encouraging for the preparation of radical cation salts, conductivity measurements demonstrate an insulator character for **Mn2**. Moreover, temperature dependence of the magnetic susceptibility follows a Curie-Weiss law, with $\theta = -1.8$ K. The weak antiferromagnetic interactions occurring at low temperatures are a likely consequence of the long-range separation of 7.1 Å between the paramagnetic metallic centers.

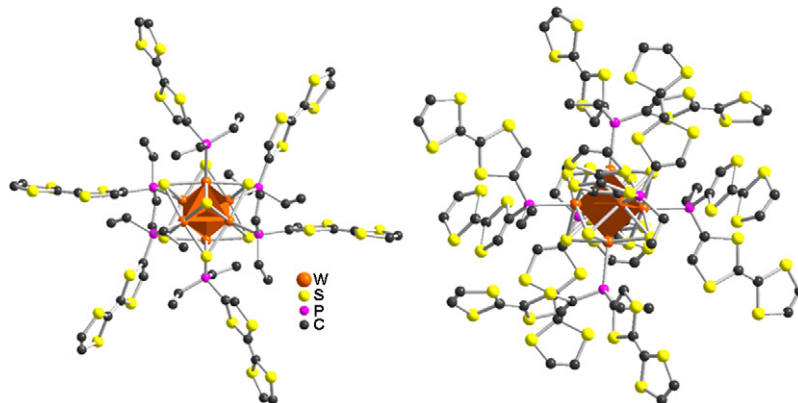


Fig. 8. X-ray structures of the electroactive clusters **W6** (left) and **W7** (right) [84].

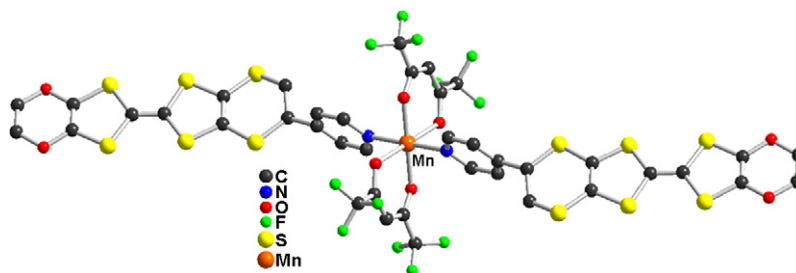


Fig. 9. Solid state structure of the complex $trans\text{-Mn}(\text{hfac})_2(\mathbf{29})$ (**Mn2**) [97].

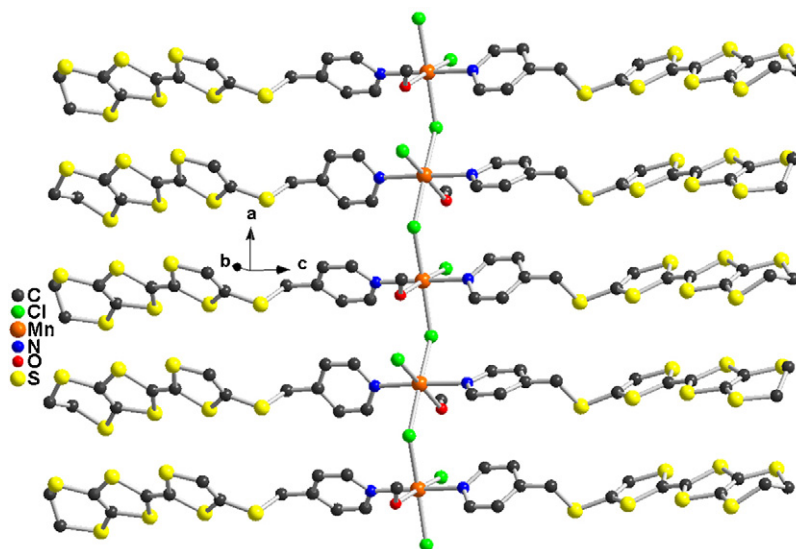
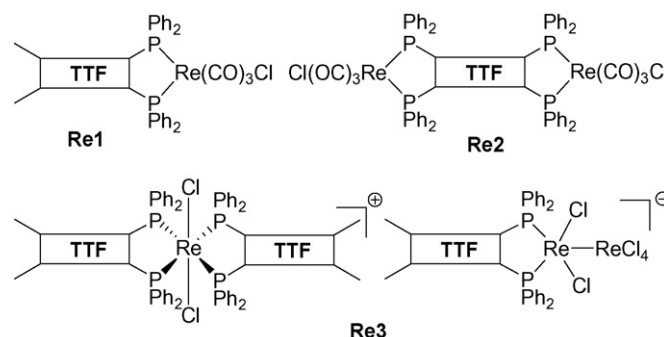


Fig. 10. Formation of polymeric chains in the structure of $[\text{Mn}(\mu\text{-Cl})\text{Cl}(\mathbf{59})_2(\text{MeOH})]_n$ (**Mn3**) [46].

A different strategy was adopted by Liu and Decurtins for the coordination of the ligand EDT-TTF-SCH₂(4'-Py) (**59**) on Mn(II) centers [46]. Slow diffusion of solutions of the ligand and of the precursor $\text{MnCl}_2 \cdot 4\text{H}_2\text{O}$ afforded crystals of the complex $[\text{Mn}(\mu\text{-Cl})\text{Cl}(\mathbf{59})_2(\text{MeOH})]_n$ (**Mn3**), for which the structural analysis revealed the polymeric nature (Fig. 10). Very interestingly, bridging μ_2 chloride ligands interconnect axially Mn(II) centers, thus leading to the formation of linear chains along the *a* direction. The metal centers present a distorted octahedral geometry, with two **59** ligands in *trans* each other, one MeOH and one terminal Cl⁻ ligands also in *trans*, completing the coordination sphere, besides the bridging chlorides. This peculiar arrangement is certainly encouraging in the perspective of oxidizing the donors, in order to have electron delocalization along the chains, since relatively short S...S intermolecular contacts of 3.89 Å are observed between consecutive TTF molecules. Moreover, even closer contacts between TTFs are established along the *b* direction, where polymeric chains alternate. A comparison between the structural parameters of the uncoordinated **59** ligand and the coordinated one demonstrates that the ligand is essentially at the neutral state in the complex **Mn3**. Mn...Mn distances within the chains, across the bridging chlorides, amount to 4.61 Å. It is thus not surprising that the magnetic measurements are consistent with an uniform antiferromagnetic chain behavior at low temperatures, with a coupling constant $J = -1.1 \text{ cm}^{-1}$.

Unlike the manganese complexes, all the rhenium complexes described so far contain only TTF-phosphines with the phosphino group directly attached to the TTF core. Those complexes based on the chelating ligands **104** and **103** (see above) are depicted in

Scheme 40. **Re1** and **Re2**, containing diamagnetic Re(I) centers, were synthesized upon thermal displacement of two CO ligands from the precursor $\text{Re}(\text{CO})_5\text{Cl}$ in the presence of the chelating phosphines **104** and **103** [95]. Although the complexation was ascertained through ³¹P NMR measurements, the *fac* stereochemistry was definitely determined by single crystal X-ray analysis. Indeed, the phosphines are *trans* to CO ligands in the equatorial plane, while the axial positions are occupied by the third CO and the chloride (Fig. 11). The 5-member metallacycle together with the adjacent dithiole ring are folded by 23–24°. In the case of **Re2**, the presence of two signals in the ³¹P NMR spectrum indicate the formation of two isomers in roughly equimolar ratio, very likely corresponding to *cis* and *trans* orientations of the two Cl ligands with respect to the TTF mean plane.



Scheme 40. TTF-phosphines Re complexes.

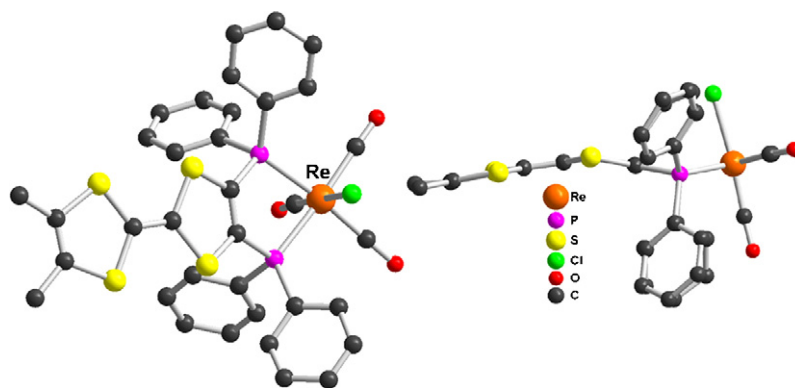


Fig. 11. X-ray structure of **Re1** (left) with a side view of the molecule (right) [95].

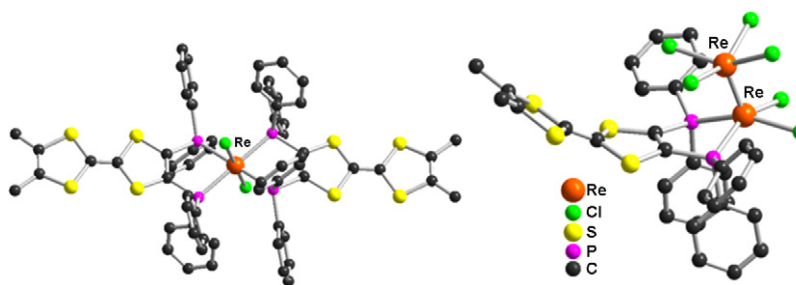


Fig. 12. Crystalline structure of the cation (left) and anion (right) of the complex salt **Re3** [98].

As for the Mo and W complexes with **104** and **103** (see Section 3.1), large anodic shifts, when compared to the uncoordinated ligands, are observed in cyclic voltammetry of both **Re1** and **Re2**, especially for the first oxidation processes, i.e. 0.25 V (**Re1**) and 0.49 V (**Re2**).

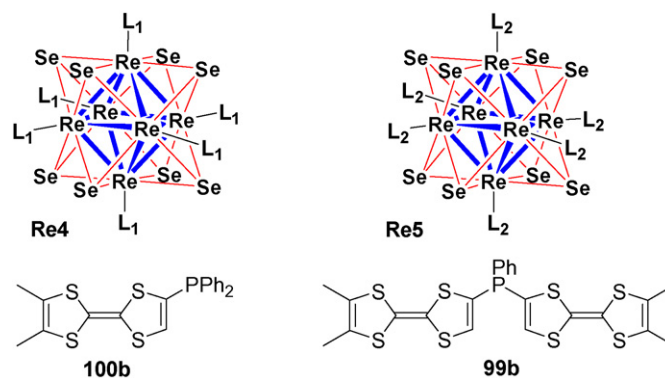
A peculiar Re-based complex (**Re3**) has been serendipitously obtained in the reaction between the ligand **104** and the Re(III) salt $[(n\text{-Bu})_4\text{N}]_2[\text{Re}_2\text{Cl}_8]$. As demonstrated by X-ray analysis (Fig. 12), the cation of this complex salt consists of a bis(chelated) $[\text{Re}(\text{III})\text{Cl}_2]^+$ fragment, while the anion contains a mixed valence Re(II)–Re(III) species formulated as $[(\mathbf{104})\text{ReCl}_2\text{ReCl}_4]^-$ [98].

Within the cation $[(\mathbf{104})_2\text{ReCl}_2]^+$, the redox active phosphines arrange in *trans* each other, while the chloride ligands occupy the axial positions (Fig. 12). Out-of-plane bends of the dithiole rings as well as bond lengths are consistent with neutral TTF species. Unexpectedly, the anion arises from the substitution of two Cl^- by one **104** ligand in the starting $[\text{Re}_2\text{Cl}_8]^{2-}$ unit, accompanied by the one electron reduction of the bimetallic $[\text{Re}_2]$ core from +6 to +5. The bond length between the two Re atoms amounts to 2.2402(9) Å, an intermediate value between a Re–Re quadruple bond and a triple bond [99]. This feature indicates a bond order of 3.5, in agreement with the mixed valence character of the bimetallic unit. The structural type encountered here, which can be considered as an intermediate towards the more common neutral complexes $\text{Re}_2\text{Cl}_4(\text{P}-\text{P})_2$, is totally unusual and it is probably due to the “special” nature of the ligand **104** (see also the chapter on Pd and Pt complexes). Several redox processes can be observed in the cyclic voltammogram of the complex salt **Re3**, which were assigned either to the oxidation of the TTF units or reduction of the Re centers in the cation or the anion, by comparison with the electrochemistry of the cation $[(\mathbf{104})_2\text{ReCl}_2]^+$ associated to the redox inert anion $[\text{BF}_4]^-$. Accordingly, a strong anodic shift of +0.26 V has been deduced for the first oxidation process of the TTFs in the cation with respect to the free **104**. Magnetic and EPR measurements revealed the paramagnetic nature of the coordinated metallic centers.

More recently, electroactive Re(III) clusters based on the $[\text{Re}_6\text{Se}_8]^{2+}$ core, and containing 6 (**Re4**) or 12 (**Re5**) *o*-DMTF units, have been synthesized upon substitution of the labile acetonitrile molecules from the precursor $[\text{Re}_6\text{Se}_8(\text{MeCN})_6][\text{SbF}_6]_2$ by the phosphines **100b** or **99b**, respectively (Scheme 41) [100].

The main objective was obviously the access to three-dimensional multiple electron donors containing an electroactive hexametallc cluster core, for which luminescence properties have been evidenced for several derivatives [101]. Ligand substitution on all the six apical sites has been definitely proved, beside ^{31}P NMR spectroscopy, by single crystal X-ray analysis in the case of the cluster **Re4**. Interestingly, the donors organize around the octahedral cluster core in two groups of three TTF units, very likely thanks to relatively short $\text{S}\cdots\text{S}$ contacts, separated by an “aromatic” equatorial region defined by the phenyl rings (Fig. 13).

Structural parameters either for the cluster core or for the TTF moieties are in the usual range, the latter having crystallized in a folded boat type conformation, often encountered within neutral



Scheme 41. TTF-phosphines containing W_6S_8 clusters.

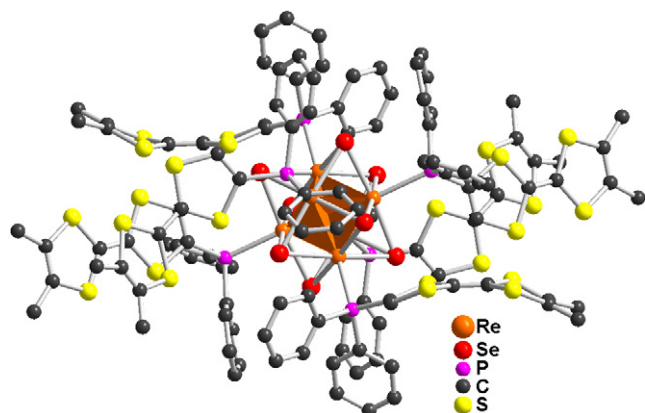


Fig. 13. Molecular structure of **Re4** [100].

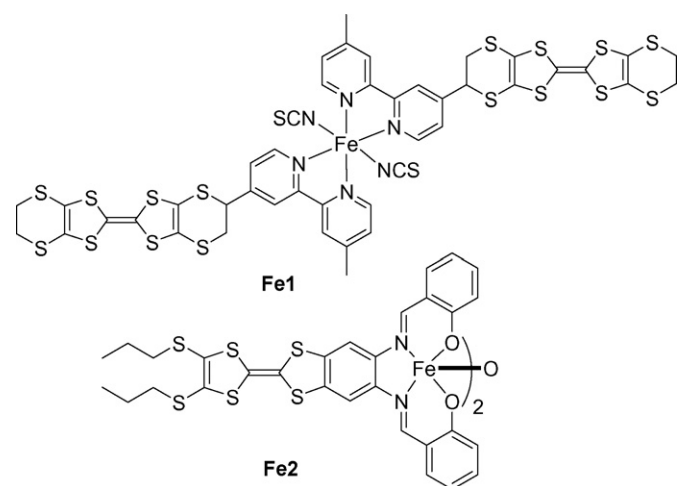
TTF derivatives. Although no crystal structure could be determined for **Re5**, containing twelve electroactive units, its formulation was assessed by NMR and also by electrospray mass spectrometry, which proved to be particularly valuable to investigate the gas phase reactivity of this family of clusters [102]. Cyclic voltammetry measurements demonstrated that all the donors oxidize simultaneously in two reversible processes, at potentials anodically shifted by +0.25 V, when compared to the free ligands, for the oxidation into radical cations. The same behavior was observed in the case of hexanuclear tungsten clusters substituted by TTF-phosphines (*vide supra*). It should be remarked once again that, despite the lack of communication between the TTF units across the cluster core, the family of $M_6Q_8[PR_n(TTF)_{3-n}]_6$ ($M=W, Re$; $Q=S, Se$) clusters presents a large interest as possible precursors for isotropic molecular conductors.

No technetium complexes containing TTF-pyridine or TTF-phosphine ligands have been reported so far.

3.3. The Fe, Ru, Os triad (group 8)

3.3.1. The Fe, Ru, Os triad with N-ligands

Only two examples of iron complexes containing N-TTF ligands have been described to date (Scheme 42), in both the TTF units being at the neutral state. The first one (**Fe1**), reported by Ouahab et al. [48], is based on a $[Fe^{II}(NCS)_2]$ fragment and two BEDT-TTF-bipyridine ligands **65**, probably *trans* disposed around the metallic center to insure an octahedral coordination environment.



Scheme 42. Iron complexes based on TTF-N ligands.

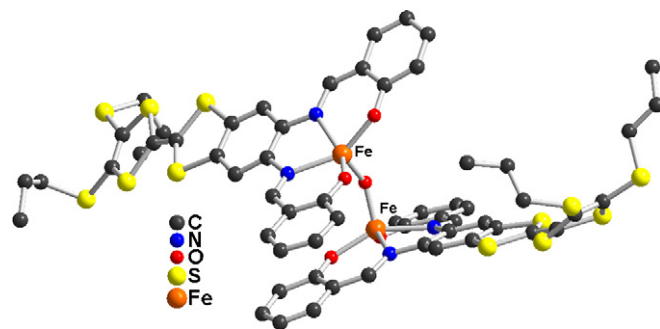


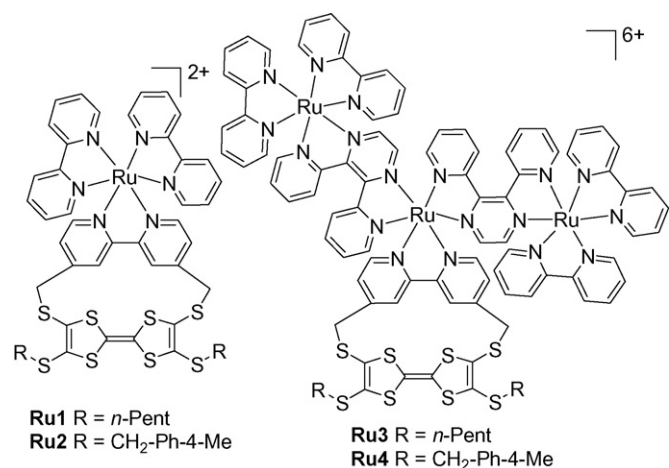
Fig. 14. Molecular structure of **Fe2**. Solvent molecules (DMF) and H atoms have been omitted [81].

UV-vis spectroscopy measurements are indicative of the presence of a metal-to-ligand charge transfer (MLCT) band, characteristic for Fe-bipyridine complexes [103], while magnetic measurements reveal a room temperature $\chi_M T$ value intermediate between high-spin Fe^{II} and low-spin Fe^{II} species. The decrease of the $\chi_M T$ product upon cooling was attributed to the zero-field splitting of Fe^{II} or to intermolecular antiferromagnetic interactions. The existence of both spin states as a mixture of HS and LS Fe^{II} in an approximated ratio of 40/60 was further substantiated through Mössbauer measurements, which show the presence of the characteristic doublets for the corresponding spin states.

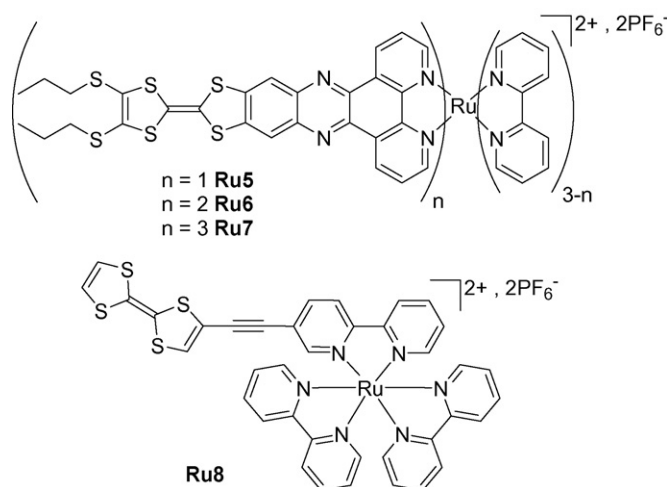
The complex **Fe2**, reported by Liu and co-workers [81], consists of two TTF-salphen (**97**) Fe^{III} units interconnected in axial positions by a μ -oxo bridge. Its synthesis involved the reaction of the TTF-bis(imine) with $FeCl_3 \cdot 6H_2O$ in the presence of triethylamine. According to the X-ray structure analysis (Fig. 14), each Fe center is coordinated in the equatorial plane to two imino N atoms and two phenoxo O atoms of the salphen unit, with Fe–N and Fe–O distances in the normal range and slight out of plane (N_2O_2) displacements for the iron atoms, amounting to 0.55–0.57 Å.

Also usual Fe–(μ -O) distances of 1.784 Å in average are measured [104], although the Fe–(μ -O)–Fe angle of $139.9(5)^\circ$ is relatively small. Bond lengths of both TTF units are consistent with donors in neutral state, which establish a couple of intermolecular $S \cdots S$ short contacts of 3.52 and 3.64 Å. The oxidation and high spin state ($S=5/2$) of the iron centers have been unambiguously established by Mössbauer measurements which show typical isomer shifts and quadrupole splitting values. The analysis of the magnetic susceptibility variation with the temperature suggests the existence of antiferromagnetic exchange interactions within the μ -oxo bridged dimer. The fit of the $\chi_M T$ curve with a $S=5/2$ dimer model afforded g and $2J$ values of 1.98(5) and $-84(1) \text{ cm}^{-1}$, in agreement with the typical values for this kind of dimers. The oxidation potentials do not vary upon coordination, as indicated by the similar values for the free ligands and their complexes, amounting to +0.55 V for **65** and its complex **Fe1** and +0.60/0.61 V (vs. SCE), for the TTF-salphen **97** and its complex **Fe2**. This occurs very likely in the case of **Fe1** because of the long-range separation between the redox active core and the coordinating groups, and in the case of **Fe2** because of the concomitant deprotonation of the phenolic oxygen atoms and coordination of the metallic center, which insures an overall equilibration of the charges. None of the complexes **Fe1** and **Fe2** has been oxidized so far into radical cation salts.

Ruthenium (II) complexes (Scheme 43), exclusively based on TTF-2,2'-bipyridine type ligands, have been prepared with the purpose of accessing antenna and charge separation systems by taking advantage of the well known photophysical properties of the $[Ru(bipy)_3]^{2+}$ unit and its related derivatives [105]. First examples have been described by Campagna et al. [49],



Scheme 43. Ru(II) complexes based on TTF-bipy ligands.



Scheme 44. Ru(II) complexes based on N-TTF ligands.

and consisted in *cis*-bipy-TTF ligands **67a** and **67b** coordinated either on [Ru(bipy)₂]²⁺ (**Ru1** and **Ru2**) or on the trinuclear unit [(bipy)₂Ru(μ-2,3-dpp)]₂Ru]⁶⁺ (**Ru3** and **Ru4**) (2,3-dpp = 2,3-bis(2'-pyridyl)-pyrazine). The counter ion is in each case PF₆⁻.

Anodic shifts of 0.13–0.15 V are observed for the first oxidation process, corresponding to the generation of the TTF radical cation, when compared to the free ligands. In the same time very weak cathodic shifts, of 0.01–0.03 V are noticed for the reduction processes centered on the substituted bipy ligand. Both features thus demonstrate a certain degree of electronic communication between the redox active sites. Undoubtedly, the most interesting aspect of these complexes concerns their luminescence properties. Accordingly, **Ru1** and **Ru2** exhibit emissions which have lifetimes of less than 1 ns, massively reduced when compared to the reference complex [Ru(bipy)₂(4,4'-Me-bipy)]²⁺ (900 ns). However, the emission arises in all the cases from a ³MLCT state, with bipy acting as acceptor. On the contrary, the luminescence is totally quenched in **Ru3** and **Ru4**, very likely because of a thermodynamically favored electron transfer from TTF to one of the peripheral Ru^{II} subunit, despite the long-range separation between the donor and the acceptor. Also an electron transfer, providing a charge-separated state TTF⁺-bipy⁻ competing with the luminescent Ru→bipy charge transfer state, was invoked for the decrease of the emission in **Ru1** and **Ru2**. These results evidenced for the very first time the role which the redox active TTF unit might play in modulating the photophysical properties of the luminescent compounds.

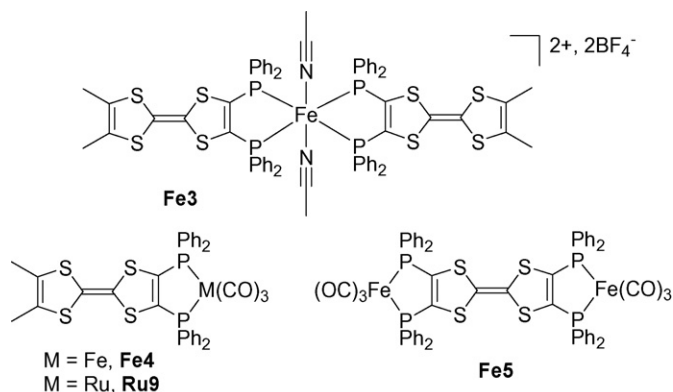
More recently, Liu and Decurtins described Ru(II) complexes containing either TTF-dppz (dppz = dipyrido-[3,2-*a*:2',3'-*c*]phenazine) ligand **71**, such as **Ru5**, **Ru6** and **Ru7** [106], or a TTF-ethynyl-bipyridine ligand **60** (**Ru8**) [47] (Scheme 44).

Interestingly, the synthetic procedure involved for the first series of compounds the condensation reaction between the Ru complex containing the phenanthroline-dione precursor and the appropriate diamino-TTF derivative to afford the pyrazino cycle. Cyclic voltammetry measurements on these complexes show that the TTF units in the complexes oxidize into radical cations at the same potentials, of about +0.3 V vs. Fc/Fc⁺, as in the uncoordinated ligands. Moreover, only in the case of **Ru7**, some intramolecular electronic interactions are likely to occur, as indicated by the broadness of the redox wave, also accompanied by a weak splitting. Photophysical investigations indicate for all the three complexes a weak emission observed around λ = 920 nm, very likely due to an intraligand charge-transfer (ILCT) fluorescence, previously evidenced in the free ligand TTF-dppz [52]. Furthermore, an intense ³MLCT emission band, characterized by a lifetime of 1040 ns and

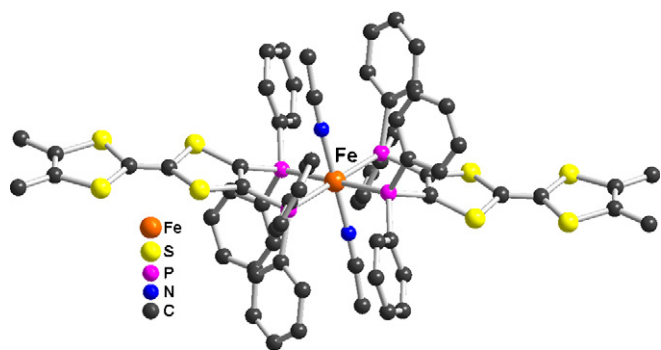
quantum efficiency of 0.014(2), appears at λ = 618 nm only in the spectrum of **Ru5**, while this emission is quenched in the case of **Ru6** and **Ru7**. An energetic diagram taking into account all the possible excited states clearly evidences that the luminescence quenching in the latter is very likely due to the population of a ligand-to-ligand charge-separated (LLCS) state with a rate constant which is larger than the intersystem crossing rate constant (*k*^{ISC}) characterizing the transition from the initially generated ¹MLCT state to the emissive ³MLCT state. The formation of the LLCS state, which relaxes to the ground state through a non-radiative charge recombination process, involves an electron transfer from a TTF, not belonging to the reduced dppz, to the formally Ru³⁺ ion. This process is favored for **Ru6** and **Ru7**, while the formation of the phosphorescent ³MLCT state dominates in the case of **Ru5**. Thus, this clear evidence for the generation of a long-lived charge-separated state in Ru(II) complexes containing appropriate TTF-based ligands encourages further efforts towards the development of such systems.

In the same trend, the complex **Ru8** was synthesized upon Sonogashira coupling between the ethynyl-TTF and the Ru(II) complex containing two bipy ligands and one 5-bromo substituted bipy ligand [47]. The more classical synthetic procedure involving the reaction between the TTF-acetylene-bipy ligand **60** and the [Ru(bipy)₂Cl₂] precursor did not afford the expected compound. This time, when compared with the previous series, the donating properties of the TTF unit are much more influenced by the coordination on the metal center, as ascertained by the relatively large anodic shifts of +0.21 and +0.22 V observed for the first and second oxidation processes of **Ru8** with respect to the free ligand. In addition, the first reduction, which is very likely based on the substituted bipyridine, occurs at a slight more positive potential (−1.04 V vs. SCE) than in the uncoordinated ligand **60** (−1.15 V vs. SCE). The absorption spectrum shows a characteristic MLCT band centered at λ = 460 nm. When the complex is excited at this wavelength, a relatively intense ³MLCT phosphorescence emission can be detected with a maximum at λ = 646 nm and lifetime τ = 1048 ns, and this despite the possibility that an electron transfer from TTF to the Ru³⁺ ion quenches the luminescence. The lower quantum efficiency with respect to the analogous complex, not containing a TTF unit, is very likely due to this feature.

Throughout these different examples, it appears that in the development of Ru complexes based on TTF-pyridine ligands the combination of the photophysical properties with the electroactivity of TTF plays a paramount role. An interesting achievement



Scheme 45. Fe and Ru complexes based on TTF-phosphines.

Fig. 15. Molecular structure of $[\text{Fe}(\mathbf{104})_2(\text{MeCN})_2](\text{BF}_4)_2$ (**Fe3**). H atoms and BF_4^- anions have been omitted [108].

would certainly be the synthesis of an optical redox commutable sensor for which the emission would be modulated by changing the TTF oxidation state.

3.3.2. The Fe, Ru, Os triad with P-ligands

The first iron complex containing TTF-phosphines has been mentioned by Dunbar et al. and involved the coordination of two chelating ligands **104** on the $[\text{Fe}^{\text{II}}(\text{MeCN})_2]^{2+}$ fragment to provide the compound formulated as $[\text{Fe}^{\text{II}}(\mathbf{104})_2(\text{MeCN})_2](\text{BF}_4)_2$ (Scheme 45) [107]. In this first report, the complex was mainly characterized by fast atom bombardment (FAB) mass spectrometry.

Later on [108], a single crystal X-ray study confirmed that the compound **Fe3** contains two bis(phosphines) *trans* coordinated in the equatorial plane to the metallic center located on an inversion center, while the axial positions are occupied by two acetonitrile molecules (Fig. 15). This provides an octahedral coordination geometry, with Fe–P (2.296 and 2.358 Å) and Fe–N (1.924 Å) distances in the normal range.

The metallacycle is folded by 28.2° about the P...P axis, while the TTF units are only slightly bended by 16.1° about the S...S hinge of the inner dithiole halves. The values for the central C=C and C–S bonds are indicative for the neutral state of the donor. The complex

Table 12

Evolution of ^{31}P NMR chemical shift ($\Delta\delta$, in ppm) in the Fe [95] and Ru [112] complexes with **104** or **103** ligands.

L (δ , ppm)	$[(\text{L})_2\text{Fe}]^{2+}$	$(\text{L})[\text{Fe}(\text{CO})_3]_n$	$(\text{L})[\text{Ru}(\text{CO})_3]$
104 (–18.8)	+74.9 (Fe3)	+105.5 (Fe4); $n=1$	+75.8 (Ru9)
103 (–18.2)	–	+105.4 (Fe5); $n=2$	–

is diamagnetic (Fe^{II} low spin, $S=0$), therefore its ^{31}P NMR could be measured. Accordingly, the chemical shift of the four equivalent P nuclei appears at $\delta = +56.1$ ppm, which represents a large downfield shift with respect to the uncoordinated **104** ($\delta = -18.8$ ppm) (see also Table 12). In addition, monitoring a solution of **Fe3** by ^{31}P NMR evidenced the transformation of the initial complex in a new one, exhibiting an even stronger downfield shift ($\delta = +76.2$ ppm), for which mass spectrometry and ^{19}F NMR results suggest the presence of a coordinated F^- or BF_4^- anion [109]. Cyclic voltammetry measurements show an anodic shift when compared to **104** of $\Delta E = +0.28$ V for the first oxidation wave, which thus corresponds to the generation of a bis-radical cation species, indicating that there is no sizeable electronic communication between the TTF units. Moreover, reversible one electron reduction processes, attributed to the sequential reduction of Fe^{II} into Fe^{I} at -0.62 V, and then Fe^{0} at -1.06 V, are observed (Table 13).

The two other examples of iron complexes based on TTF-phosphines known to date have been synthesized upon reaction of either the diphosphine **104** (**Fe4**) or the tetraphosphine **103** (**Fe5**) with the precursor $\text{Fe}_2(\text{CO})_9$ [95]. Downfield shifts of about $\Delta\delta = +106$ ppm when compared to the respective free ligands are observed in ^{31}P NMR spectra of the complexes (Table 12). The structure of the complexes has been ascertained by single crystal X-ray study. In both cases the phosphino groups are *cis* chelated on iron which further contains three CO ligands within a distorted trigonal bipyramid (tbp) (Fig. 16), a stereochemistry often encountered in similar $\text{Fe}(\text{CO})_3$ complexes with unsaturated diphosphines [110].

The equatorial plane is formed by one phosphino and two CO ligands, while the other phosphine and CO occupy the axial positions. Folding angles of $21.1(1)^\circ$ and $10.2(1)^\circ$ in **Fe4** (two independent molecules in the asymmetric unit) and $2.0(1)^\circ$ in **Fe5** are observed along the P...P hinges, thus suggesting, together with the value measured in the previous example (see above), a relatively large flexibility for this type of metallamacrocycle. The most interesting aspect of these complexes is undoubtedly related to their electrochemical behavior, since the first oxidation process occurring at low potentials (Table 13) is attributed to the formation of paramagnetic Fe^{I} species. In the case of **Fe5**, the metallic centers Fe^{0} are simultaneously oxidized into Fe^{I} . This feature is in agreement with reports in the literature mentioning the reversible one-electron oxidation of $\text{P}_2\text{Fe}^{\text{0}}(\text{CO})_3$ complexes in non-coordinating solvents [111]. Also in our case, full reversibility of this process was observed in CH_2Cl_2 , while in MeCN ligand substitution probably takes place. Upon increasing the potential, oxidation of TTF into radical cation and then dication is observed in **Fe4**, whereas in **Fe5** the oxidation of the TTF core seems to be much more difficult to achieve and the process is not reversible. However, upon repetitive cycling of a solution of **Fe4** in CH_2Cl_2 in a potential range encompassing the

Table 13

Cyclic voltammetry data for Fe and Ru complexes with **104** or **103** ligands (potentials expressed in V referenced vs. SCE, ΔE with respect to the free ligand in mV, 0.1 M TBAPF₆ in CH_2Cl_2) [95,112].

Compound	E_{ox}^1 ($\text{M}^{\text{0}}/\text{M}^{\text{1+}}$)	ΔE_{ox}^2 (TTF ²⁺ /TTF ⁺)	ΔE_{ox}^3 (TTF ²⁺ /TTF ⁺)	E_{red}^1 ($\text{M}^{\text{2+}}/\text{M}^{\text{1+}}$)	E_{red}^1 ($\text{M}^{\text{1+}}/\text{M}^{\text{0}}$)
Fe3		+280 (vs. 104)	+120 (vs. 104)	–0.62	–1.06
Fe4	0.28	+410 (vs. 104)	+370 (vs. 104)		
Fe5	0.31	+710 (irr.) (vs. 103)	not obs.		
Ru9	0.39 (irr.)	+440 (irr.) (vs. 104)	+410 (irr.) (vs. 104)		

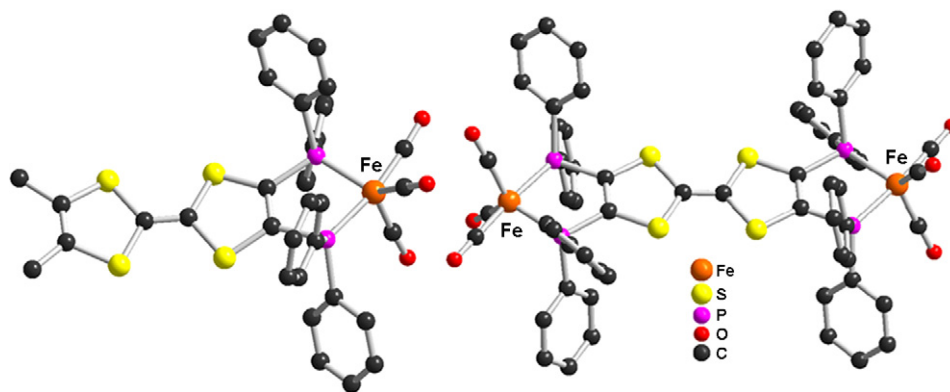
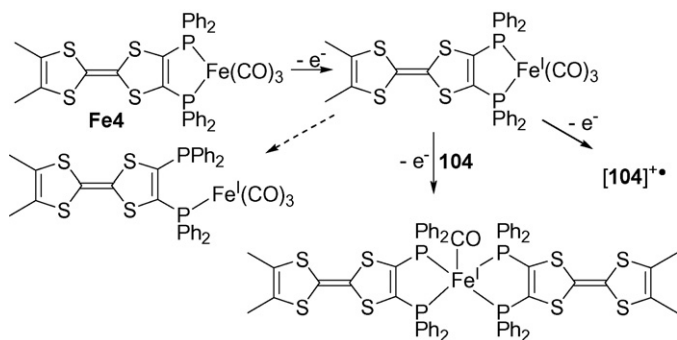


Fig. 16. Molecular structures of $(104)Fe(CO)_3$ (**Fe4**) (left) and $(103)[Fe(CO)_3]_2$ (**Fe5**) (right) [95].

oxidation of TTF, either to $TTF^{•+}$ or TTF^{2+} , a decrease of the intensity of the oxidation wave Fe^0/Fe^I simultaneous to the appearance of the redox couples for the free ligand is observed [112]. This indicates that in those experimental conditions the oxidized species $[Fe4]^{2+}$, containing in principle one organic radical as $TTF^{•+}$ and one paramagnetic metal as Fe^I d^7 center, is not stable and decomposes gradually into **104** and unidentified iron-based fragments. When the potential reaches only values slightly above the formation of Fe^I species, the redox process Fe^0/Fe^I appears to be stable at the timescale of the experiment, even at low scan rates. EPR measurements corroborated with theoretical calculations at DFT level were performed in order to characterize the chemically or electrochemically oxidized species from an electronic distribution point of view and also to determine their stability. Accordingly, the triplet observed after the first oxidation is clearly metal-centered, the unpaired electron on iron being coupled with the two equivalent ^{31}P atoms, with experimental hyperfine coupling constants of 22.5 G in agreement with the calculated ones of 21.53 G [112]. As soon as the oxidation is conducted with more than one equivalent of chemical oxidant, e.g. $AgClO_4$, or at a potential higher than the one required for the second oxidation of the compound, the typical heptuplet signal for the free $[104]^{•+}$ ligand is observed, indicating the total decoordination at this stage. Moreover, a solution of singly oxidized compound $[(104)Fe^I(CO)_3]^+$ slowly evolves upon standing at room temperature towards a single coordinated complex, suggesting that even this first metal-centered oxidized compound exhibits moderate kinetic stability. When the oxidation of **Fe4** takes place in the presence of a second equivalent of **104**, a bis-coordinated $[(104)_2Fe^I]^+$ complex is likely formed, according to the quintet EPR signal arising from the isotropic coupling with four ^{31}P nuclei (Scheme 46).



Scheme 46. Species issued from the oxidation of **Fe4** detected by EPR spectroscopy.

The unique TTF-phosphine-based ruthenium complex (**Ru9**) reported so far contains the diphosphine **104** coordinated to the $Ru(CO)_3$ fragment and was prepared from the precursor $Ru_3(CO)_{12}$ (Scheme 45) [112]. Its structure, ascertained by single crystal X-ray study, shows a metal center in a slightly distorted trigonal bipyramidal environment, with a planar 5-member ring metallacycle, as well as essentially planar dithiole halves (Fig. 17).

Unlike the iron counterpart **Fe4**, cyclic voltammetry measurements show an irreversible oxidation of Ru^0 into the paramagnetic Ru^I d^7 species. This instability did not allow further investigations of the diverse oxidized intermediates. More electron donating or sterically hindered phosphines are probably needed in order to stabilize these species.

3.4. The Co, Rh, Ir triad (group 9)

3.4.1. The Co, Rh, Ir triad with N-ligands

In general, the utilization of the Co^{II} center in coordination chemistry relies mainly on its strong anisotropy as a consequence of the large spin-orbit coupling [113]. Two different families of Co^{II} complexes containing TTF-pyridines have been reported so far. The first one, described by Liu and Decurtins [114,45], is based on the coordination of the $CoBr_2$ fragment by tetradentate 4,5-bis(2-pyridyl-methylsulfanyl)-4',5'-ethylenedithio-TTF ligands such as **51**, **54a** and **54b** to give **Co1**, **Co2** and **Co3**, respectively (Scheme 47), and has been conventionally synthesized upon reaction of the ligands with the $CoBr_2 \cdot H_2O$ precursor in MeCN. Alternatively, the 2-pyridyl units have been replaced on the EDT-TTF-bis(thiomethyl) scaffold by 2-quinolinyl fragments in **54c** to afford the corresponding Co^{II} complex **Co4** [45].

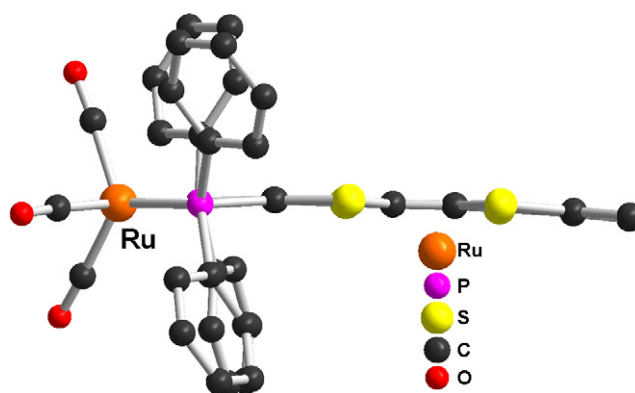
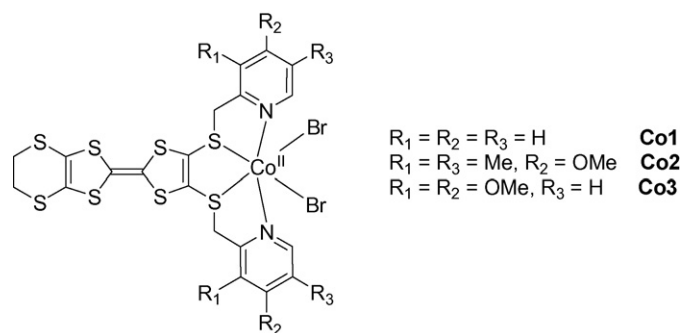


Fig. 17. Molecular structures of $(104)Ru(CO)_3$ (**Ru9**) [112].



Scheme 47. Monometallic Co^{II} complexes with TTF-pyridines.

The solid state structures have been determined in the case of the complexes **Co1** (Fig. 18) [114] and **Co2** [45], showing in each case a distorted octahedral coordination pattern around the Co^{II} center, as well as a segregation of the inorganic and donor moieties in the packing diagrams, thus favoring the establishment of some short intermolecular $\text{S} \cdots \text{S}$ contacts. The equatorial coordination plane is formed by the two bromide anions, with $\text{Co}-\text{Br}$ distances of 2.49–2.52 Å, and the two sulfanyl sulfur atoms, with $\text{Co}-\text{S}$ distances of 2.51–2.54 Å, while the axial positions are occupied by the pyridyl N atoms, with $\text{Co}-\text{N}$ distances of 2.17 Å. The bond angle $\text{N}-\text{C}-\text{N}$ of 158.7° exhibits the greatest deviation from the octahedral geometry. Similar characteristics are observed for the complex **Co2**.

Electrochemistry investigations on this series of complexes revealed small anodic shifts when compared to the free ligands, for the first oxidation processes generating TTF radical cations, ranging between 30 mV (**Co3**) and 110 mV (**Co4**). This is very likely due to the relative short distance between the redox active unit and the coordinated metal. Magnetic susceptibility measurements performed on the complex **Co1** indicated a typical paramagnetic behavior for isolated Co^{II} ions $S = 3/2$.

The second series of Co^{II} complexes (**Co5–Co7**, Scheme 48) was reported by Ouahab et al. and consists in the combination of $[\text{Co}^{\text{II}}_2]$ dimers [22] or $[\text{Co}^{\text{II}}_2\text{M}^{\text{II}}]$ ($\text{M}^{\text{II}} = \text{Co}^{\text{II}}, \text{Mn}^{\text{II}}$) trimers [115] stabilized by bridging benzoate PhCOO^- ligands, with monodentate TTF-ethenyl-pyridines **14a** and **14b**.

The key step in the preparation of the complexes involves the *in situ* generation of the benzoate upon oxidation of benzaldehyde by nitrate salts of the transition metal, followed by the addition of the ligand and crystallization by slow diffusion [116]. The fine-tuning of the experimental conditions affords either bimetallic

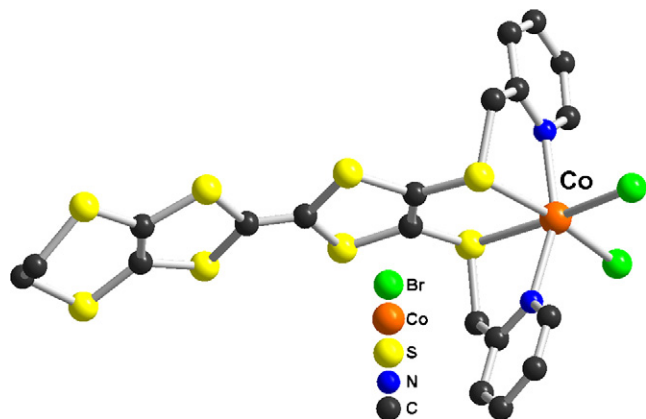
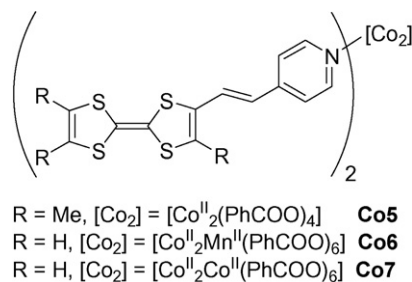


Fig. 18. Molecular structure of **Co1** [114].



Scheme 48. Bi- and trimetallic Co^{II} complexes with TTF-pyridines.

(**Co5**) or trimetallic (**Co6–Co7**) complexes. **Co5** crystallized as centrosymmetric dimer, with the metal located in a distorted square pyramidal environment if neglecting the $\text{Co}-\text{Co}$ contact (Fig. 19).

The base of the pyramid is formed by four oxygen benzoate ligands which bridge the metals, thus affording the classical paddlewheel morphology for this motif, with $\text{Co}-\text{O}$ distances ranging between 2.019(3) and 2.075(4) Å, while the apical position is occupied by the nitrogen pyridyl atom. Interestingly, the comparison of the crystallographic parameters measured at 293 and 100 K reveals that the $\text{Co}-\text{Co}$ distance strongly decreases from 2.772(2) Å (293 K) to 2.694(2) Å (100 K). This variation, nicely explained in terms of orbital interaction, is likely due to the decrease of the thermal population of the first excited state, characterized by the promotion of an electron from the bonding HOMO σ orbital to the low lying σ^* LUMO orbital of the $[\text{Co}_2]$ fragment. The population of this excited state, besides the weakening effect on the $\text{Co}-\text{Co}$ interaction, confers a paramagnetic character to the $[\text{Co}_2]$ entity. Indeed, magnetic susceptibility measurements show a steady decrease to zero of the $\chi_{\text{M}}T$ curve when lowering the temperature, clearly indicating that the ground state is non-magnetic. The magnetic data, fitted by a singlet–triplet model with the Bleaney–Bowers equation, yielded an exchange coupling constant $J = -420 \text{ cm}^{-1}$, thus proving the existence of metal–metal interactions. A nice expansion of this first report consisted in the synthesis of the two trinuclear heterometallic **Co6** and homometallic **Co7** complexes based on the same type of building blocks [115]. The trimetallic unit $[\text{Co}^{\text{II}}_2\text{M}^{\text{II}}(\text{PhCOO})_6]$, generated through the same experimental procedure, contains now on the apical positions of the lateral Co^{II} ions the non-methylated TTF-ethenyl-pyridine ligand **14a**. As shown by single crystal X-ray analysis, there are four $\mu_2(\eta_1, \eta_1)$ and two $\mu_2(\eta_1, \eta_2)$ bridging carboxylates, the two complexes being isostructural with the central ion located on an inversion center (**Co7** in Fig. 20).

The central ion (Co^{II} or Mn^{II}) is hexacoordinated by six oxygen benzoate atoms within octahedral geometry, while the outer Co^{II} centers are linked to four oxygen and one nitrogen pyridyl atoms in a distorted trigonal bipyramid. The $\text{Co}-\text{O}$ distance with the bridging η_2 oxygen amounts to 2.370(4) Å, while the other three $\text{Co}-\text{O}$ bonds are shorter by 0.4 Å in average. These parameters impose a $\text{Co} \cdots \text{Co}$

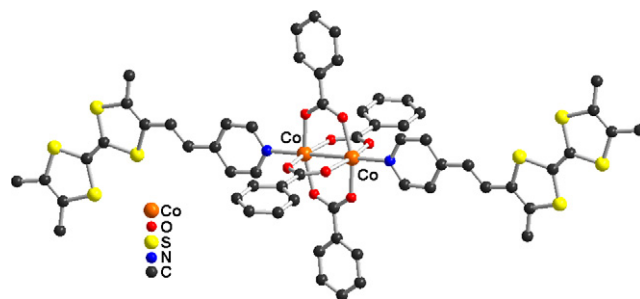


Fig. 19. Molecular structure of **Co5** [22].

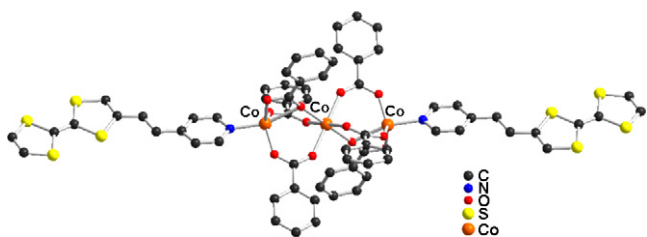


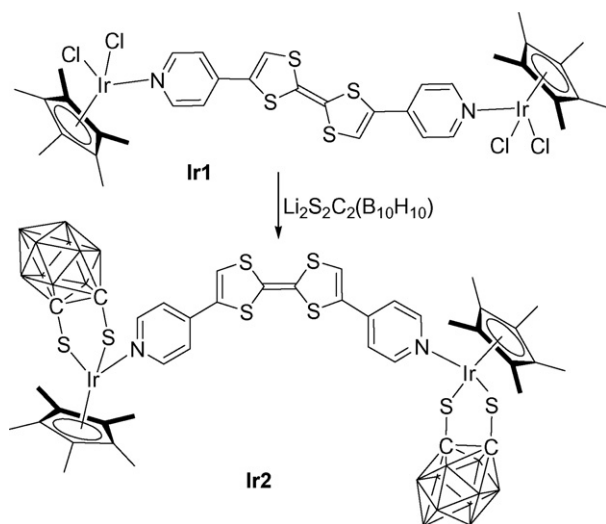
Fig. 20. Molecular structure of **Co7** [115].

distance of 3.56 Å, much longer than in the previous case (*vide supra*). Accordingly, the magnetic interactions within the trinuclear brick can be explained through a superexchange mechanism. However, the interactions are rather weak, as demonstrated by magnetic measurements. The ground state of the complex **Co6** can be clearly described as a $S = 1/2$ with antiferromagnetically coupled isotropic S_{Mn} to two S_{Co} , such as it was deduced from the drop of the $\chi_M T$ curve below 100 K. The situation is more complex in the case of **Co7**, however the decrease of the $\chi_M T$ curve suggests once again antiferromagnetic interactions between the neighboring metal ions, with probably a ferrimagnetic ground state.

The preparation of a Co^{II} complex with the ligand TTF-salphen **97** has been mentioned by Liu and Decurtins in the report describing the complex **Fe2** (*vide supra*, Scheme 42) [81], yet with no X-ray structural studies, nor magnetic measurements. Further studies will certainly be devoted to the chemical or electrochemical oxidation of all these Co^{II} complexes in order to ally in the solid state conducting and magnetic properties.

Besides the cobalt complexes, only one example involving a heavier metal of this group 9 and a TTF-N ligand has been reported. The somewhat “exotic” bimetallic compound **Ir2** consists in two $(Cp^*)Ir^{III}[S_2C_2(B_{10}H_{10})]$ (Cp^* = pentamethyl-cyclopentadienyl, $[S_2C_2(B_{10}H_{10})]$ = 1,2-dicarba-*closo*-dodecaborane (12)-1,2-dithiolate) bridged by the bis(4'-pyridyl)-TTF ligand **12** (Scheme 49) [18]. Its synthesis was achieved upon chloride replacement from the precursor **Ir1**, itself prepared from the bis(pyridine)-TTF ligand and the dimer $[Cp^*IrCl_2]_2$, by treatment with the dilithio salt of the carborane-dithiolate. An unexpected *E-Z* isomerisation was noticed during the substitution reaction.

The structure of **Ir2** has been proved by single crystal X-ray analysis. It appears that the carborane clusters point in opposite directions and the Ir^{III} centers lie in a distorted octahedral coordi-



Scheme 49. Ir-TTF-pyridine complexes.

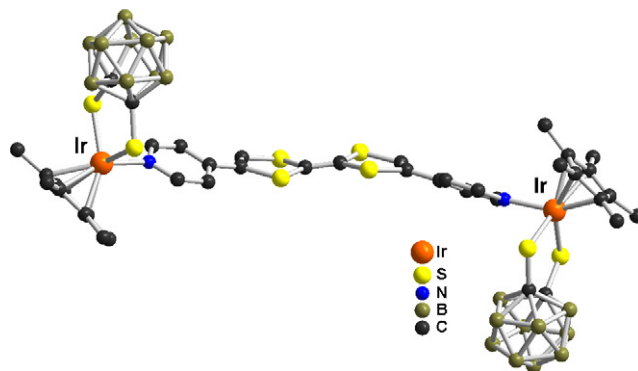
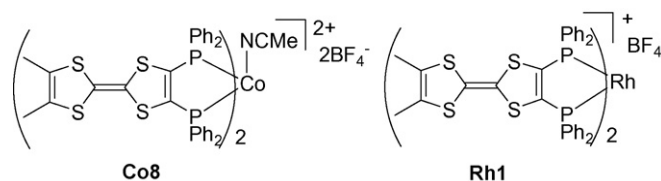


Fig. 21. Molecular structure of **Ir2** [18].



Scheme 50. Group 9 TTF-phosphines complexes.

nation geometry formed by the Cp^* ligand, one nitrogen pyridine and two sulfur atoms (Fig. 21).

The Ir–N bond amounts to 2.135(7) Å, while a twist of 16.7° is observed between the pyridine ligands and the TTF mean plane. Alternatively, the diselena, instead of dithio, compounds have been also prepared. No electrochemical data have been reported for these complexes.

3.4.2. The Co, Rh, Ir triad with P-ligands

Although the Co^{II} complex **Co8** (Scheme 50) containing two TTF-phosphines **104** was mentioned already in 1998 [107], its solid state structure and full characterization were only recently reported [108].

The X-ray study revealed that the Co^{II} center is pentacoordinated within a square pyramid environment, as already observed in Co^{II} phosphine complexes [117] by two chelating bis(phosphines) in equatorial plane and one acetonitrile molecule in apical position (Fig. 22).

Folding angles of 30.16° and 17.76° along the $P \cdots P$ axes can be measured for the two 5-member rings metallacycles. The dithiole rings are bended as well, a classical feature for neutral donors. The paramagnetism of the complex prevented its characterization by



Fig. 22. Molecular structure of **Co8**. H atoms, BF_4^- anions and crystallization MeCN molecules have been omitted [108].

Table 14

Cyclic voltammetry data for Co and Rh complexes with **104** (potentials expressed in V referenced vs. Ag/AgCl, ΔE with respect to the free ligand **104** in mV, 0.1 M TBAPF₆ in CH₂Cl₂).

Complex	E_{ox}^1 (ΔE_{ox}^1) (TTF ^{•+} /TTF)	E_{ox}^2 (ΔE_{ox}^2) (TTF ²⁺ /TTF ^{•+})	E_{red}^1 (M ²⁺ /M ¹⁺)	E_{red}^1 (M ¹⁺ /M ⁰)	Reference
Co8	+0.63 (+170)	+1.03 (+160)	−0.91 ^{irr}	−1.19 ^{irr}	[108]
Rh1	+0.62 (+160)	+1.01 (+100)			[89]

³¹P NMR. Magnetic susceptibility measurements as a function of temperature are consistent with a spin state $S = 3/2$ at high temperatures, with an important spin-orbit coupling, while an effective $S' = 1/2$ state is indicated for the low temperatures regime. However, EPR measurements in solution shows an anisotropy due to the interaction with the ⁵⁹Co ($I = 7/2$) nucleus, which suggests a $S = 1/2$ ground state, typical for an octahedrally coordinated Co^{II} center. Coordination by a second molecule of solvent in solution is very likely to occur. Cyclic voltammetry measurements demonstrate concomitant oxidation of both TTF units into radical cations, and then dications, at potentials anodically shifted by +170 and +160 mV, respectively, when compared to the free ligand (Table 14). In addition, irreversible reduction of the metal center into Co^I, and then Co⁰, is also observed.

Attempts to prepare a Rh^{II} complex upon reaction of the bimetallic [Rh₂(MeCN)₁₀](BF₄)₄ with the same diphosphine **104** resulted in the one electron reduction of the metal accompanied by the formation of the mononuclear [Rh^I(**104**)₂](BF₄) complex **Rh1** (Scheme 50) [89]. As expected for a Rh^I d⁸ ion, a square planar coordination geometry is observed (Fig. 23), with the metal occupying an inversion center. The dithiole rings bearing the phosphines are rather strongly folded by 24.2(2)° along the S··S axis, while the metallacycles are bended only by 8.26(66)° along the P··P hinges. A strong downfield shift of $\Delta\delta = +69.8$ ppm for the ³¹P NMR resonance with respect to the free phosphine, together with the splitting of the signal because of the ¹J_{Rh-P} coupling constant of 133.8 Hz are observed. As for the Co^{II} complex previously described, similar anodic shifts for the oxidation potentials have been measured (Table 14).

3.4.3. The Co, Rh, Ir triad with N,S or P,N-ligands

So far, only a couple of complexes containing mixed chelating ligands have been described, and they concern EDT-TTF-oxazolines functionalized in *ortho* position with SMe (**92a**) or PPh₂ (**91b**) groups, thus insuring a second coordination site beside the oxazoline nitrogen (Scheme 51). Moreover, these examples are among the very few known chiral metal complexes based on the TTF unit.

The neutral cobalt complex **Co9** was synthesized in racemic form upon reaction of the racemic ligand TTF-SMe-Me-oxazoline **92a** with the precursor Co^{II}(hfac)₂ in non-coordinating solvents such as CH₂Cl₂ [118]. The metallic center lies in a distorted octahe-

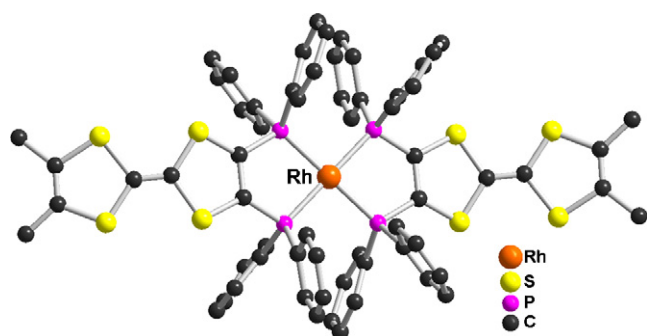
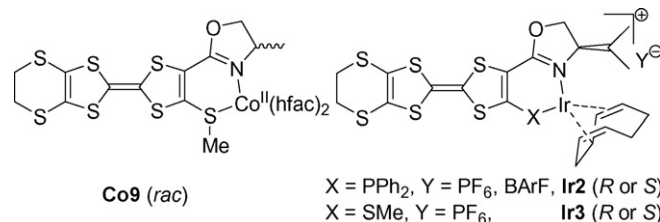


Fig. 23. Molecular structure of **Rh1**. H atoms, BF₄[−] anion and crystallization H₂O molecules have been omitted [89].



Scheme 51. Group 9 TTF-oxazolines complexes.

dral coordination environment, with three oxygen and the nitrogen atoms in the equatorial plane and the fourth oxygen and the sulfur atom in the apical positions (Fig. 24).

The Co–S distance of 2.524(1) Å is much longer than the usual Co–S (thioether) bond lengths ranging from 2.17 to 2.35 Å. Both enantiomers are equally disordered on the same crystallographic site, therefore all the four possible diastereomers (Δ,R), (Δ,S), (Λ,S) and (Λ,R) are present in the crystal. Within the crystal, the shortest Co··Co distance amounts to 8.71 Å, thus suggesting that the metallic centers are very likely isolated.

The phosphino-oxazolines (**Ir2**) and thiomethyl-oxazolines (**Ir3**) iridium (I) complexes have been synthesized in order to be used as catalysts in the enantioselective hydrogenation reaction of imines (see Section 5) [119].

3.5. The Ni, Pd, Pt triad (group 10)

3.5.1. The Ni, Pd, Pt triad with N-ligands

Surprisingly, only a few metal complexes with the nickel triad have been described so far with N or P TTF-containing ligands (Scheme 52).

For example, tetrathiafulvalene itself with a single 4-pyridyl group was engaged with Ni(acac)₂ to form the neutral *trans* complex [(**5a**)₂Ni(acac)₂] **Ni1** (Fig. 25), which exhibits the expected $S = 1$ spin configuration for a Ni²⁺ ion in an octahedral environment [14].

Several Ni complexes were investigated by Liu and Decurtins, based on the bis-pyridyl chelate TTFs **51**. The NiCl₂ complex **Ni2** (Fig. 26) shows an octahedral coordination with the Ni ion *cis* coordinated to two chloride ions bound to two *trans* pyridyl nitrogen atoms and two sulfanyl sulfur atoms [114]. The TTF unit is coplanar with the NiCl₂ moiety. Magnetic measurements

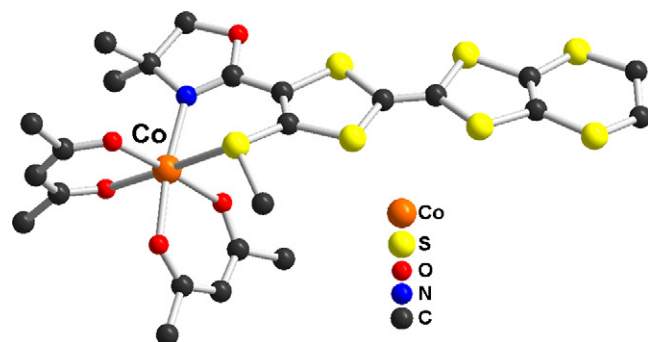
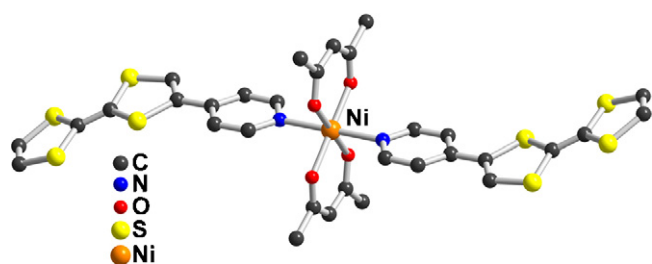
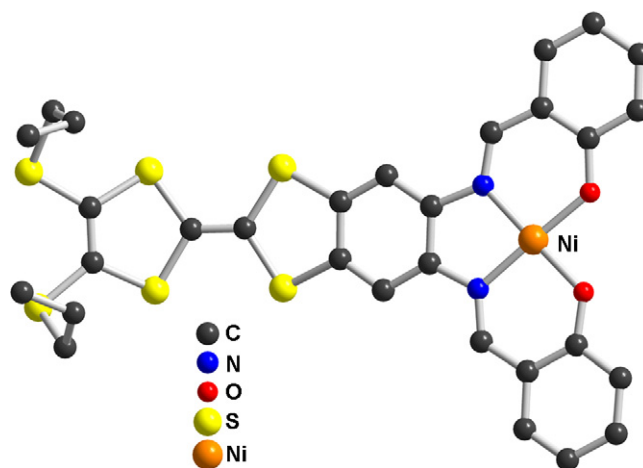
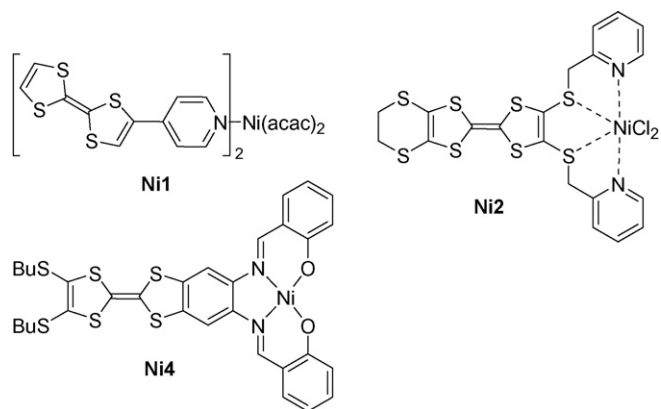
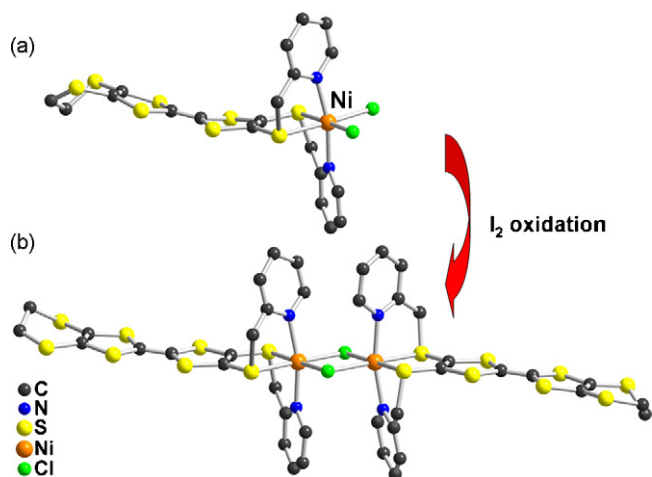


Fig. 24. Molecular structure of (*rac*)-**Co9** [118].



(SQUID) confirmed the $S = 1$ configuration expected for this octahedral geometry. Since the electrochemical studies showed that the reversibility of the TTF oxidation waves was not modified upon complexation, this complex **Ni2** was oxidized chemically with I_2 by layer diffusion technique [120] to afford an original dinuclear μ -chloro-bridged Ni(II) complex **Ni3** formulated as $[Ni_2(\mu-Cl)_2(51^{+})_4]^{4+}(I_3^-)_4(I_2)_3 \cdot (H_2O)_2 \cdot (THF)_3$ [121]. The distorted octahedral Ni(II) coordination moiety and its bond lengths are at first sight very similar to those of the neutral mononuclear compound **Ni2**, only two chlorides change from terminal to bridging ligands. The solid state and electronic properties of this salt will be described in more detail in Section 4.3.

The same authors very recently described the Ni complex **Ni4** of an original tetrathiafulvalene-fused Schiff-base ligand **97** [81].



The coordination geometry around the Ni atom (Fig. 27) is square-planar, with geometrical features which compare well with those of known substituted $[Ni(salen)]$ complexes [122]. The electrochemical properties associated with the TTF redox core in **97** are essentially not modified in the **Ni4** complex.

Pd and Pt complexes were also described with the *meta*-pyridyl carbamoyl TTF ligand **33** (Scheme 53), engaged with $[Pd(dppp)]^{2+}$ and $[Pt(dppp)]^{2+}$ moieties [33]. Indeed, this kind of precursors has been widely used in the construction of molecular or supramolecular assemblies, by coordinating the two remaining free *cis* positions with various pyridine- or bipyridine-based ligands [123]. The reaction of $[M(dppp)](OTf)_2$, $M = Pd, Pt$ with the *meta*-pyridyl carbamoyl TTF derivative **33** afforded the desired complexes **Pd1**, **Pt1** formulated as $[(33)_2M(dppp)](OTf)_2$.

The reaction was easily followed by ^{31}P NMR spectroscopy, characterized by an upfield shift (relative to the free $[(dppp)Pd](OTf)_2$ complex) of $\Delta\delta = -16.6$ ppm for **Pd1**, by a downfield shift ($\Delta\delta = 21.0$ ppm) for **Pt1**. Interestingly, in the case of the latter, a diastereoisomeric pair (*meso* and *anti-dl* racemic) was formed at room temperature in a ratio 5:8, indicating that the rotation barrier is much higher than for the Pd analog. As a consequence, only crystal of the more fluxional salt **Pd1** could be obtained (Fig. 28). The Pd atom is in a square-planar environment, *cis* coordinated by two TTF-amido-pyridines, whose conformations are highly distorted, mainly around the NH-Py bond. The conformation of the complex is of *anti* type, the centrosymmetric dimers observed in the structure correspond to the *dl* racemic pairs of enantiomers. Note also the strong distortions from planarity of one of the two TTF cores in the complex.

3.5.2. The Ni, Pd, Pt triad with P-ligands

The very first metal complexes of a TTF P-ligand were reported in 1992 by Fourmigué, based on the chelating *o*-Me₂TTF diphosphine **104** (Scheme 54) [83].

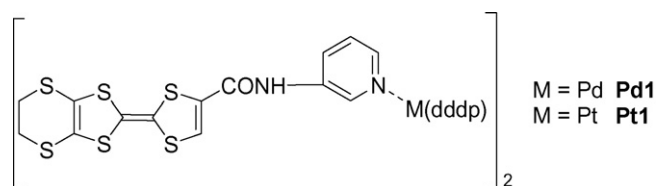


Fig. 26. (a) Molecular geometry of the **Ni2** complex in its neutral form and [114] (b) its oxidation product **Ni3**, in its polyiodide salt [120].

Scheme 53.

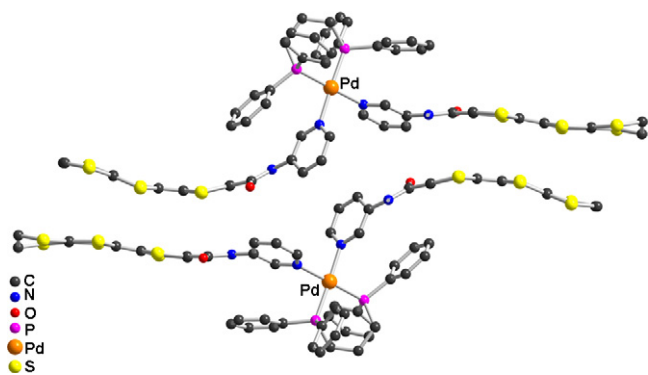
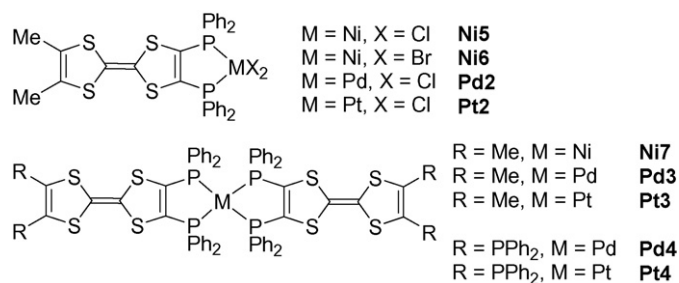


Fig. 28. A view of the face-to-face association of the **Pd1** complexes in the solid state [33].



Scheme 54. Group 10 metal complexes of the chelating diphosphine **104**.

Its square-planar, diamagnetic NiCl_2 and NiBr_2 complexes noted **Ni5** and **Ni6** are characterized by a strong ^{31}P NMR coordination chemical shift, $\Delta\delta = \delta(\text{complex}) - \delta(\text{ligand})$, around 60–70 ppm. Indeed, the P atoms in **Ni5** and **Ni6** complexes are observed at 41.3 and 48.8 ppm, respectively while the free diphosphine **104** exhibits a resonance at -18.8 ppm. The diamagnetic character of the two salts, inferred from the NMR results, is attributable to a square-planar configuration, as confirmed by the X-ray crystal structure determination of **Ni6**, as CHCl_3 solvate. The analogous PdCl_2 and PtCl_2 complexes **Pd2** and **Pt2** were described later on and behave similarly. Their CHCl_3 solvates are isomorphous with **Ni6** [124] (Fig. 29) and they are all three characterized by hydrogen bonding interaction between the chloride anion and the acidic hydrogen atom of the chloroform molecules. ^{31}P NMR data show similar strong downfield shifts upon complexation, $\Delta\delta_{\text{Pd2}} = 66.3$ ppm and $\Delta\delta_{\text{Pt2}} = 46.3$ ppm. Based on these ^{31}P NMR data, an interesting com-

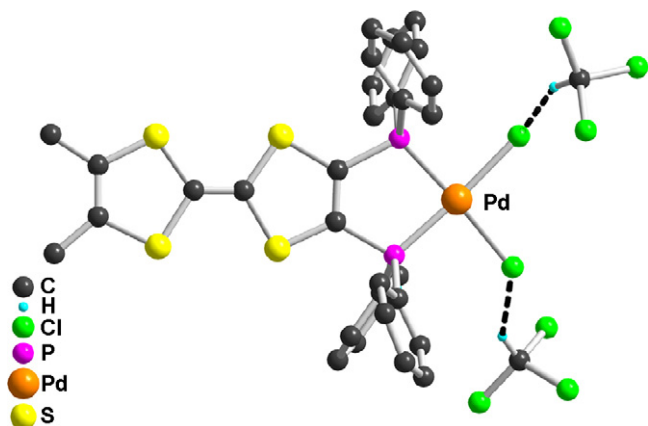


Fig. 29. A view of **Pd2** showing the square-planar geometry and the C–H...Cl hydrogen bonds [124].

Table 15

Evolution of ^{31}P NMR coordination chemical shift ($\Delta\delta$, in ppm) in **Ni5**, **Pd2** and **Pt2** and the analogous dppe complexes.

L	(L) NiCl_2	(L) PdCl_2	(L) PtCl_2	Reference
dppe	72.1	81.5	58.5 ($^1J_{\text{P-Pt}} = 3618$ Hz)	[125]
104	60.1	66.3	46.3 ($^1J_{\text{P-Pt}} = 3640$ Hz)	[83,124]

parison can be performed between the prototypical dppe chelating diphosphine and **104** (Table 15).

We observe a systematic decrease of the $\Delta\delta$ values, whatever the nature of the metal, indicating an enhancement of the M-to-P π retrodonation due to the unsaturated character of the **104** ligand when compared with dppe. Similar effects were already encountered for example in the conjugated dppen analog [126]. The slight increase of the $^1J_{\text{P-Pt}}$ coupling constant when going from dppe to **104** also demonstrates the stronger σ -bonding character of the **104** ligand. Electrochemical investigations of the three chloride complexes **Ni5**, **Pd2** and **Pt2** show a strong anodic shift of the TTF oxidation waves upon coordination, from 0.34 V for the first oxidation wave of the free ligand to 0.57 V for **Ni5** in the same conditions. The reactivity of the PdCl_2 and PtCl_2 complexes **Pd2** and **Pt2** was investigated toward chlorine abstraction with $\text{Ti}(\text{OTf})_4$, in the hope to free some coordination sites for further formation of extended networks of supramolecular assemblies upon coordination with various bipyridines. However, it appeared that a $\text{Ti}(\text{OTf})_4$ adduct was systematically obtained without any chloride abstraction, an adduct formulated as $[(\text{104})\text{MCl}_2 \cdot \text{Ti}(\text{OTf})_4]$ and structurally characterized [124].

Homoleptic complexes **Ni7**, **Pd3**, **Pt3** (Scheme 54) incorporating only the **104** ligand were also obtained by Dunbar starting from the “naked” metal cations $[\text{M}(\text{CH}_3\text{CN})_x][\text{BF}_4]_2$ ($\text{M} = \text{Ni}$, $x = 6$ [127]; $\text{M} = \text{Pd}$, $x = 4$ [128], $\text{M} = \text{Pt}$, $x = 4$ [129]) under the general formula: $[(\text{104})_2\text{M}][\text{BF}_4]_2$ ($\text{M} = \text{Ni}$, Pd , Pt) [108]. The three **Ni7**, **Pd3** and **Pt3** complexes, isolated as toluene solvate, are isomorphous (Fig. 30). They exhibit a square-planar geometry with averaged Ni–P, Pd–P and Pt–P distances of 2.255, 2.343 and 2.340 Å, respectively. The TTF units are now strongly distorted from planarity, with a folding of the phosphine-functionalized dithiole ring by 31 – 32° , by contrast with the $[(\text{104})\text{MCl}_2]$ **Ni5**, **Pd2** and **Pt2** complexes where the TTF was essentially planar. The molecular packing is characterized by a face-to-face organization of the TTF moieties, most probably stabilized by an extended set of S...S van der Waals interactions (Fig. 30).

A large downfield shift of the ^{31}P NMR resonance (Table 16) was observed for all three complexes, measured at 42.3 and 43.9 ppm for the Ni and Pd complexes **Ni7** and **Pd3** while the Pt complex **Pt3** showed a singlet at 35.8 ppm with platinum satellites ($^1J_{\text{Pt-P}} = 2357$ Hz). Electrochemical investigations showed no sign of interaction between the two TTF moieties through the chelated metal atom. The first two-electron reversible oxidation wave was observed at 0.68, 0.64 and 0.70 V vs. Ag/AgCl for the **Ni7**, **Pd3** and **Pt3** complexes respectively, to be compared with the first oxidation potential of **104** reported at 0.46 V in the same conditions.

The tetraphosphine ligand **103** (Scheme 32) contains *trans* binding sites that can be used to join metals in oligomeric arrays and its reaction was accordingly investigated with the labile starting materials mentioned above $[\text{M}(\text{CH}_3\text{CN})_4][\text{BF}_4]_2$. Soluble products

Table 16

Evolution of ^{31}P NMR coordination chemical shift ($\Delta\delta$, in ppm) in the homoleptic complexes with ligands **104** or **103**.

L	$[(\text{L})_2\text{Ni}]^{2+}$	$[(\text{L})_2\text{Pd}]^{2+}$	$[(\text{L})_2\text{Pt}]^{2+}$	Reference
104	61.1 (Ni7)	62.7 (Pd3)	54.6 (Pt3 , $^1J_{\text{P-Pt}} = 2357$ Hz)	[108]
103	–	60.4 (Pd4)	51.4 (Pt4 , $^1J_{\text{P-Pt}} = 2401$ Hz)	[131]

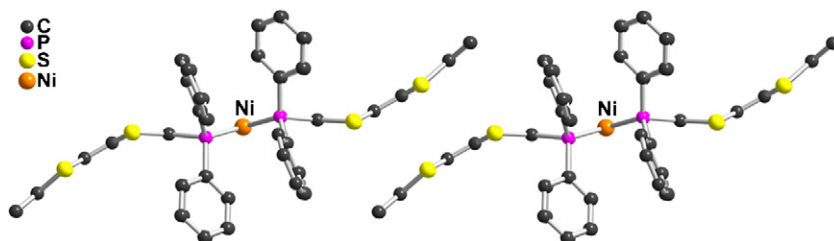


Fig. 30. A view of the solid state arrangement in **Ni7**, [(**104**)₂Ni](BF₄)₂·3(toluene) [108].

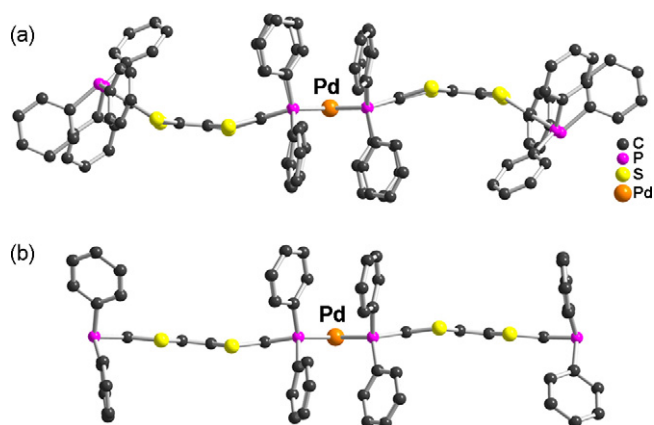
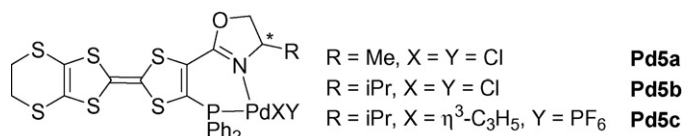


Fig. 31. A side view of the **Pd4** complexes in their (a) CH₂Cl₂ solvate and (b) CH₂Cl₂/toluene solvate [131].

which exhibit a single ³¹P resonance – indicative of a structure without phosphorus end groups [130] – were isolated and formulated as {[(**103**)M][BF₄]₂]_n, but could not be crystallized. The simplest entity of these oligomers, that is the homoleptic mononuclear complexes were thus described [131]. By using the same metallic precursors with an excess of **103**, the dicationic complexes **Pd4** and **Pt4** [(**103**)₂M]²⁺ (M = Pd, Pt) were isolated as BF₄[−] salts and structurally characterized, either as CH₂Cl₂ or as CH₂Cl₂/toluene solvates. They adopt the same square planar geometry around the metal cation in the four crystal structures but, as shown in Fig. 31, different folding angles for the dithioether rings of the TTF core and different orientations of the outer, non-coordinated PPh₂ groups. Because of the presence of these free PPh₂ groups on the outer ends of the complexes, the ³¹P{¹H} NMR spectra exhibit now two resonance lines, one at −18 ppm attributed to the free PPh₂ moieties, one at +41.6 ppm (for **Pd4**) or +32.6 ppm (for **Pt4**, with ¹J_{P–Pt} = 2401 Hz) for the coordinated phosphines. As shown in Table 16, the coordination chemical shifts Δδ are slightly smaller while the ¹J_{P–Pt} coupling constants are comparable.

3.5.3. The Ni, Pd, Pt triad with P,N-ligands

Complexes of the P,N ligands are limited to those based on the tetrathiafulvalene phosphino-oxazolines **91a** and **91b** (Scheme 55). Pd salts have been investigated for their possible use in asymmetric catalytic reactions, by analogy with the phosphino-oxazolines initially developed by Pfaltz [132], Helmchen et al. [133] and Williams



Scheme 55. Palladium phosphino-oxazoline complexes.

[134]. Indeed, the incorporation of TTF – rather than ferrocene – as backbone for phosphino-oxazoline ligands opens the way to a new class of redox active chiral ligands which would eventually allow an electrochemical modulation of the catalytic processes thanks to the electroactive TTF core [135].

The PdCl₂ complex **Pd5a** of the racemic methyloxazoline derivative was first described and structurally characterized (Fig. 32) [74]. The metal adopts a square-planar geometry while the TTF core exhibits strong distortions from planarity. An anodic shift of 0.24 V for the two TTF redox waves is observed upon complexation, in the same range that observed with the chelating diphosphine **104** (See Section 5). In order to increase the steric hindrance of the oxazoline substituent of these chiral auxiliaries, the *isopropyl*-oxazoline derivatives were investigated in palladium catalyzed asymmetric allylic alkylation [75]. The Pd precatalysts were generated from the reaction of the free optically pure (*R*) or (*S*) ligand with [Pd(η³-C₃H₅)Cl] to give, after TlPF₆ addition the series of cationic Pd complexes [Pd(η³-C₃H₅)(**91b**)] [PF₆] **Pd5c**. These complexes exhibit a sizeable, albeit smaller than the PdCl₂ complex, anodic shift of the TTF first redox potential (0.18 V), yet showing a full reversibility. A salt of the oxidized TTF species was even obtained upon oxidation with NOSbF₆, formulated as [Pd(η³-C₃H₅)(**91b**)] [PF₆] [SbF₆], its optical activity has been confirmed through circular dichroism measurements.

3.6. The Cu, Ag, Au triad (group 11)

3.6.1. The Cu, Ag, Au triad with N-ligands

A large number of different Cu(I) and Cu(II) complexes has been described with N-based TTF ligands and they are detailed below (Scheme 56). They differ by the nature of the ligand (pyridine but also phenanthrolines, phthalocyanines) and its separation from the TTF core. These complexes are *a priori* particularly attractive in the context of this review article because the redox potential of the Cu(II)/Cu(I) system coordinated with pyridine, bipyridine or

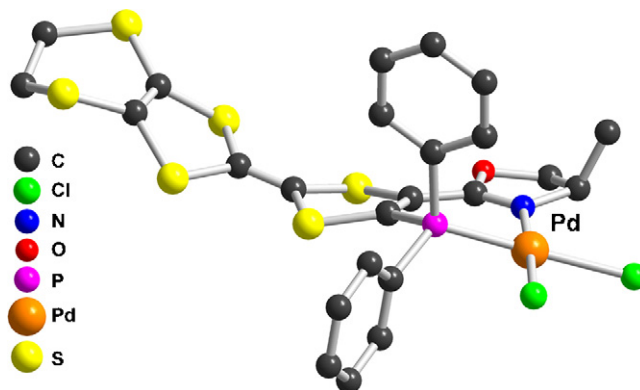
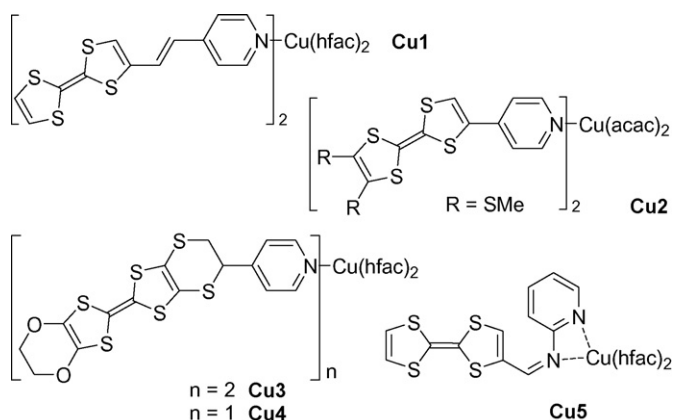


Fig. 32. A view of **Pd5a**, the PdCl₂ complex of the racemic methyl-oxazoline derivative **91a**. Only one of the two enantiomers is shown [74].



Scheme 56.

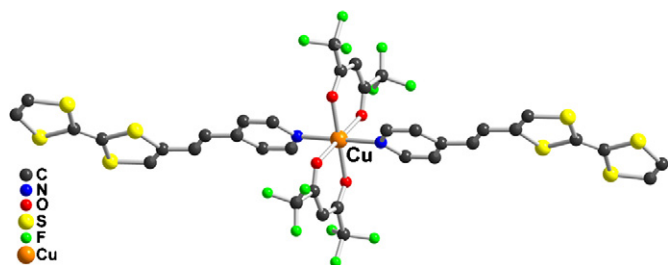
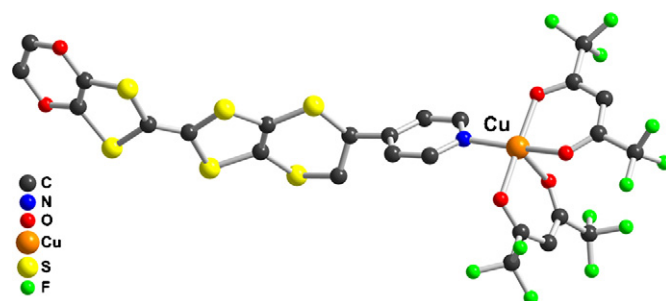
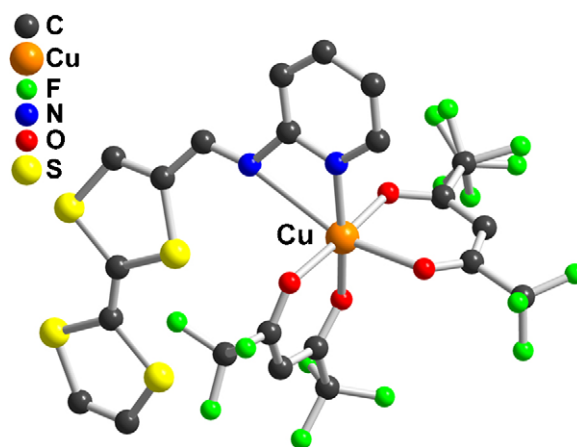
phenanthroline ligands can be close to that of the TTF⁺/TTF redox system, opening possibilities for mixed-valence systems.

Perhaps the first and best example of copper complex, **Cu1**, was reported by Ouahab in 2001 [136]. It is based on the *trans* coordination of a Cu(hfac)₂ complex with the TTF-CH=CH-4-Py ligand **14a** (Fig. 33). The paramagnetic nature of the complex is attributed to the *S* = 1/2 configuration of the Cu(II) center.

The complex oxidizes in two successive reversible redox waves at +0.42 and +0.83 V, each of them involving 2e⁻, indicating that the TTF center are simultaneously oxidized. Its electrocrystallization in the presence of ⁿBu₄NPF₆ afforded a mixed-valence salt, (**Cu1**)⁺, formulated as [Cu(hfac)₂(**14a**)₂](PF₆)·2CH₂Cl₂ [137]. This represents the very first example of a complex based on a TTF ligand, where the TTF itself is oxidized to the cation radical state, and more interestingly, into an appealing mixed-valence state. Its magnetic behavior will be described in more detail in Section 4. The electrocrystallization of the neutral **Cu1** complex in the presence of the smaller BF₄⁻ anion allowed for the isolation of a novel salt where now each TTF is oxidized to the radical cation [138], that is (**Cu1**)²⁺, formulated as [Cu(hfac)₂(**14a**)₂](BF₄)₂·2CH₂Cl₂.

Other Cu(hfac)₂ or Cu(acac) complexes such as **Cu2–4** have been described (Scheme 56) [31,139]. While *trans* octahedral complexes (**Cu2** and **Cu3**) are obtained when using two equivalents of donor ligands **8** and **29**, penta-coordinated *cis* complex **Cu4** was also isolated with **29**, as shown in Fig. 34. In most complexes, as already observed above with **Cu1**, the redox potential of the TTF core is not affected at all by coordination. Only in the case of **Cu2** where the pyridine is directly conjugated with the TTF core, a cathodic shift upon coordination was observed since the free ligand **8** oxidizes at 0.494 and 0.797 V vs. SCE while the *trans* complex [Cu(acac)₂(**8**)₂] oxidizes at 0.475 and 0.777 V vs. SCE.

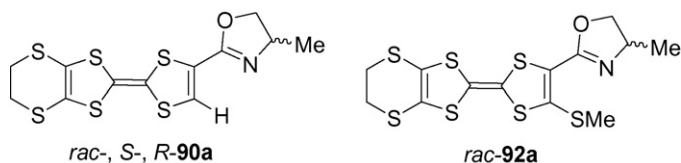
A bidentate imine TTF derivative **17** was also engaged in a Cu(hfac) complex **Cu5** [23]. As shown in Fig. 35, the Cu^{II} adopts a distorted octahedral geometry, with bonding in the equatorial plane

Fig. 33. A view of the neutral complex [Cu(hfac)₂(**14a**)₂] **Cu1** [136].Fig. 34. A view of one of the two crystallographically independent molecules of the penta-coordinated *cis* complex **Cu4** [31].Fig. 35. A view of **Cu5** with the TTF imine ligand **17** [23].

of three O atom of the hfac ligands and the N atom of the pyridine. The imine N2 atom and one hfac O atom (O3) complete the coordination sphere, with a Cu–O3 distance (2.1999(19) Å) longer than the three equatorial Cu–O distances that range between 1.9474(17) and 1.9737(18) Å.

Comparable *cis* complexes of [Cu(hfac)₂] were also isolated with the racemic, *R*- and *S*-TTF-methyloxazolines derivatives **90a** and **92a**, providing the first complete series of metal complexes with chiral tetrathiafulvalenes (Scheme 57) [118].

Indeed, they all form with [Cu(hfac)₂] a 1:1 adduct formulated as **Cu6**: [(**90a**)Cu(hfac)₂] and **Cu7**: [(**92a**)Cu(hfac)₂]. Both complexes oxidize at the same potential as the starting TTF ligand. The Cu(II) adopts a distorted square pyramidal coordination geometry with a weaker interaction with a sulfur atom of the TTF dithiole ring (Fig. 36), with Cu···S_{TTF} distances in a 2.91–3.04 Å range. The basal plane is formed by three oxygen atoms (Cu–O: 1.90–1.96 Å) and the nitrogen atom of the oxazoline (Cu–N: 1.96–1.98 Å), while the last oxygen atom of the hfac ligands is located in the apical position, at a longer Cu–O distance (2.19–2.22 Å). Surprisingly, the introduction in **Cu7** of a complementary-SMe group located α to the oxazoline ring in **92a** does not modify this coordination scheme (Fig. 36c). The racemic complex [(rac)-**90a**][Cu(hfac)₂] rac-**Cu6** crystallizes in



Scheme 57.

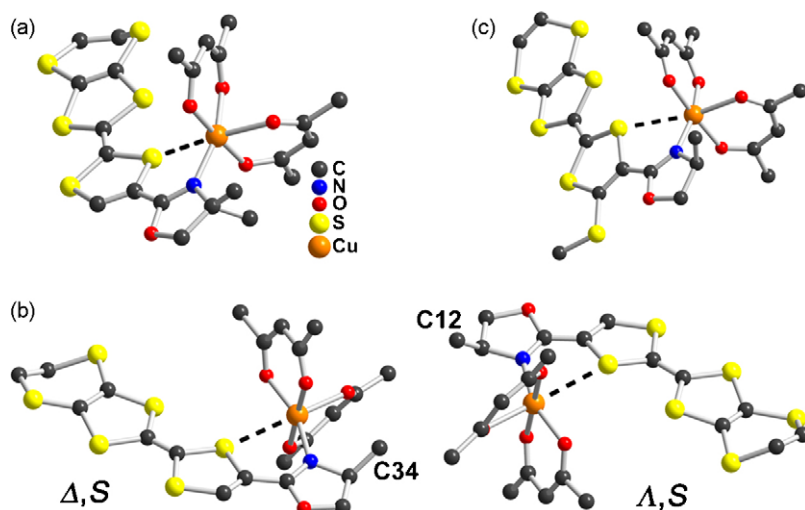


Fig. 36. Detail of the coordination sphere of the Cu(II) species in: (a) *rac*-**Cu6**, (b) (*S*)-**Cu6**, (the two diastereoisomers Δ,S and Λ,S are shown), (c) *rac*-**Cu7**. The fluorine atoms of the hfac ligands have been omitted for clarity [118].

the triclinic P-1 space group with the methyl group of the oxazoline disordered on two positions (C12A, C12B in Fig. 36a). On the other hand, the enantiopure complexes obtained with (*R*)-**90a** and (*S*)-**90a** crystallize in the chiral P1 space group with almost identical cell parameters. This implies the presence of two crystallographically independent molecules in the enantiopure complexes, described as (Λ,S) and (Δ,S) diastereoisomers (Fig. 36b and c) if one considers the distorted octahedral coordination configuration around the Cu(II) atoms. Investigation of the magnetic properties of **Cu6** and **Cu7** showed a Curie-type behavior attributed to the presence of non-interacting Cu(II) species with $g=2.12$ – 2.16 .

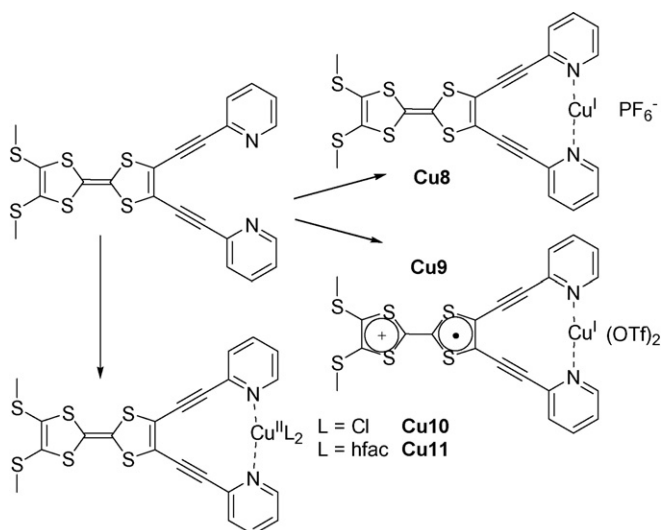
A beautiful series of copper complexes (Scheme 58) has been described by Iyoda starting from the 4',5'-bis(methylthio)-4,5-bis(2-pyridylethynyl)tetrathiafulvalene **23** [26]. Its rigid, chelating geometry allowed for the isolation of several Cu^I and Cu^{II} salts, with possibilities for charge-transfer interactions between the TTF and the copper center (Fig. 37).

Indeed, while the reaction of the free ligand **23** with [Cu(CH₃CN)₄]PF₆ afforded the Cu^I complex **Cu8**, the reaction with Cu^{II}(OTf)₂ led to the TTF oxidation with concomitant Cu^{II} reduction and complexation. As a consequence, the triflate salt **Cu9** is

best described as a TTF cation radical, associated with a Cu^I complex. On the other hand and based on EPR results, the Cu^{II}Cl₂ and Cu^{II}(hfac)₂ complexes **Cu10** and **Cu11** are essentially seen as real Cu^{II} complex with no TTF oxidation.

Other investigations of possible charge-transfer reactions between a TTF core and a Cu^{II} species were based on pyrazino-fused TTF **75** or **80a** (Scheme 59). Copper complexes were obtained by co-crystallization with CuCl₂ to afford respectively **Cu12** (75·CuCl₂) [72], **Cu13** (80a·CuCl₂) [71], or **Cu14** (80a₂·80a·Cu₃Cl₄) [71].

In **Cu12**, ESR and SQUID measurements demonstrated that the oxidation states are TTF⁰ and Cu²⁺ while the Cu^{II} species form uniform magnetic chains (Fig. 38a), which can find their origin, either in a direct interaction (Cu^{II}...Cu^{II} distance at



Scheme 58. Copper (I) and (II) of the bis(2-pyridylethynyl)tetrathiafulvalene **23**.

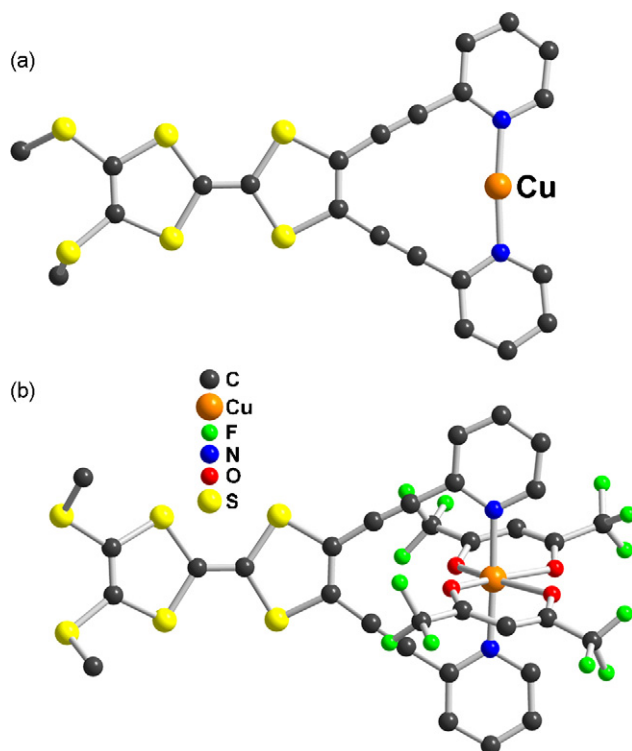
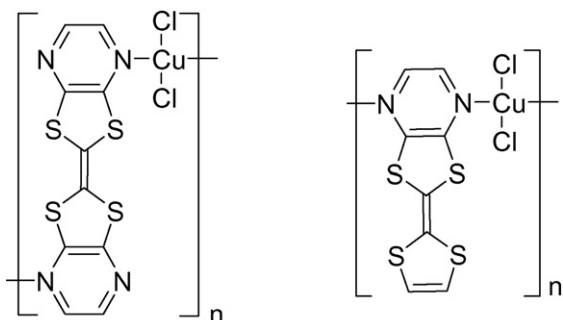


Fig. 37. Molecular structures of (a) the Cu^I **Cu8** and (b) the Cu^{II} **Cu11** complexes [26].



Scheme 59. Supramolecular complexes **Cu12** ($75 \cdot \text{CuCl}_2$) left and **Cu13** ($80\text{a}^+ \cdot \text{CuCl}_2$) right.

3.87 Å), a super-exchange interaction through Cl^- atom ($\text{Cl}^- \cdots \text{Cu}$ distance at 2.99 Å) or through the coordinated bis(pyrazino)-tetrathiafulvalene molecule. Since the bis-pyrazino-TTF **75** oxidize at rather high potentials, the monopyrazino derivative **80a** was

also investigated with the hope that reaction with CuCl_2 will lead to oxidized TTFs salts, as indeed observed in **Cu13** and **Cu14**. In the former, the two nitrogen atoms of the pyrazine ring are engaged in the coordination, leading to the formation of $[-\text{CuCl}_2-\mathbf{80a}-]_\infty$ chains (Fig. 38b). **Cu13** exhibits antiferromagnetic interactions ($2J/k = -20 \text{ K}$), attributed to the Cu^{II} species interacting into layers and behaves as a semiconductor ($\sigma_{\text{RT}} = 10^{-4} \text{ S cm}^{-1}$ and $E_a = 0.33 \text{ eV}$), due to partial doping with the CuCl_2 . On the other hand, a commensurate charge transfer takes places in **Cu14** (Fig. 38c), which is characterized by non-coordinated mixed-valence $(\mathbf{80a})_2^{\bullet+}$ species organized into layers with a so-called α'' motif, separated from each other by anionic layers formed by another **80a** molecule, coordinated to a copper (I) Cu_3Cl_4 one-dimensional motif with two kinds of Cu^{I} : one has a tetragonal CuCl_3N geometry with a full Cu occupancy while the other has a bent CuCl_2 geometry with half the occupancy. Due to this partial charge transfer and two-dimensional segregation, this salt exhibits a sizeable conductivity ($\sigma_{\text{RT}} = 10^{-1} \text{ S cm}^{-1}$ and $E_a = 0.15 \text{ eV}$) with a magnetic behavior (uniform spin chain with $2J/k = -42 \text{ K}$)

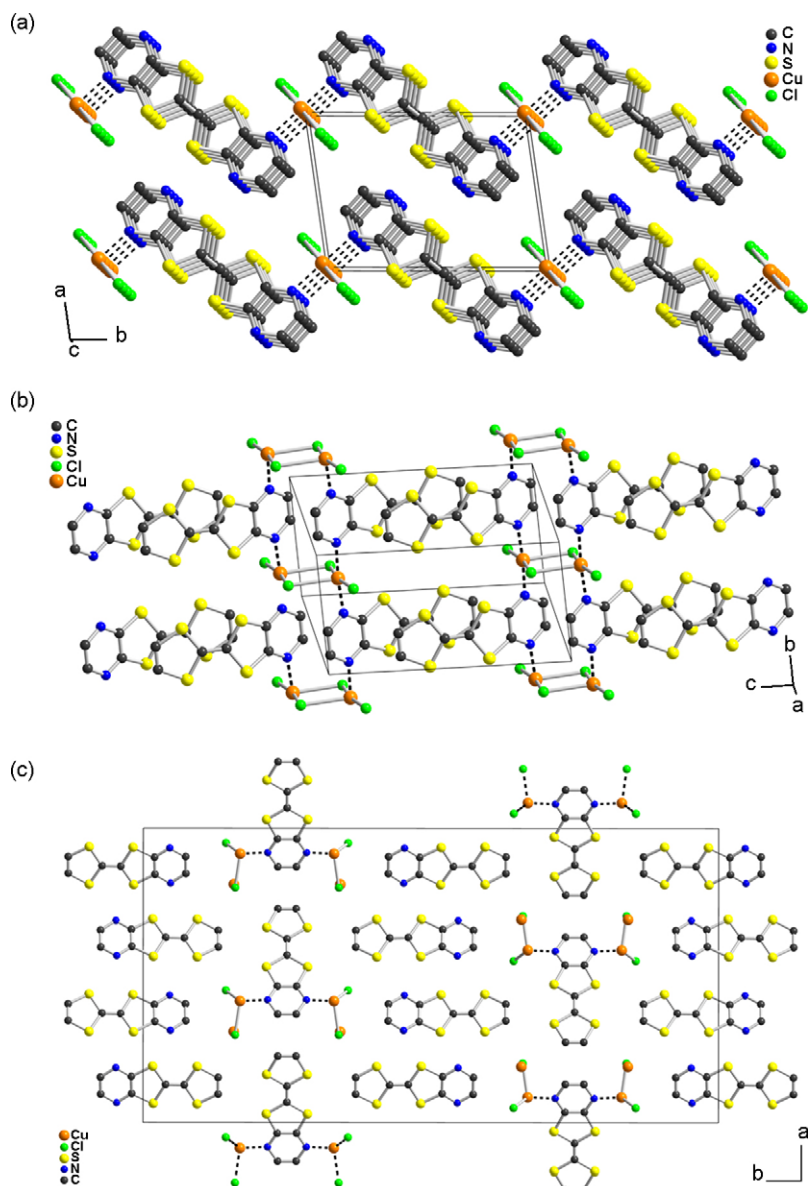
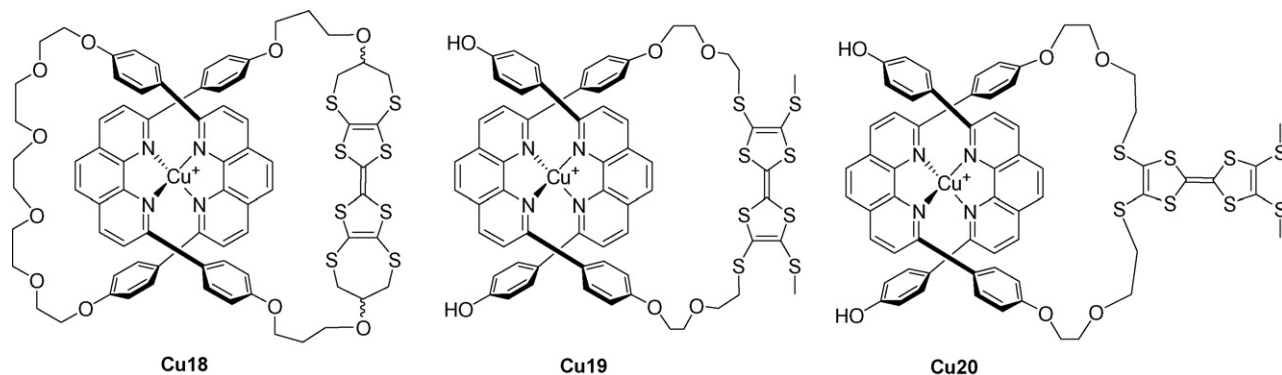


Fig. 38. (a) The solid-state organization in **Cu12**, showing the square-planar geometry around the Cu^{II} cation and the columns of CuCl_2 moieties running along c [72]. (b) The structure of **Cu13** [71]. (c) A projection view of the unit cell of **Cu14** showing the layered structure [71].



Scheme 60. Catenates and macrocycles.

attributed, on the basis of calculated overlap integrals, to a one-dimensional interaction between magnetic ($80a$) $_2^{\bullet-}$ species along *a*.

Among the different 2,2'-bipyridine molecules incorporating the tetrathiafulvalenyl core (see Section 2.1.6), the amide derivative **64** has been engaged in Cu(I)/Cu(II) complexes, upon reaction with either CuPF_6 or $\text{Cu}(\text{OTf})_2$, affording the bis(bipyridine) complexes **Cu15**: $[(\mathbf{64})_2\text{Cu}]\text{PF}_6$ and **Cu16**: $[(\mathbf{64})_2\text{Cu}](\text{OTf})_2$ or the mono-bipyridine complex **Cu17**: $[(\mathbf{64})\text{Cu}(\text{DMF})_3](\text{OTf})_2$ [140]. Redox behavior of the Cu(I) complex shows three successive oxidation waves, with the first one attributed to the Cu(I)/Cu(II) oxidation process, the two others to the TTF core. The reduction scan shows that the generated Cu(II) species reduces at much lower potential, a consequence of solvent coordination of the Cu(II) species which most probably stabilizes with solvent coordination into a square planar pyramidal or distorted octahedral geometry. X-ray crystal structure of **Cu17** (Fig. 39) shows a square planar pyramidal coordination sphere around the Cu(II) ion, with the basal plane formed by the two nitrogen atoms of the bipyridine and two oxygen atoms of coordinated DMF molecules, while a third DMF molecule occupies the apical position.

Phenanthroline Cu^I complexes incorporating a tetrathiafulvalene core in macrocyclic systems (**72**, **73a** and **73b**) have been also reported (Scheme 60), either as catenanes [53] in **Cu18** or in open macrocycles [54] such as **Cu19** or **Cu20**. Catenate **Cu18** was only characterized by its mass spectrum and its ¹H NMR spectrum which shows the presence of two diastereoisomeric species in a 77:23 ratio. Macrocycles **Cu19** and **Cu20** were essentially characterized by cyclic voltammetry and differential pulse voltammetry. Interestingly, large anodic shifts of both the first and second oxidation wave of the TTF are observed relative to the free macrocycle, as a result of the electrostatic influence exerted by the Cu⁺ metal ion. The Cu⁺ is oxidized into Cu²⁺ species in between the two TTF redox processes (Table 17). It should be stressed also that the generated Cu²⁺ species is not expelled but maintained in the complex since

Table 17

Differential pulse voltammetry data (vs. Ag/AgCl) in CH_2Cl_2 containing 0.1 M NBu_4PF_6 .

Compound	$E_{\text{ox}}^1/\text{V} (\text{TTF}^{\bullet+}/\text{TTF})$	$E_{\text{ox}}^2/\text{V} (\text{Cu}^{2+}/\text{Cu}^+)$	$E_{\text{ox}}^3/\text{V} (\text{TTF}^{2+}/\text{TTF}^{\bullet+})$
Cu19	0.56	0.70	0.82
Cu20	0.54	0.69	0.82

the second TTF oxidation is also affected by the presence of the Cu²⁺ species.

As already mentioned for its Ni complex (**Ni4**), the tetradentate tetrathiafulvalene-based salphen molecule **97** has also been engaged in Cu(II) coordination to afford **Cu21** (Scheme 61) [81], with a structure very close to that of **Ni4** (Fig. 27). Electrochemical properties of **Cu21** are essentially those of the free ligand **97**, together with an added reversible reduction wave at -1.16V (vs. Ag/AgCl, in CH_2Cl_2) attributed to the Cu²⁺/Cu⁺ redox couple.

3.6.2. The Cu, Ag, Au triad with P-ligands

Cu(I) and Ag(I) complexes with the chelating diphosphine **104** have been reported as homoleptic bis(diphosphine) complexes $[(\mathbf{104})_2\text{Cu}]^+$ and $[(\mathbf{104})_2\text{Ag}]^+$ [108]. As shown in Fig. 40 for $[(\mathbf{104})_2\text{Ag}]^+$, the d¹⁰ metal cation in both complexes occupies the center of a distorted tetrahedron with P–M–P angles within each metallacycle of $\approx 84^\circ$ for Ag and $\approx 90^\circ$ for Cu. Within the complex, one TTF moiety exhibits an almost planar conformation while the other is strongly bent along the S...S axis of the dithiole ring bearing the PPh₂ groups. Both complexes exhibit a 120–140 mV anodic shift of the TTF oxidation potentials, to be compared with the 220 (Ni), 180 (Pd) or 240 (Pt) mV anodic shifts observed in the square-planar d⁸ complexes mentioned above in Section 3.5.2. This reduced shift is probably attributable to the reduced cationic charge of the metallic center in the Cu⁺ and Ag⁺ complexes, when compared with the dicationic Ni²⁺, Pd²⁺ or Pt²⁺ centers. The corresponding Au³⁺ complex has not been described yet to check this assumption but several

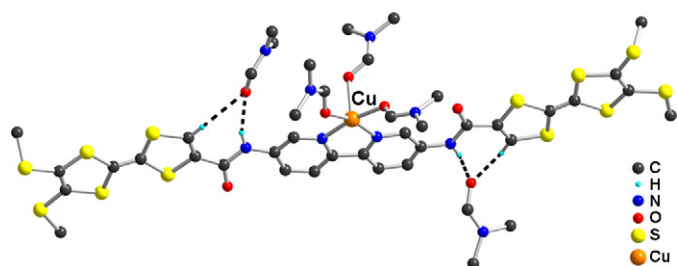
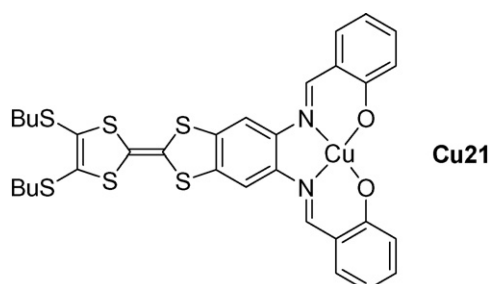


Fig. 39. View of **Cu17**, showing the complementary hydrogen-bonding of the amidic N–H and TTF C–H toward the carbonyl oxygen atom of DMF molecules [140].



Scheme 61.

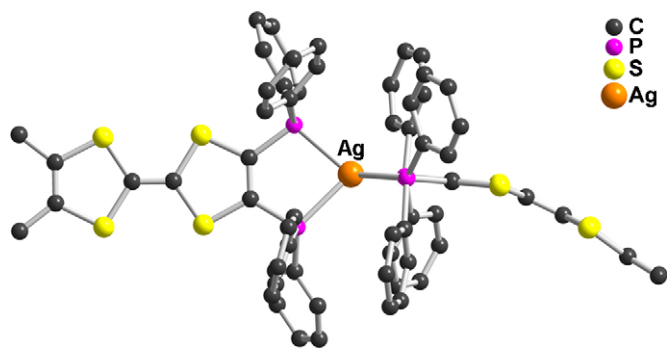
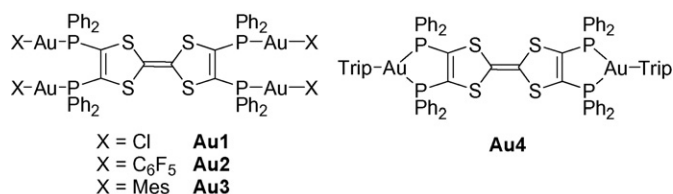


Fig. 40. A view of the tetrahedral Ag^+ complex with **104** [108].



Scheme 62. Gold (I) complexes of the tetraphosphine **103**.

Au(I) complexes were reported by Laguna (Scheme 62), based on the tetradentate **103** ligand [141].

Indeed, reaction of **103** with $[\text{AuX}(\text{tht})]$ ($\text{X} = \text{Cl}, \text{C}_6\text{F}_5$; tht = tetrahydrothiophene) or $[\text{Au}(\text{Mes})(\text{AsPh}_3)]$ ($\text{Mes} = 2,4,6\text{-Me}_3\text{-C}_6\text{H}_2$) afforded the tetranuclear complexes $[(\text{103})(\text{AuX})_4]$, **Au1** ($\text{X} = \text{Cl}$), **Au2** ($\text{X} = \text{C}_6\text{F}_5$) and **Au3** ($\text{X} = \text{Mes}$) while the use of the more sterically demanding $[\text{Au}(\text{Trip})(\text{AsPh}_3)]$ ($\text{Trip} = 2,4,6\text{-Pr}_3\text{C}_6\text{H}_2$) provided the dinuclear derivative **Au4**, $[\text{103}(\text{AuTrip})_2]$ [141]. The chelating coordination of **103** in **Au4** was inferred from the observation of one singlet in the $^{31}\text{P}\{^1\text{H}\}$ in its NMR spectrum. Cyclic voltammetry experiments for the four complexes reveals a strong anodic shift of the oxidation potentials of the TTF core, with the first oxidation wave shifted by 500, 430, 380 and 240 mV, relative to the free ligand. The anodic shift in **Au1** (500 mV) represents the largest value reported so far, a consequence of (i) the four metallic center coordinated to the TTF and (ii) the electronegativity of the Cl^- counter ion, by comparison with C_6F_5^- or Mes^- . **Au1** was also the only complex structurally characterized. As shown in Fig. 41, the coordination around the gold atoms deviates slightly from linearity, which is typical for Au(I)

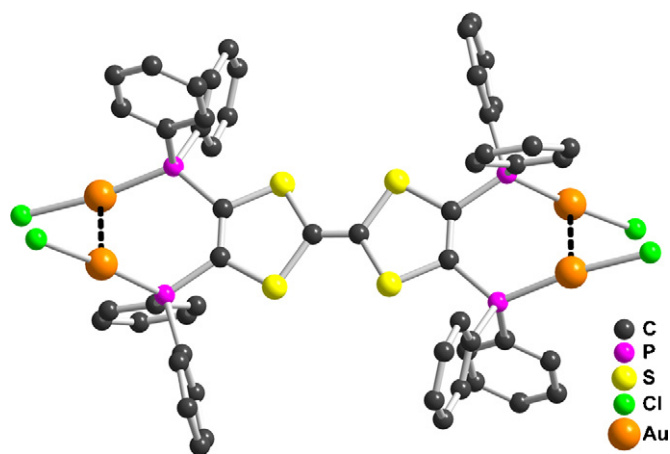
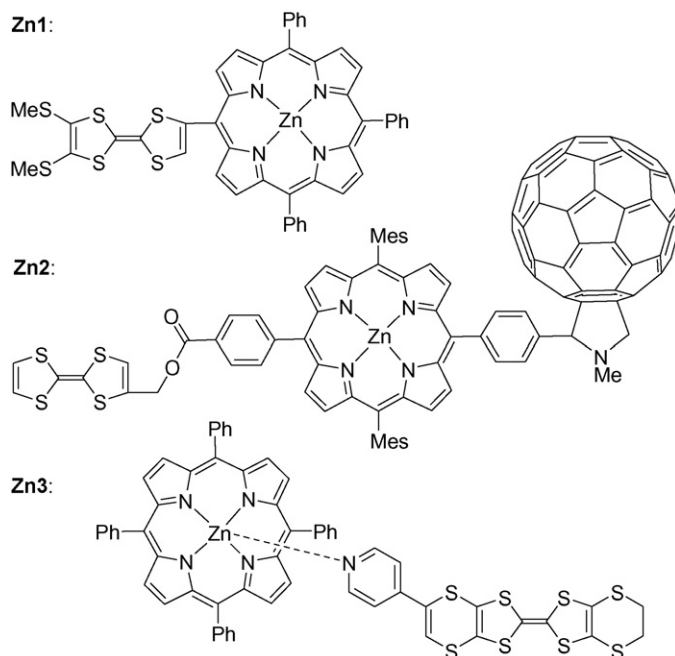


Fig. 41. A view of **Au1**, showing the aurophilic $\text{Au}\cdots\text{Au}$ interaction (dotted line) [141].



Scheme 63. Zn porphyrins complexes incorporating a TTF moiety.

complexes, with P-Au-Cl angles of $174.41(10)$ and $172.10(10)^\circ$. A short intramolecular $\text{Au}\cdots\text{Au}$ interaction at $3.0081(8)\text{\AA}$ denotes the presence of aurophilic interactions.

3.7. The Zn, Cd, Hg triad (group 12)

Zn complexes incorporating a TTF ligand essentially involve Zn porphyrins and phthalocyanines, with the TTF covalently linked to the macrocyclic motif, as shown below for **Zn1** or **Zn2** (Scheme 63). They were developed as molecular fluorescence switches taking advantage of the TTF redox couple as triggers to eventually adjust the luminescence of light-emitting fragments such as ZnTPP.

The cyclic voltammogram of **Zn1** exhibit four reversible oxidation waves [142]. The two first ones at 0.52 and 0.93 V (vs. Ag/AgCl) are attributed to the TTF core while the two others at 1.07 and 1.27 V are due to the ZnTPP system. Compared with the non-metalled porphyrin, a coordination anodic shift of 50 mV affects the first oxidation wave. The oxidation of the Zn tetraphenylporphyrin, usually observed at 0.84 and 1.15 V under the same conditions, is shifted here to more anodic potentials, due to the Coulombic influence of the initially oxidized dicationic TTF^{2+} moiety. These effects are purely electrostatic as the UV-vis. spectrum of **Zn1** is interpreted in terms of simple superposition of the electronic transitions of the two constituents, supporting non-conjugation through the orthogonal *meso* linkage. A 75–80% quenching of the fluorescence of the simple ZnTPP is observed in **Zn1**. No such electrochemical shifts are observed in **Zn2** [143], where the three redox centers (TTF, ZnTPP and C_{60}), are almost independent. On the other hand, photochemical investigations of **Zn2** showed that a transient charge-separated state $\text{TTF}^+\text{-ZnTPP}^+\text{-C}_{60}^{\bullet-}$ is formed by ultrafast electron transfer with a time constant of 1.5 ps. The final $\text{TTF}^+\text{-ZnTPP}^+\text{-C}_{60}^{\bullet-}$ state is generated with a quantum yield of 16% and has also a lifetime of 660 ns.

Another approach toward such molecular switches consists in using a TTF derivatized with a pyridine ring, such as **28**, to directly coordinate a Zn porphyrin to give **Zn3** [144]. Red shift of the Soret and Q bands of the ZnTPP confirmed the axial coordination.

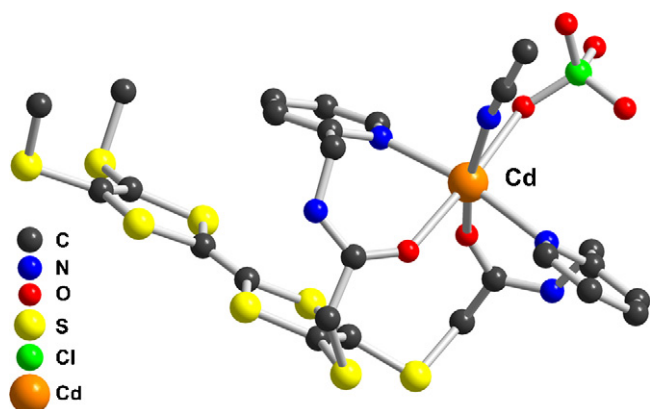
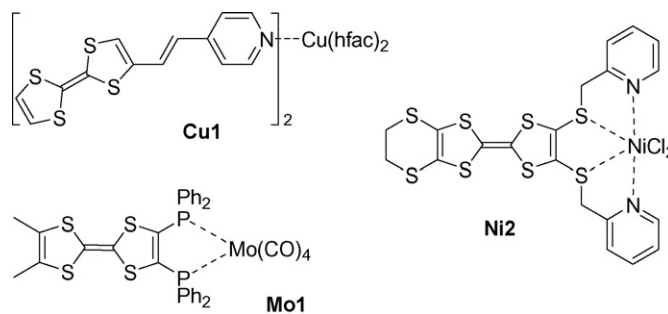


Fig. 42. View of the cadmium complex **Cd1**, based on the bipyridyl molecule **37** [35].



Scheme 64. The three complexes isolated as TTF cation radicals.

electronic properties associated with the radical nature of the TTF core.

4.1. Cation radical salts of the copper complex **Cu1**

As described in Section 3.6.1, the electrocrystallization of the copper complex **Cu1** in the presence of ${}^n\text{Bu}_4\text{NPF}_6$ affords a mixed-valence salt, $(\text{Cu1})^+$, formulated as $[\text{Cu}(\text{hfac})_2(\mathbf{14a})_2](\text{PF}_6)_2 \cdot 2\text{CH}_2\text{Cl}_2$ [137] while its electrocrystallization in the presence of the smaller BF_4^- anion allows for the isolation of a $(\text{Cu1})^{2+}$ salt formulated as $[\text{Cu}(\text{hfac})_2(\mathbf{14a})_2](\text{BF}_4)_2 \cdot 2\text{CH}_2\text{Cl}_2$ [138]. As shown in Table 18, the progressive oxidation of the TTF core in **14a**, from an oxidation state of 0 to 0.5 and 1 leads to a marked lengthening of the central C=C double bond with concomitant shortening of the internal C–S bonds. This general effect in TTF salts is due to the nature of the TTF HOMO, which is C=C bonding and C–S antibonding. The coordination of the pyridine group does not appear to be affected by the oxidation state of the TTF. In other words, coordination through pyridine is strong and the complexes tolerate very well the oxidation, without any de-coordination.

The organization of the radical molecules in the solid state differs in the two salts. Indeed in the mixed valence PF_6^- salt (Fig. 43), the TTF cores organize into dyads with a bond-over-ring overlap (Fig. 44) and short S··S intra-dyad distances (3.59 and 3.65 Å), to be compared with the larger inter-dyad interaction with the shortest S··S contacts amounting to 4.30 Å. Therefore, the salt can be described as mixed-valence $(\text{TTF})_2^{\bullet+}$ species, essentially isolated from each other, hence the insulating character of the salt. However, the magnetic susceptibility, well fitted by a Curie–Weiss law with $\theta = -3.8\text{K}$, was attributed to the sole contribution of Cu^{2+} species, on the basis of the room-temperature effective moment μ_{eff} of $1.84(3)\mu_{\text{B}}$, compatible with a $S = 1/2$ system with $g \approx 2.1$. The absence of the contribution of the mixed-valence $(\text{TTF})_2^{\bullet+}$ species was tentatively attributed to a possible charge disproportionation, with randomly alternating, magnetically silent, neutral $(\text{TTF})_2$ and dicationic $(\text{TTF})_2^{2+}$ dyads.

In the fully oxidized BF_4^- salt (Fig. 45) [138], the TTF dyads exhibit much shorter intra-dyad S··S contacts (at 3.50 and 3.29 Å) than above, but also shorter inter-dyad contacts, at 3.67 and 4.0 Å. However, due to the strong association within these $(\text{TTF})_2^{2+}$ dyads, the EPR spectra are dominated by the contribution of the Cu^{2+} species ($g = 2.11$). An intense signal centered at 2.008 is recovered

Table 18

Evolution of the bond distances within the $[\text{Cu}(\text{hfac})_2(\mathbf{14a})_2]$ complexes upon TTF oxidation. ρ is the averaged oxidation state of each TTF.

	ρ	C=C (Å)	Aver (C–S) (Å)	N–Cu (Å)	Reference
Cu1	0	1.317 (11)	1.763	2.030 (8)	[136]
(Cu1)⁺	0.5	1.370 (9)	1.734	2.016 (2)	[137]
(Cu1)²⁺	1	1.398 (4)	1.722	2.013 (2)	[138]

The fluorescence quenching reached 50% when one equiv. ligand molecule **28** was added.

Several Zn phthalocyanines have been also reported [145,146], however without any sizeable interaction between the four TTF redox centers. Other porphyrines, phthalocyanines and analogs such as pyrazino-porphyrines appended with four or eight TTF moieties have been also described as free ligands [147,148] or as Zn^{2+} , Ni^{2+} , or Cu^{2+} complexes [149,150] and will not be described in more detail here.

Finally, one single cadmium complex has been recently reported and structurally characterized [35]. It is based on the bis(pyridyl) derivative **37** (See Scheme 10). Its binding ability in the presence of Cd^{2+} was first evidenced by ${}^1\text{H}$ NMR, affording a constant formation for a 1:1 complex of $10^{4.9 \pm 0.1} \text{L mol}^{-1}$, also confirmed by UV–vis spectroscopy. A small anodic shift (+60 mV) was also observed upon complexation on the first oxidation wave, while the second oxidation wave was displaced by 110 mV, indicating that the metal is not expelled upon TTF oxidation, at variance with many other complexes. In the solid state, the complex **Cd1** adopts an octahedral coordination (Fig. 42), with two nitrogen atoms of the two pyridyl moieties, two oxygen atoms of the amidic functions, one acetonitrile nitrogen atom and one perchlorate oxygen atom while the second perchlorate anion does not participate in metal binding.

4. Cation radical salts of TTF metal complexes

A large number of metal complexes associating the redox active tetrathiafulvalenyl core have been described above in Section 3. In almost all of them, the first oxidation wave is fully reversible and associated with the TTF redox moiety. We have seen that complexes with pyridine ligands and analogs exhibit a limited anodic shift of the TTF first oxidation potential of the free ligand while complexes of TTF phosphines with the PPh_2 groups directly linked to the TTF core exhibit a 200–250 mV anodic shift, whatever the nature of the metallic group. In most cases, no mention was made of a possible de-coordination of the metal upon TTF oxidation. In those favorable conditions, it is therefore expected that most of these complexes can potentially be oxidized to the cation radical state, and organized in the solid state to afford interesting conducting and/or magnetic properties, which would eventually combine the delocalized $S = 1/2$ radical species of the TTF radical with the $S \geq 1/2$ spin of the metal fragment. As a matter of fact, only a tiny handful of such systems have been reported so far (Scheme 64). Three of them, based on the copper complex **Cu1**, the molybdenum complex **Mo1** and the nickel complex **Ni2** will be described in more detail in this paragraph in chronological order, with a special emphasis on their structural and

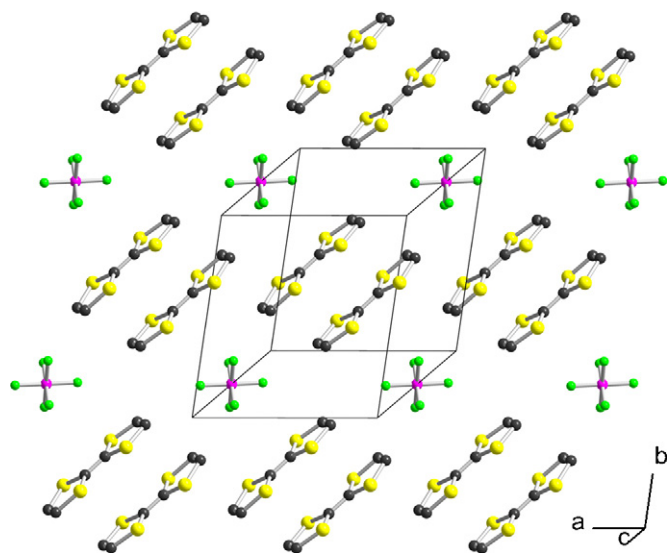


Fig. 43. Organization of the TTF dyads in the mixed-valence salt $[\text{Cu1}](\text{PF}_6)_2 \cdot 2\text{CH}_2\text{Cl}_2$ [137].

upon dissolution of the salt in DMF where the organic dyads are destroyed, a signature of the TTF cation radical.

4.2. Cation radical salts of the molybdenum complex **Mo1**

The electrocrystallization of complex **Mo1** in the presence of the Linquist anion $\text{Mo}_6\text{O}_{19}^{2-}$ afforded a 2:1 salt, formulated as $(\text{Mo1})_2(\text{Mo}_6\text{O}_{19})$ where each TTF is oxidized to the cation radical state ($\rho = 1$) [96]. From a structural point of view (Fig. 46), only the TTF moiety of the complex is affected by the oxidation, with a lengthening of the central C=C bond (1.388(5) Å vs. 1.345(5) Å in the neutral complex) and shortening of the central C–S bonds, particularly within the dithiole ring bearing the two methyl groups (1.705 Å vs. 1.744 Å in the neutral complex) while the shortening is much less pronounced in the dithiole ring bearing the organometallic complex (1.726 Å vs. 1.758 Å in the neutral complex). A very interesting feature is also the variation of the IR absorption frequencies of the carbonyl ligands upon TTF oxidation. Shifts towards larger wave numbers are observed upon oxidation for the four carbonyl absorption bands, a trend which can be rationalized in terms of a lower degree of π -back retrodonation from metal-d to CO- π^* orbitals, as a consequence of a weaker electron density on the metal in the oxidized complex.

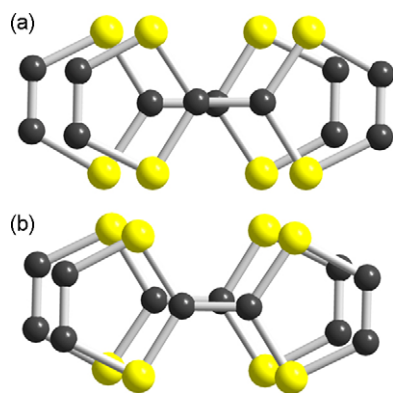


Fig. 44. A projection view perpendicular to the molecular planes of the TTF dyads in: (a) the mixed-valence $[\text{Cu1}](\text{PF}_6)_2 \cdot 2\text{CH}_2\text{Cl}_2$ salt [137] and (b) the fully oxidized $[\text{Cu1}](\text{BF}_4)_2 \cdot 2\text{CH}_2\text{Cl}_2$ salt [138].

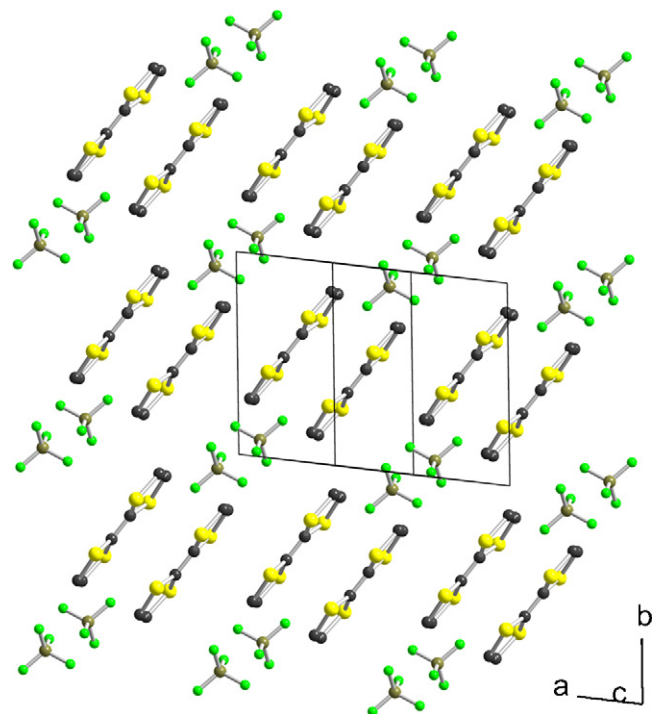


Fig. 45. Organization of the TTF dyads in the 1:1 salt $[\text{Cu1}](\text{BF}_4)_2 \cdot 2\text{CH}_2\text{Cl}_2$ [138].

At variance with the previous examples based on **Cu1**, the steric demand of the bulky diphenylphosphino groups most probably hinders here the face-to-face arrangement of the TTF cores. As shown in Fig. 47, the sole interactions between the $\text{TTF}^{\bullet+}$ radical species develop along *b*, giving rise to the formation of a uniform spin chain system. The temperature dependence of the molar magnetic susceptibility confirms this structural description with the molar magnetic susceptibility which exhibits a rounded maximum at around 11 K. A fit of this Heisenberg spin chain, with the Bonner–Fisher model affords $J/k = -17$ K, demonstrating the presence of weak but sizeable intermolecular interactions attributed to the S3...S4 contact.

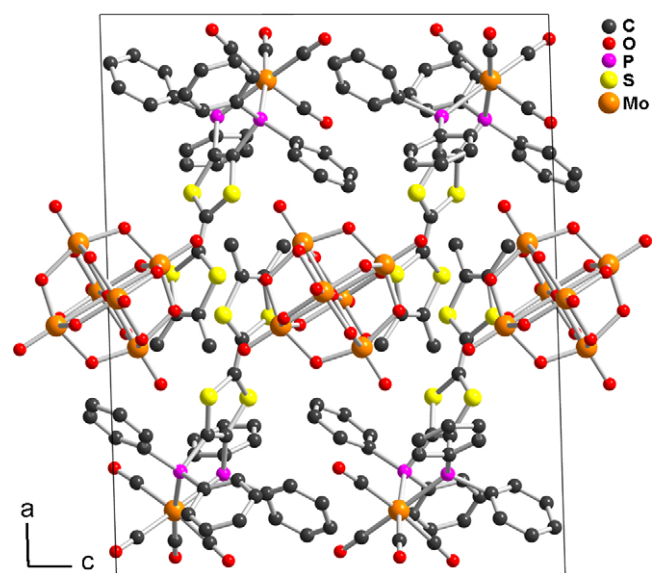


Fig. 46. Projection view along *b* of the unit cell of $(\text{Mo1})_2(\text{Mo}_6\text{O}_{19})$ [96].

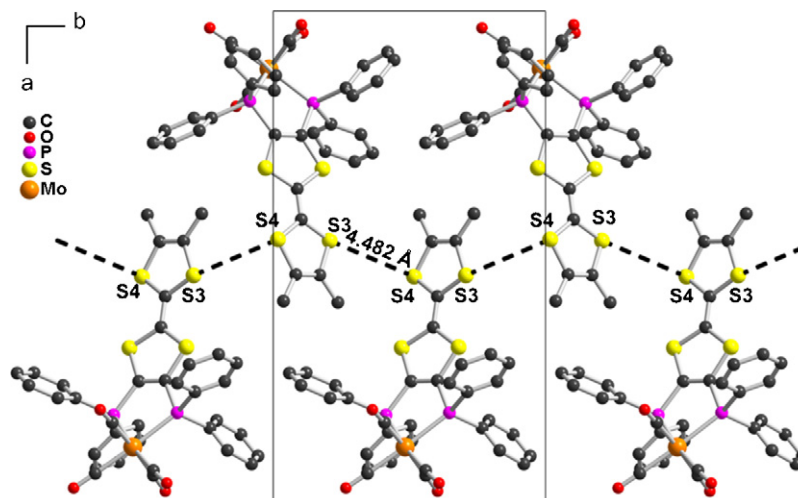
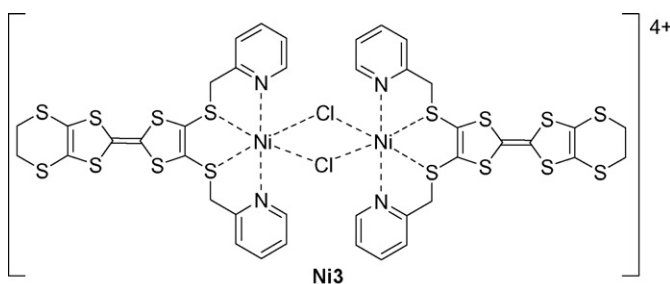


Fig. 47. A view of the uniform spin chain formed by the oxidized $(\text{Mo1})^{\bullet+}$ species in $(\text{Mo1})_2(\text{Mo}_6\text{O}_{19})$ [96].



Scheme 65. Structure of the oxidized complex **Ni3**.

4.3. Cation radical salts of the nickel complex **Ni2**

As already mentioned above in Section 3.5.1, oxidation of the mononuclear complex **Ni2** with iodine afforded a binuclear complex (Scheme 65) formulated as $[\text{Ni}_2(\mu\text{-Cl})_2(\mathbf{51}^{\bullet+})_2]^{4+}(\text{I}_3^-)_4(\text{I}_2)_3 \cdot (\text{H}_2\text{O})_2 \cdot (\text{THF})_3$. The analysis of the structural properties of the complex anionic polyiodide network observed here gives a total I_{18}^{4-} formula, that is a 4+ charge for the **Ni3** complex [121].

This implies then that each TTF moiety is oxidized to the cation radical state. One observes indeed the classical C=C bond lengthening and C–S bond shortening usually observed upon TTF oxidation, but also and more interestingly, a modification of the Ni atom coordination sphere, with a noticeable shortening of the Ni–S bond distances (Table 19) while the Ni–N and Ni–Cl distances remain essentially the same. This tends to indicate that the oxidation strengthens the Ni–S interaction. Theoretical calculations will be needed to ascertain this overlooked point.

Table 19
Evolution of the bond distances in the Ni coordination sphere of **Ni2** and **Ni3**, depending on the degree of oxidation of the TTF core.

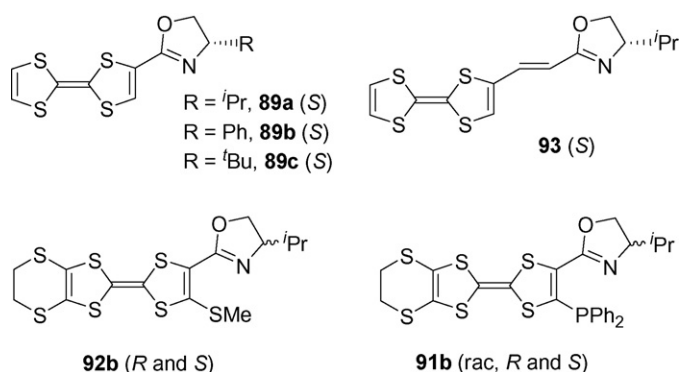
Compound	ρ	Ni–S (Å)	Ni–N (Å)	Ni–Cl (Å)	Reference	
Ni2	mol A	0	2.427 (2)	2.116 (4)	2.344 (2)	[114]
			2.442 (1)	2.127 (5)	2.375 (1)	
	mol B		2.421 (1)	2.098 (5)	2.364 (1)	
			2.425 (1)	2.099 (4)	2.373 (1)	
Ni3	1		2.369 (5)	2.070 (17)	2.365 (5)	[121]
			2.402 (5)	2.098 (19)	2.391 (5)	

In the solid state, TTF moieties are far apart from each other, the salt is insulating and its magnetic behavior, characterized by the simultaneous presence of $S=1/2$ TTF $^{\bullet+}$ and $S=1$ Ni $^{2+}$ species, has been interpreted by a ferromagnetic Ni $^{2+}$ /Ni $^{2+}$ interaction ($J_{\text{Ni}}=5 \text{ cm}^{-1}$), weak antiferromagnetic interactions, attributed to intramolecular Ni $^{2+}$ /TTF $^{\bullet+}$ interactions ($J_{\text{rad}}=-1 \text{ cm}^{-1}$) together with the effect of the zero-field splitting (ZFS) of the Ni(II) dimer, approximated with a model showing an axial geometry ($D=-10 \text{ cm}^{-1}$).

5. Catalytic applications of complexes based on TTF ligands

Besides the obvious interest in multifunctional molecular materials, another attractive field of investigation related to the TTF-containing ligands concerns homogenous catalysis based on transition metal complexes. The peculiarity of these catalysts with respect to the vast majority of transition metal complexes utilized in various catalytic processes relies on their electroactive behavior. This feature could possibly induce a modulation of the reactivity of the metal complex used as catalyst upon changing the oxidation state of the electroactive ligand [135]. Nevertheless, little attention has been paid up to date to the use of TTF ligands in catalytic reactions. In this respect, Bryce et al. first reported catalytic studies with TTF ligands involving the series of TTF-oxazolines **89a–c** and **93** (Scheme 66) [73].

Assuming that the vicinal sulfur atom of the TTF core would act as second coordination site beside the oxazoline nitrogen atom,



Scheme 66. TTF-oxazoline derivatives investigated in catalytic reactions.

Table 20
Asymmetric allylic substitution reactions with chiral TTF-oxazoline ligands.

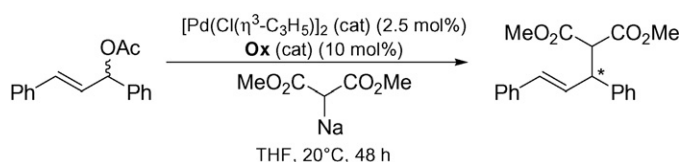
Ligand	Time (h)	Conv (%)	ee (%)	Reference
89a (S)	48	29	21 ^a	[73]
89b (S)	48	28	17 ^a	[73]
89c (S)	48	trace	–	[73]
93 (S)	72	trace	–	[73]
92b (R)	18	12	26 ^b	[75]
91b (R)	18 (70)	10 (21)	85 (80) ^b	[75]

^a Determined by ¹H NMR in the presence of Pr(hfc)₃.

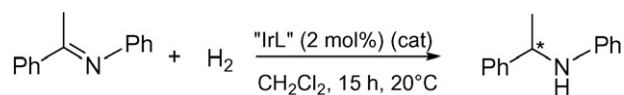
^b Determined by HPLC on a Daicel® Chiralpack® AD column.

these TTF-mono-oxazolines have been applied in the asymmetric allylic alkylation (AAA) reaction [73], which constitutes one of the most straightforward strategies for the formation of stereoselective carbon–carbon bonds [151]. However, the activities and selectivities demonstrated by the ligands **89a–c** and **93** were rather modest, since only the ligands **89a** and **89b** shown measurable activity and selectivity, with about 29% (**89a**) and 28% (**89b**) yield and 21% (**89a**) and 17% (**89b**) ee (Table 20), in the reaction of the standard substrate (*rac*)-(*E*)-1,3-diphenyl-3-acetoxy-prop-1-ene with the sodium salt of dimethyl malonate in the presence of allyl-palladium chloride dimeric precursor (Scheme 67). According to the authors, the modest activity might be due to a tightly bound Pd–ligand complex, with slow turnover, while the low selectivity was attributed to the fact that the nucleophilic attack occurs *trans* to the nitrogen atom, which would be in this case the best π-acceptor.

Among the numerous ligands tested in this already “classical” reaction, phosphino-oxazoline auxiliaries have largely proved their efficiency [152]. Taking into account this evidence, the synthesis of a series of EDT-TTF-phosphino-oxazolines (**91b** in Scheme 66) was reported together with their application in the same AAA reaction catalyzed by palladium [75]. In parallel, EDT-TTF-thiomethyl-oxazolines (**92b**) have been also prepared and tested. The test reaction was the same as in the previous study, with the difference that the nucleophile was generated in situ from neutral dimethylmalonate, *N,O*-bis(trimethylsilyl)acetamide (BSA) and potassium acetate (KOAc). The Pd precatalysts were generated from the reaction of the free optically pure (*R*) or (*S*) ligand with [Pd(η³-C₃H₅)Cl]₂ to give, after TlPF₆ addition the series of cationic Pd complexes [Pd(η³-C₃H₅)(**91b**)]PF₆ **Pd5c**. These complexes exhibit a sizeable, albeit smaller than the PdCl₂ complex (see Section 3.5.3), anodic shift of the TTF first redox potential (0.18 V), yet showing a full reversibility. Albeit the observed conversions are modest (up to 20%), the enantioselectivities are rather high, up to 85% with the ¹Pr-oxazoline derivatives (see Table 20). As expected, the use of the racemic ligands provided the racemic mixture of the allyl-malonate, with the same activity as the optically pure counterparts. Interestingly, an enhancement of Δee% = 55% resulted from the use of the ¹Pr- rather than the Me-oxazoline derivatives. The results were modest when EDT-TTF-mono-oxazolines or thiomethyl-oxazolines **92b** have been used. The Tsuji-Trost reaction was also carried out with the oxidized TTT-Pd complexes such as [**Pd5c**][SbF₆], in order to evaluate a possible electromodulation



Scheme 67. Asymmetric allylic alkylation with the ligands **89a–c** and **93**.



Scheme 68. Asymmetric hydrogenation of imines.

of the catalytic center upon changing the electronic density around the metal. However, when engaged in the asymmetric allylic alkylation reaction, this oxidized salt afforded a conversion and selectivity quite similar to those found with the non-oxidized complexes. This behavior was tentatively explained by the in situ reduction of TTF^{•+} in TTF, either by Pd(0) species or by the basic reaction medium.

One of the most applied strategies for the synthesis of enantiopure amines consists of the catalytic asymmetric hydrogenation of imines. Iridium complexes, involving the Ir^I/Ir^{III} couple, with phosphino-oxazoline ligands are particularly efficient for this type of catalytic reaction [153]. The different cationic enantiopure or racemic **Ir2** and **Ir3** complexes (see Scheme 51) [119] which contain an isopropyl group on the oxazoline ring, have been conventionally prepared upon reaction between the ligands **92b** or **91b** and the precursor [Ir(COD)Cl]₂ (COD = cycloocta-1,5-diene), followed by the chloride abstraction in the presence of PF₆[−] or BArF₂₄[−] (BArF₂₄[−] = tetrakis[3,5-bis(trifluoromethyl)-phenyl]borate) salts. The latter is a non-coordinating anion which usually leads to an enhancement of the enantiomeric excess. The coordination of the ligands TTF-phosphino-oxazolines (TTF-PHOX) to the Ir^I center induces a downfield shift of +22.7 ppm in ³¹P NMR with respect to the free ligand. The best results in terms of selectivity and catalytic activity for the hydrogenation reaction of the standard substrate *N*-benzylmethyl-phenylimine (Scheme 68) have been obtained with the complexes **Ir2**.

Indeed, total conversions were observed within several hours, with enantiomeric excesses reaching up to 68% ee at room temperature in chiral amine, with the BArF₂₄[−] anion (Table 21).

Variation of the temperature did not lead to any improvement of the selectivity; on the contrary, lower temperatures induce a massive decrease of the conversions, very likely because of solubility problems. When the hydrogenation reaction was carried out with the oxidized **Ir2** complex, thus containing the radical cation salt of TTF, a drastic loss in selectivity (23% ee) and activity (20% yield) was observed after 15 h, although the conversion reached up to 70% after 70 h. Nevertheless, it is difficult to assign this difference with respect to the neutral ligand to either an electronic modulation on the metallic center provided by the change in the oxidation state of the ligand, or to other catalytic species generated in the reaction mixture under the reductive conditions.

However, these first results in asymmetric allylic alkylation and hydrogenation of imines are certainly promising in view of developing electroactive ligands which could induce a redox control on the catalytic processes.

Table 21
Asymmetric hydrogenation of imines [119].

Ligand	Anion	T (°C)	Conv (%) ^a	ee (%) ^b
92b (R)	PF ₆ [−]	20	7	not determined
91b (R)	PF ₆ [−]	20	100	57 (R)
91b (R)	PF ₆ [−]	5	20	56 (R)
91b (R)	PF ₆ [−]	50	100	58 (R)
91b (R)	BArF [−]	20	100	68 (R)
91b (R)	BArF [−]	−10	22	69 (R)

^a Determined by GPC.

^b Determined by HPLC on a Chiralpack OJ column.

6. Conclusions and perspectives

In this review paper, which is unprecedented with respect to the topic addressed, we presented in an exhaustive manner the electroactive ligands based on the TTF unit and phosphorous and nitrogen coordinating groups, together with their coordination metallic complexes. It turns out that all the phosphorous ligands described so far are phosphines. However, as superior pnicogen homologues, we reported also a couple of examples concerning TTF-stibines. While the nitrogen ligands containing TTF units are much more various, e.g. pyridines, pyrazines, bipyridines, imines, etc., yet the common feature of most of them is the sp^2 hybridization of the nitrogen atom. Accordingly, we have focused our attention mainly on TTF-phosphines and on different families of TTF-N sp^2 ligands, also because metallic complexes have been described only with these precursors. The synthetic methodologies employed for the preparation of TTF-N ligands are very diverse, and they include carbon–carbon bond formation reactions, condensation reactions between reactive precursors of TTF's and nitrogen heterocycles, alkylation reactions of TTF thiolates with halogenated pyridines, or Wittig type condensation reactions. On the contrary, the synthesis of TTF-phosphines or stibines is limited to a couple of methods, i.e. reaction of lithiated TTF's with halogeno-phosphines or -stibines in the case of direct linkage between TTF and coordinating group, and nucleophilic substitution of TTF-thiolates with halogeno-alkyl-phosphines, protected as boranes, in the case of long chain TTF-phosphines. It is clear then that, at the present day, one has access to a huge library of electroactive phosphines or pyridines and derivatives containing the electrodonating TTF unit, available for further metal coordination. One particular aspect which should be emphasized at this point throughout all the examples concerns the electron donating ability of the TTF core, which is only scarcely affected upon association with the coordinating group. Indeed, when the phosphino group is directly attached to the TTF unit, the similar electronegativities of phosphorous and carbon atoms do not favor a large variation in electron density on TTF. On the other hand, in TTF-N ligands, the electronegative nitrogen atom is rather remote from TTF across the linker. Undoubtedly, the largest variation is observed when the TTF unit is fused with the nitrogen heterocycle, like in TTF-pyrazines. Despite the large number of ligands itemized to date, only a restricted collection of metal complexes, with a maximum of about 15 examples in the case of copper (I or II), has been described so far, but also with no example for metals such as chromium or osmium, thus suggesting that there is still a lot of room for further developing this field. All the reported complexes for each triad of transition metals have been reviewed, with a special focus on their solid-state structures and properties. One interesting aspect is related to the variation of the oxidation potential of TTF ligand upon metal complexation. As a general trend, within the complexes based on TTF-N ligands, there is little change on the oxidation potential, very likely because of the large separation between the TTF and the metallic fragment. On the contrary, anodic shifts of $\Delta E = 200\text{--}250$ mV are observed in the case of TTF-phosphines complexes with the phosphino groups directly attached to the TTF core, indicating undoubtedly that the coordinated metal influences the electron donating properties. In the series of metal carbonyl complexes, the modulation of the electronic density on the metal with the oxidation state of TTF can be also evaluated from the shift of the IR absorption frequencies of CO ligands. Another interesting possibility which can occur is the mixed valence state, when the oxidation potentials of TTF and metal are very close. Since in many of the reported complexes, the metal is paramagnetic, their magnetic properties have been determined and they are characteristic either for Curie or Curie–Weiss type behaviors, or, in one case, for antiferromagnetic uniform spin

chains. Clearly, the presence of magnetic interactions in such complexes is interesting in view of their combination with conducting properties due to the activation of donors upon partial oxidation. The coexistence or interplay of itinerant π type electrons with localized d (or even f) electrons arising from the same molecule will be a highly valuable achievement within the multifunctional materials field. However, in the few examples described so far containing oxidized TTF units, strong dimerization or lack of interaction caused by the steric hindrance did not allow extensive electron delocalization in the solid. Another peculiar aspect is related to the properties of the Ru^{II} complexes, in which the presence of an electroactive ligand is likely to control their luminescence upon changing the oxidation state of TTF. Finally, an interesting development, which for the moment is only at its infancy, appears to be the utilization of appropriately designed redox active ligands in catalytic processes. In this case, a tuning of the reactivity and electron density on the metallic center is likely to be achieved by switching between the oxidation states of TTF. Some first results on TTF-oxazoline derivatives demonstrated already the efficiency of such ligands in a couple of catalytic reactions.

Acknowledgement

This work was supported by the CNRS, University of Rennes I and University of Angers.

References

- [1] (a) J.M. Williams, J.R. Ferraro, R.J. Thorn, K.D. Carlson, U. Geiser, H.H. Wang, A.M. Kini, M.-H. Whangbo, *Organic Superconductors (Including Fullerenes)*, Synthesis, Structure, Properties and Theory, Prentice Hall, 1992; (b) M.R. Bryce, *J. Mater. Chem.* 5 (1995) 1469; (c) J.L. Segura, N. Martin, *Angew. Chem. Int. Ed.* 40 (2001) 1372.
- [2] P. Batail, *Chem. Rev.* 104 (2004) 4887 (and the following articles of this thematic issue).
- [3] (a) M. Kurmoo, A.W. Graham, P. Day, S.J. Coles, M.B. Hurthouse, J.L. Caulfield, J. Singleton, F.L. Pratt, W. Hayes, L. Ducasse, P. Guionneau, *J. Am. Chem. Soc.* 117 (1995) 12209; (b) E. Coronado, J.R. Galan-Mascaros, C.J. Gomez-Garcia, V. Laukhin, *Nature* 408 (2000) 447.
- [4] H. Tanaka, Y. Okano, H. Kobayashi, W. Suzuki, A. Kobayashi, *Science* 291 (2001) 285.
- [5] E. Coronado, P. Day, *Chem. Rev.* 104 (2004) 5419.
- [6] (a) T. Enoki, A. Miyazaki, *Chem. Rev.* 104 (2004) 5449; (b) L. Ouahab, T. Enoki, *Eur. J. Inorg. Chem.* (2004) 933.
- [7] (a) G. Schukat, A.M. Richter, E. Fanghanel, *Sulfur Rep.* 7 (1987) 155; (b) G. Schukat, E. Fanghanel, *Sulfur Rep.* 14 (1993) 245; (c) G. Schukat, E. Fanghanel, *Sulfur Rep.* 18 (1996) 1; (d) G. Schukat, E. Fanghanel, *Sulfur Rep.* 24 (2003) 1.
- [8] (a) M. Bendikov, F. Wudl, D.F. Perepichka, *Chem. Rev.* 104 (2004) 4891; (b) J. Yamada, H. Akutsu, H. Nishikawa, K. Kikuchi, *Chem. Rev.* 104 (2004) 5057; (c) M. Iyoda, M. Hasegawa, Y. Miyake, *Chem. Rev.* 104 (2004) 5085; (d) J.O. Jeppesen, M.B. Nielsen, J. Becher, *Chem. Rev.* 104 (2004) 5115; (e) J.M. Fabre, *Chem. Rev.* 104 (2004) 5133; (f) A. Gorgues, P. Hudhomme, M. Sallé, *Chem. Rev.* 104 (2004) 5151; (g) D. Lorcy, N. Bellec, *Chem. Rev.* 104 (2004) 5185.
- [9] T. Nagawa, Y. Zama, Y. Okamoto, *Bull. Chem. Soc. Jpn.* 57 (1984) 2035.
- [10] M. Iyoda, Y. Kuwatani, N. Ueno, M. Oda, *J. Chem. Soc. Chem. Commun.* (1992) 158.
- [11] M. Iyoda, M. Fukuda, M. Yoshida, S. Sasaki, *Chem. Lett.* (1994) 2369.
- [12] A.J. Moore, A.S. Batsanov, M.R. Bryce, J.A.K. Howard, V. Khodorkovsky, L. Shapiro, A. Shames, *Eur. J. Org. Chem.* (2001) 73.
- [13] S. Bouguessa, A.K. Gouasmia, S. Golhen, L. Ouahab, J.-M. Fabre, *Tetrahedron Lett.* 44 (2003) 9275.
- [14] L. Wang, B. Zhang, J. Zhang, *Inorg. Chem.* 45 (2006) 6860.
- [15] M. Chahma, X.S. Wang, A. van des Est, M. Pilkington, *J. Org. Chem.* 71 (2006) 2750.
- [16] E. Cerrada, J. Garrido, M. Laguna, N. Lardiés, I. Romeo, *Synth. Met.* 102 (1999) 1709.
- [17] O.P.-L. Levi, J.Y. Becker, A. Ellern, V. Khodorkovsky, *Tetrahedron Lett.* 42 (2001) 1571.
- [18] Y.-F. Han, J.-S. Zhang, Y.-J. Lin, J. Dai, G.-X. Jin, *J. Organomet. Chem.* 692 (2007) 4545.
- [19] (a) R. Andreu, I. Malfant, P.G. Lacroix, P. Cassoux, *Eur. J. Org. Chem.* 3 (2000) 737; (b) R. Andreu, I. Malfant, P.G. Lacroix, P. Cassoux, *Synth. Met.* 102 (1999) 1575.

- [20] R. Andreu, J. Garin, J. Orduna, G.J. Ashwell, M.A. Amiri, R. Hamilton, *Thin Sol. Films* 408 (2002) 236.
- [21] H. Xue, X.-J. Tang, L.-Z. Wu, L.-P. Zhang, C.-H. Tung, *J. Org. Chem.* 70 (2005) 9727.
- [22] N. Benbellat, K.S. Gavrilenco, Y. Le Gal, O. Cador, S. Golhen, A. Gouasmia, J.-M. Fabre, L. Ouahab, *Inorg. Chem.* 45 (2006) 10440.
- [23] M. Chahma, N. Hassan, A. Alberola, H. Stoeckli-Evans, M. Pilkington, *Inorg. Chem.* 46 (2007) 3807.
- [24] J.-Y. Balandier, A. Belyasmine, M. Sallé, *Eur. J. Org. Chem.* (2008) 269.
- [25] Y.-P. Zhao, L.-Z. Wu, G. Si, Y. Liu, H. Xue, L.-P. Zhang, C.-H. Tung, *J. Org. Chem.* 72 (2007) 3632.
- [26] E. Isomura, K.-I. Tokuyama, T. Nishinaga, M. Iyoda, *Tetrahedron Lett.* 48 (2007) 5895.
- [27] L.M. Goldenberg, J.Y. Becker, O.P.-T. Levi, V.Y. Khodorkovsky, M.R. Bryce, M.C. Petty, *J. Chem. Soc., Chem. Commun.* (1995) 475.
- [28] L.M. Goldenberg, J.Y. Becker, O.P.-T. Levi, V.Y. Khodorkovsky, L.M. Shapiro, M.R. Bryce, J.P. Cresswell, M.C. Petty, *J. Mater. Chem.* 7 (1997) 901.
- [29] W. Xu, D. Zhang, H. Li, D. Zhu, *J. Mater. Chem.* 9 (1999) 1245.
- [30] J.-P. Griffiths, R.J. Brown, P. Day, C.J. Matthews, B. Vital, J.D. Wallis, *Tetrahedron Lett.* 44 (2003) 3127.
- [31] A. Ota, L. Ouahab, S. Golhen, O. Cador, Y. Yoshida, G. Saito, *New J. Chem.* 29 (2005) 1135.
- [32] A.S.F. Boyd, G. Cooke, F.M.A. Duclairoir, V.M. Rotello, *Tetrahedron Lett.* 44 (2003) 303.
- [33] T. Devic, N. Avarvari, P. Batail, *Chem. Eur. J.* 10 (2004) 3697.
- [34] H. Lu, W. Xu, D. Zhang, D. Zhu, *Chem. Commun.* (2005) 4777.
- [35] C. Benhaoua, M. Mazari, N. Mercier, F. Le Derf, M. Sallé, *New J. Chem.* 32 (2008) 913.
- [36] Q. Wang, P. Day, J.-P. Griffiths, H. Nie, J.D. Wallis, *New J. Chem.* 30 (2006) 1790.
- [37] B. Girmay, J.D. Kilburn, A.E. Underhill, K.S. Varma, M.B. Hursthouse, M.E. Harman, J. Becher, G. Bojesen, *J. Chem. Soc. Chem. Commun.* (1989) 1406.
- [38] C. Jia, D. Zhang, X. Guo, S. Wan, W. Xu, D. Zhu, *Synthesis* (2002) 2177.
- [39] S. Bouguessa, K. Hervé, S. Golhen, L. Ouahab, J.-M. Fabre, *New J. Chem.* 27 (2003) 560.
- [40] M. Jørgensen, K.A. Lestrup, K. Bechgaard, *J. Org. Chem.* 56 (1991) 5684.
- [41] S.-X. Liu, S. Dolder, M. Pilkington, S. Decurtins, *J. Org. Chem.* 67 (2002) 3160.
- [42] C. Jia, D. Zhang, Y. Xu, W. Xu, H. Hu, D. Zhu, *Synth. Met.* 132 (2003) 249.
- [43] N. Benbellat, Y. Le Gal, S. Golhen, A. Gouasmia, L. Ouahab, J.-M. Fabre, *Eur. J. Org. Chem.* (2006) 4237.
- [44] S.-X. Liu, S. Dolder, E.B. Rusanov, H. Stoeckli-Evans, S. Decurtins, *C. R. Chimie* 6 (2003) 657.
- [45] M. Mosimann, S.-X. Liu, G. Labat, A. Neels, S. Decurtins, *Inorg. Chim. Acta* 360 (2007) 3848.
- [46] C. Jia, S.-X. Liu, C. Ambrus, A. Neels, G. Labat, S. Decurtins, *Inorg. Chem.* 45 (2006) 3152.
- [47] C. Goze, S.-X. Liu, C. Leiggenger, L. Sanguinet, E. Levillain, A. Hauser, S. Decurtins, *Tetrahedron* 64 (2008) 1345.
- [48] K. Hervé, S.-X. Liu, O. Cador, S. Golhen, Y. Le Gal, A. Bousseksou, H. Stoeckli-Evans, S. Decurtins, L. Ouahab, *Eur. J. Inorg. Chem.* (2006) 3498.
- [49] S. Campagna, S. Serroni, F. Puntoriero, F. Loiseau, L. De Cola, C.J. Kleverlaan, J. Becher, A.P. Sørensen, P. Hascoet, N. Thorup, *Chem. Eur. J.* 8 (2002) 4461.
- [50] C.-J. Fang, Z. Zhu, W. Sum, C.-H. Xu, C.H. Yan, *New J. Chem.* 31 (2007) 580.
- [51] K. Sako, Y. Misaki, M. Fujiwara, T. Maitani, K. Tanaka, H. Tatemitsu, *Chem. Lett.* 31 (2002) 592.
- [52] (a) C. Jia, S.-X. Liu, C. Tanner, C. Leiggenger, A. Neels, L. Sanguinet, E. Levillain, S. Leutwyler, A. Hauser, S. Decurtins, *Chem. Eur. J.* 13 (2007) 3804; (b) C. Jia, S.-X. Liu, C. Tanner, C. Leiggenger, L. Sanguinet, E. Levillain, S. Leutwyler, A. Hauser, S. Decurtins, *Chem. Commun.* (2006) 1878.
- [53] T. Jørgensen, J. Becher, J.-C. Chambron, J.-P. Sauvage, *Tetrahedron Lett.* 35 (1994) 4339.
- [54] K.S. Bang, M.B. Nielsen, R. Zubarev, J. Becher, *Chem. Commun.* (2000) 215.
- [55] G.C. Papavassiliou, S.Y. Yiannopoulos, J.S. Zambounis, *Mol. Cryst. Liq. Cryst.* 120 (1985) 333.
- [56] G.C. Papavassiliou, S.Y. Yiannopoulos, J.S. Zambounis, *J. Chem. Soc., Chem. Commun.* (1986) 820.
- [57] G.C. Papavassiliou, G.A. Mousdis, S.Y. Yiannopoulos, V.C. Kakoussis, J.S. Zambounis, *Synth. Met.* 27 (1988) B373.
- [58] (a) G.C. Papavassiliou, G.A. Mousdis, A. Terzis, C. Raptopoulou, K. Murata, T. Konoike, Y. Yoshino, *Synth. Met.* 120 (2001) 743; (b) G.C. Papavassiliou, G.A. Mousdis, A. Terzis, C. Raptopoulou, K. Murata, T. Konoike, Y. Yoshino, A. Graja, A. Łapiński, *Synth. Met.* 135/136 (2003) 651.
- [59] S. Kimura, H. Suzuki, T. Maejima, M. Suto, K. Yamashita, S. Ichikawa, H. Mori, H. Moriyama, T. Mochida, Y. Nishio, K. Kajita, *J. Phys. IV France* 114 (2004) 521.
- [60] R. Suizu, T. Imakubo, *Org. Biomol. Chem.* 1 (2003) 3629.
- [61] Naraso, J. Nishida, M. Tomura, Y. Yamashita, *Synth. Met.* 153 (2005) 389.
- [62] (a) G.C. Papavassiliou, S.Y. Yiannopoulos, J.S. Zambounis, K. Kobayashi, K. Umemoto, *Chem. Lett.* 16 (1987) 1279; (b) S. Kimura, K. Yamashita, H. Suzuki, S. Ichikawa, H. Mori, Y. Nishio, K. Kajita, *Synth. Met.* 153 (2005) 437.
- [63] M. Tomura, Y. Yamashita, *Acta Cryst. E57* (2001) o307.
- [64] Naraso, J. Nishida, S. Ando, J. Yamaguchi, K. Itaka, H. Koinuma, H. Tada, S. Tokito, Y. Yamashita, *J. Am. Chem. Soc.* 127 (2005) 10142.
- [65] Naraso, J. Nishida, D. Kumaki, S. Tokito, Y. Yamashita, *J. Am. Chem. Soc.* 128 (2006) 9598.
- [66] K. Lahlii, A. Moradpour, C. Bowlas, F. Menou, P. Cassoux, J. Bonvoisin, J.-P. Launay, G. Dive, D. Dehareng, *J. Am. Chem. Soc.* 117 (1995) 9995.
- [67] S. Frenzel, K. Müllen, *Synth. Met.* 80 (1996) 175.
- [68] N. Avarvari, M. Fourmigué, *Chem. Commun.* (2004) 2794.
- [69] K. Lahlii, A. Moradpour, C. Merienne, C. Bowlas, *J. Org. Chem.* 59 (1994) 8030.
- [70] S. Dolder, S.-X. Liu, E. Beurer, L. Ouahab, S. Decurtins, *Polyhedron* 25 (2006) 1514.
- [71] S. Ichikawa, S. Kimura, K. Takahashi, H. Mori, G. Yoshida, Y. Manabe, M. Matsuda, H. Tajima, J. Yamaura, *Inorg. Chem.* 47 (2008) 4140.
- [72] S. Ichikawa, S. Kimura, H. Mori, G. Yoshida, H. Tajima, *Inorg. Chem.* 45 (2006) 7575.
- [73] A. Chesney, M.R. Bryce, *Tetrahedron: Asymmetry* 7 (1996) 3247.
- [74] C. Réthoré, M. Fourmigué, N. Avarvari, *Chem. Commun.* (2004) 1384.
- [75] C. Réthoré, I. Suisse, F. Agbossou-Niedercorn, E. Guillaumon, R. Llusar, M. Fourmigué, N. Avarvari, *Tetrahedron* 62 (2006) 11942.
- [76] C. Réthoré, N. Avarvari, E. Canadell, P. Auban-Senzier, M. Fourmigué, *J. Am. Chem. Soc.* 127 (2005) 5748.
- [77] C. Réthoré, A. Madalan, M. Fourmigué, E. Canadell, E.B. Lopes, M. Almeida, R. Clérac, N. Avarvari, *New J. Chem.* 31 (2007) 1468.
- [78] T. Murata, Y. Morita, K. Fukui, K. Sato, D. Shiomi, T. Takui, M. Maesato, H. Yamochi, G. Saito, K. Nakasui, *Angew. Chem. Int. Ed.* 43 (2004) 6343.
- [79] Y. Morita, T. Murata, H. Yamochi, G. Saito, K. Nakasui, *Synth. Met.* 135/136 (2003) 579.
- [80] T. Murata, Y. Morita, Y. Yakiyama, Y. Nishimura, T. Ise, D. Shiomi, K. Sato, T. Takui, K. Nakasui, *Chem. Commun.* (2007) 4009.
- [81] J.-C. Wu, S.-X. Liu, T.D. Keene, A. Neels, V. Mereacre, A.K. Powell, S. Decurtins, *Inorg. Chem.* 47 (2008) 3452.
- [82] M. Fourmigué, P. Batail, *J. Chem. Soc. Chem. Commun.* (1991) 1370.
- [83] M. Fourmigué, P. Batail, *Bull. Soc. Chim. Fr.* 129 (1992) 29.
- [84] M. Yuan, B. Ülgüt, M. McGuire, K. Takada, F.J. DiSalvo, S. Lee, H. Abruña, *Chem. Mater.* 18 (2006) 4296.
- [85] M. Fourmigué, Y.-S. Huang, *Organometallics* 12 (1993) 797.
- [86] F. Gerson, A. Lamprecht, M. Fourmigué, *J. Chem. Soc., Perkin Trans. II* (1996) 1409.
- [87] D.C. Green, *J. Org. Chem.* 44 (1979) 1476.
- [88] M. Fourmigué, S. Jarshow, P. Batail, *Phosph. Sulfur Silicon* 75 (1993) 175.
- [89] M. Fourmigué, C.E. Uzelmeier, K. Boubekeur, S.L. Bartley, K.R. Dunbar, *J. Organomet. Chem.* 529 (1997) 343.
- [90] P. Pellon, E. Brulé, N. Bellec, K. Chamontin, D. Lorcy, *J. Chem. Soc., Perkin Trans. I* (2000) 4409.
- [91] P. Pellon, G. Gachot, J. Le Bris, S. Marchin, R. Carlier, D. Lorcy, *Inorg. Chem.* 42 (2003) 2056.
- [92] G. Gachot, P. Pellon, T. Roisnel, D. Lorcy, *Eur. J. Inorg. Chem.* 13 (2006) 2604.
- [93] S.S. Kuduva, N. Avarvari, M. Fourmigué, *J. Chem. Soc., Dalton Trans.* (2002) 3686.
- [94] M. Ashikawa, H.M. Yamamoto, A. Nakao, R. Kato, *Tetrahedron Lett.* 47 (2006) 8937.
- [95] N. Avarvari, D. Martin, M. Fourmigué, *J. Organomet. Chem.* 643/644 (2002) 292.
- [96] N. Avarvari, M. Fourmigué, *Chem. Commun.* (2004) 1300.
- [97] L. Ouahab, F. Iwahori, S. Golhen, R. Carlier, J.-P. Sutter, *Synth. Met.* 133/134 (2003) 505.
- [98] C.E. Uzelmeier, S.L. Bartley, M. Fourmigué, R. Rogers, G. Grandinetti, K.R. Dunbar, *Inorg. Chem.* 37 (1998) 6706.
- [99] (a) F.A. Cotton, K.R. Dunbar, L.R. Falvello, M. Tomas, R.A. Walton, *J. Am. Chem. Soc.* 105 (1983) 4950; (b) F.A. Cotton, J.G. Jennings, A.C. Price, K. Vidyasager, *Inorg. Chem.* 29 (1990) 4138.
- [100] S. Perruchas, N. Avarvari, D. Rondeau, E. Levillain, P. Batail, *Inorg. Chem.* 44 (2005) 3459.
- [101] (a) C. Guilbaud, A. Deluzet, B. Domercq, P. Molinié, C. Coulon, K. Boubekeur, P. Batail, *Chem. Commun.* 1867 (1999); (b) T.G. Gray, C.M. Rudzinski, D. Nocera, R.H. Holm, *Inorg. Chem.* 38 (1999) 5932.
- [102] D. Rondeau, S. Perruchas, N. Avarvari, P. Batail, K. Vekey, *J. Mass. Spectr.* 40 (2005) 60.
- [103] S. Schenker, P.C. Stein, J.A. Wolny, C. Brady, J.J. McGarvey, H. Toftlund, A. Hauser, *Inorg. Chem.* 40 (2001) 134.
- [104] D.M. Kurtz Jr., *Chem. Rev.* 90 (1990) 585.
- [105] (a) V. Balzani, A. Juris, M. Venturi, S. Campagna, S. Serroni, *Chem. Rev.* 96 (1996) 759; (b) E.R. Batista, R.L. Martin, *J. Phys. Chem. A* 109 (2005) 3128.
- [106] C. Goze, C. Leiggenger, S.-X. Liu, L. Sanguinet, E. Levillain, A. Hauser, S. Decurtins, *ChemPhysChem* 8 (2007) 1504.
- [107] J.M. Asara, C.E. Uzelmeier, K.R. Dunbar, J. Allison, *Inorg. Chem.* 37 (1998) 1833.
- [108] C.E. Uzelmeier, B.W. Smucker, E.W. Reinheimer, M. Shatruk, A.W. O'Neal, M. Fourmigué, K.R. Dunbar, *Dalton Trans.* (2006) 5259.
- [109] R.V. Honeychuck, W.H. Hersh, *Inorg. Chem.* 28 (1989) 2869.
- [110] L.-S. Luh, L.-K. Liu, *Inorg. Chim. Acta* 206 (1993) 89.
- [111] P.K. Baker, N.G. Connelly, B.M.R. Jones, J.P. Maher, K.R. Somers, *J. Chem. Soc. Dalton Trans.* (1980) 579.
- [112] C. Gouverd, F. Biaso, L. Cataldo, T. Berclaz, M. Geoffroy, E. Levillain, N. Avarvari, M. Fourmigué, F.-X. Sauvage, C. Wartelle, *Phys. Chem. Chem. Phys.* 7 (2005) 85.
- [113] R.L. Carlin, *Magneto-chemistry*, Springer, Berlin, 1986.

- [114] S.-X. Liu, S. Dolder, P. Franz, A. Neels, H. Stoeckli-Evans, S. Decurtins, *Inorg. Chem.* 42 (2003) 4801.
- [115] K.S. Gavrilenko, Y. Le Gal, O. Cador, S. Golhen, L. Ouahab, *Chem. Commun.* (2007) 280.
- [116] K.S. Gavrilenko, S.V. Punin, O. Cador, S. Golhen, L. Ouahab, V.V. Pavlishchuk, *J. Am. Chem. Soc.* 127 (2005) 12246.
- [117] J.K. Stalick, P.W.R. Corfield, D.W. Meek, *Inorg. Chem.* 12 (1973) 1668.
- [118] A.M. Madalan, C. Réthoré, N. Avarvari, *Inorg. Chim. Acta* 360 (2007) 233.
- [119] C. Réthoré, F. Riobé, M. Fourmigué, N. Avarvari, I. Suisse, F. Agbossou-Niedercorn, *Tetrahedron: Asymmetry* 18 (2007) 1877.
- [120] S.-X. Liu, C. Ambrus, S. Dolder, A. Neels, G. Labat, S. Decurtins, *J. Low Temp. Phys.* 142 (2006) 457.
- [121] S.-X. Liu, C. Ambrus, S. Dolder, A. Neels, S. Decurtins, *Inorg. Chem.* 45 (2006) 9622.
- [122] (a) M.M. Bhadbhade, D. Srinivas, *Inorg. Chem.* 32 (1993) 5458;
(b) L.G. Marzilli, M.F. Summers, N. Bresciani, E. Pahor, J.-P. Charland, L. Randaccio, *J. Am. Chem. Soc.* 107 (1985) 6680;
(c) P. Cassoux, A. Gleizes, *Inorg. Chem.* 19 (1980) 665;
(d) S.-S. Zhang, B. Yang, Y.-F. Wang, X.-M. Li, K. Jiao, *Asian J. Chem.* 17 (2005) 929.
- [123] (a) P.J. Stang, J. Fan, B. Olenyuk, *Chem. Commun.* (1997) 1453;
(b) J. Fan, J.A. Whiteford, B. Olenyuk, M.D. Levin, P.J. Stang, E.B. Fleischer, *J. Am. Chem. Soc.* 121 (1999) 2741;
(c) T. Habicher, J.-F. Nierengarten, V. Gramlich, F. Diederich, *Angew. Chem. Int. Ed. Engl.* 37 (1998) 1916;
(d) F. Würthner, A. Sautter, D. Schmid, P.J.A. Weber, *Chem. Eur. J.* 7 (2001) 894.
- [124] T. Devic, P. Batail, M. Fourmigué, N. Avarvari, *Inorg. Chem.* 43 (2004) 3136.
- [125] (a) A.R. Sanger, *J. Chem. Soc. Dalton Trans.* (1977) 1972;
(b) S.T. Liu, J.T. Chen, S.M. Peng, Y.L. Hsiao, M.C. Cheng, *Inorg. Chem.* 29 (1990) 1169.
- [126] (a) S.-X. Xiao, W.C. Trogler, D.E. Ellis, Z. Berkovitch-Yellin, *J. Am. Chem. Soc.* 105 (1983) 7033;
(b) D.S. Marynick, *J. Am. Chem. Soc.* 106 (1984) 4064.
- [127] B.J. Hathaway, D.G. Holah, A.E. Underhill, *J. Chem. Soc.* (1962) 244.
- [128] R.R. Thomas, A. Sen, *Inorg. Synth.* 26 (1989) 128.
- [129] A. DeRenzi, A. Panunzio, A. Vitagliano, *J. Chem. Soc. Chem. Commun.* (1976) 47.
- [130] P.-W. Wang, M.A. Fox, *Inorg. Chem.* 33 (1994) 2938.
- [131] B.W. Smuker, K.R. Dunbar, *Dalton Trans.* (2000) 1309.
- [132] A. Pfaltz, *Acta Chem. Scand. B* 50 (1996) 189.
- [133] G. Helmchen, S. Kudis, P. Sennhenn, H. Steinhagen, *Pure Appl. Chem.* 69 (1997) 513.
- [134] J.M.J. Williams, *Synlett* (1996) 705.
- [135] (a) A.M. Allgeier, C.A. Mirkin, *Angew. Chem. Int. Ed.* 37 (1998) 894;
(b) C.K.A. Gregson, V.C. Gibson, N.J. Long, E.L. Marshall, P.J. Oxford, A.J.P. White, *J. Am. Chem. Soc.* 128 (2006) 7410.
- [136] F. Iwahori, S. Golhen, L. Ouahab, R. Carlier, J.-P. Sutter, *Inorg. Chem.* 40 (2001) 6541.
- [137] F. Setifi, L. Ouahab, S. Golhen, Y. Yoshida, G. Saito, *Inorg. Chem.* 42 (2003) 1791.
- [138] K. Hervé, Y. Le Gal, L. Ouahab, S. Golhen, O. Cador, *Synth. Metals* 153 (2005) 461.
- [139] Q.-Y. Zhu, Y. Liu, Y. Zhang, G.-Q. Bian, G.-Y. Niu, J. Dai, *Inorg. Chem.* 46 (2007) 10065.
- [140] T. Devic, D. Rondeau, Y. Sahin, E. Levillain, R. Clérac, P. Batail, N. Avarvari, *Dalton Trans.* (2006) 1331.
- [141] E. Cerrada, C. Diaz, M.C. Diaz, M.B. Hursthouse, M. Laguna, M.E. Light, *Dalton Trans.* (2002) 1104.
- [142] S. Sadaïke, K. Takimiya, Y. Aso, T. Otsubo, *Tetrahedron Lett.* 44 (2003) 161.
- [143] P.A. Liddell, G. Kodis, L. de la Garza, J.L. Bahr, A.L. Moore, T.A. Moore, D. Gust, *Helv. Chim. Acta* 84 (2001) 2765.
- [144] X. Xiao, W. Xu, D. Zhang, H. Xu, H. Lu, D. Zhu, *J. Mater. Chem.* 15 (2005) 2557.
- [145] (a) Y. Hu, G. Lai, Y. Shen, Y. Li, *Dyes Pigments* 66 (2005) 49;
(b) Y. Hu, G. Lai, Y. Schen, Y. Li, *Monatshfte Chem.* 135 (2004) 1167.
- [146] C. Loosli, C. Jia, S.-X. Liu, M. Haas, M. Dias, E. Levillain, A. Neels, G. Labat, A. Hauser, S. Decurtins, *J. Org. Chem.* 70 (2005) 4988.
- [147] (a) J. Becher, T. Brimert, J.O. Jeppesen, J.Z. Pedersen, R. Zubarev, T. Bjornholm, N. Reitzel, T.R. Jensen, K. Kjaer, E. Levillain, *Angew. Chem. Int. Ed.* 40 (2001) 2497;
(b) J.O. Jeppesen, J. Becher, *Eur. J. Org. Chem.* (2003) 3245;
(c) H. Li, J.O. Jeppesen, E. Levillain, J. Becher, *Chem. Commun.* (2003) 846.
- [148] M.A. Blower, M.R. Bryce, W. Devonport, *Adv. Mater.* 8 (1996) 63.
- [149] J. Sly, P. Kasak, E. Elba-Nadal, C. Rovira, L. Gorriç, P. Thordarson, D.B. Amabilino, A.E. Rowan, R.J.M. Nolte, *Chem. Commun.* (2005) 1255.
- [150] C. Wang, M.R. Bryce, A.S. Batsanov, J.A.K. Howard, *Chem. Eur. J.* 3 (1997) 1679.
- [151] B.M. Trost, M.L. Crawley, *Chem. Rev.* 103 (2003) 2921.
- [152] G. Helmchen, A. Pfaltz, *Acc. Chem. Res.* 33 (2000) 336.
- [153] (a) A. Lightfoot, P. Schnider, A. Pfaltz, *Angew. Chem. Int. Ed.* 37 (1998) 2897;
(b) A. Trifonova, J.S. Diesen, P.G. Andersson, *Chem. Eur. J.* 12 (2006) 2318.